NPS68-86-002

NAVAL POSTGRADUATE SCHOOL

Monterey, California

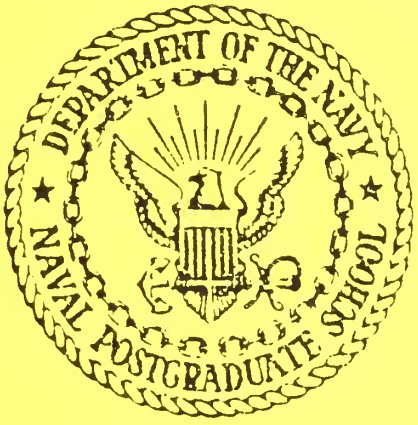

PRELIMINARY INVESTIGATION OF OPTIMUM FREQUENCY FOR SOUND PROPAGATION IN SHALLOW SOUND CHANNELS

Suk Wang Yoon
Calvin R. Dunlap
Wendy L. Bradfield-Smith

July 1986

Approved for public release-distribution unlimited

Prepared for:
Space and Naval Warfare Systems Command

ington, D.C. 20363-5100

NAVAL POSTGRADUATE SCHOOL
Monterey, California

Rear Admiral R. C. Austin
Superintendent

David Schrady
Provost

The work reported herein was supported by funds provided by the Commander, Space and Naval Warfare Systems Command.

This report was prepared by:

SECURITY CLASSIFICATION OF THIS PAGE *(When Date Entered)*

REPORT DOCUMENTATION PAGE

READ INSTRUCTIONS BEFORE COMPLETING FORM

1. REPORT NUMBER: NPS 68-86-002
2. GOVT ACCESSION NO.:
3. RECIPIENT'S CATALOG NUMBER:

4. TITLE *(and Subtitle)*: Preliminary Investigation of Optimum Frequency for Sound Propagation in Shallow Sound Channels

5. TYPE OF REPORT & PERIOD COVERED: Technical Report

6. PERFORMING ORG. REPORT NUMBER:

7. AUTHOR(s):
Suk Wang Yoon
Calvin R. Dunlap
W.L. Bradfield-Smith

8. CONTRACT OR GRANT NUMBER(s): N003985WRU007

9. PERFORMING ORGANIZATION NAME AND ADDRESS:
Naval Postgraduate School
Monterey, CA 93943

10. PROGRAM ELEMENT, PROJECT, TASK AREA & WORK UNIT NUMBERS:

11. CONTROLLING OFFICE NAME AND ADDRESS:
Space and Naval Warfare Systems Command

12. REPORT DATE: July 1986

13. NUMBER OF PAGES: 106

14. MONITORING AGENCY NAME & ADDRESS *(if different from Controlling Office)*:
Naval Postgraduate School
Department of Oceanography
Monterey, CA 93943

15. SECURITY CLASS. *(of this report)*: UNCLASSIFIED

15a. DECLASSIFICATION/DOWNGRADING SCHEDULE:

16. DISTRIBUTION STATEMENT *(of this Report)*:
Approved for public release - distribution unlimited

17. DISTRIBUTION STATEMENT *(of the abstract entered in Block 20, if different from Report)*:

18. SUPPLEMENTARY NOTES:

19. KEY WORDS *(Continue on reverse side if necessary and identify by block number)*:
Shallow sound channel
Deep sound channel
FACT
FACT 9H
Parabolic Equation
PE model
Acoustic transmission loss

20. ABSTRACT *(Continue on reverse side if necessary and identify by block number)*:
Optimum frequency for propagation of sound in shallow sound channels was studied using two acoustic transmission loss models. The split-step Parabolic Equation model (a full-wave model) and the Fast Asympotic Coherent Transmission loss model, version 9H (a ray-tracing model) were tested against experimental data collected by Dosso and Chapman in the northeast Pacific Ocean. The models were found to be valid predictors of optimum frequency for the shallow sound channel observed by Dosso and Chapman. Both models were then used to predict optimum frequency for two sound velocity profiles obtained in a high-latitude

DD FORM 1 JAN 73 1473 EDITION OF 1 NOV 65 IS OBSOLETE
S/N 0102-LF-014-6601

Unclassified
SECURITY CLASSIFICATION OF THIS PAGE *(When Date Entered)*

deep ocean basin under summer conditions exhibiting shallow sound channels. As expected, the split-step Parabolic Equation (PE) model adequately predicted optimum frequencies for these cases. The Fast Asymptotic Coherent Transmission loss model, version 9H (FACT 9H) model did not produce reasonable results for optimum frequencies.

ABSTRACT

Optimum frequency for propagation of sound in shallow sound channels was studied using two acoustic transmission loss models. The split-step Parabolic Equation (PE) model, a full-wave model; and the Fast Asymptotic Coherent Transmission loss model, version 9H (FACT 9H), a ray-tracing model; were tested against experimental data collected by Dosso and Chapman (1984) in the northeast Pacific Ocean. The models were found to be valid predictors of optimum frequency for the shallow sound channel observed by Dosso and Chapman. Both models were then used to predict optimum frequency for two sound velocity profiles obtained in a high-latitude deep ocean basin under summer conditions, exhibiting shallow sound channels. As expected, the split-step PE model adequately predicted optimum frequencies for these cases. The FACT 9H model did not produce reasonable results for optimum frequencies.

TABLE OF CONTENTS

LIST OF TABLES

LIST OF FIGURES

PREFACE

The Environmental Acoustic Research Group at the Naval Postgraduate School(NPS) is engaged in research to establish beneficial and detrimental environmental effects important to present and future Navy acoustics systems.

Pursuant to the above objectives, environmental and acoustics models are used to interpret and predict the complex results obtained when actual experimental or operational scenarios are utilized. The present work is part of a series of investigations concerning shallow sound channels in ASW [Ref. 1].

The Environmental Acoustic Research Group presently consists of 7 professors from the Departments of Oceanography, Physics and Electrical and Computer Engineering. About 10 NPS graduate students are participating in the research group.

I. INTRODUCTION

A. BACKGROUND

Despite technological advances in ship silencing, the acoustic signature produced by a submarine's main propulsion system and auxiliary machinery remains the single most easily exploited tool for detecting, tracking and localizing the submarine. The transmission of sound through the ocean is predictable given a sufficiently well-defined knowledge of the environment, the source and the receiver. Transmission phenomena can become extremely complex, even for relatively simple sound velocity profiles.

Acoustic transmission loss models have been developed for implementation on digital computers. The models generally take one of two approaches: either solving the acoustic wave equation or employing ray-tracing techniques. Both approaches require assumptions, simplifications and approximations. For real situations some models will predict transmission loss more accurately than others depending on the computational technique involved, the method of solution and the extent to which the model accepts real conditions for boundaries at the sea surface, the sea floor and between different water masses.

The situation of interest here is one of the more complicated cases: the shallow sound channel. This situation develops in higher latitudes of the world's oceans, where precipitation is heavy and evaporation is small. A sound velocity profile reveals the presence of a mixed layer resulting from winds and turbulence which may extend from the surface to depths of several tens of meters. Below the mixed layer a shallow sound channel (SSC) is formed by a

combination of temperature and salinity gradients, resulting in a sound speed minimum (channel axis) at roughly 80 to 200 meters. The lower edge of the SSC is bounded by an area of rapidly increasing sound speed. Below the SSC the combined effects of decreasing temperature and increasing pressure can also result in a second or deep sound channel (DSC) with an axis at about 800 to 1000 meters in mid-latitudes. Sound channels act as acoustic waveguides, trapping certain frequencies and allowing them to propagate especially well, while other frequencies "leak" out of the channel and propagate poorly. A more complete discussion of the theoretical background for this paper is contained in Chapter II.

The various layers and channels discussed above occupy the top several hundred to one thousand meters of the oceans. Submarines operate within these depths. These features of the sound velocity profile strongly affect the propagation of the submarine's acoustic signature, and the active and passive operation of the submarine's sonar equipment and that of its hunters. Antisubmarine warfare (ASW) operators must understand these effects and have some means of predicting them. With reliable predictions operators will be able to select frequencies and modes of operation to maximize the effectiveness of their sonar equipment in detecting and tracking the submarine.

B. OBJECTIVE

This study seeks to use two acoustic transmission loss models to predict the behavior of sound in typical shallow sound channels. Both models are available at the Naval Postgraduate School (NPS), accessed through the IBM 3033 computer.

The first model, the split-step Parabolic Equation (PE) model, uses a parabolic approximation to the basic wave

equation and solves for pressure levels as a function of range. It is considered to be a low-frequency (below 800 Hz) model, since higher frequencies require large amounts of computational time. It is not commonly used in support of fleet operations due to the large computational times required.

The second model, the Fast Asymptotic Coherent Transmission loss model version 9H (FACT 9H), employs ray-tracing techniques to predict the amount of acoustic energy arriving at a receiver as a function of range. This model is less rigorous in predicting the effects of different types of boundaries and it does not allow for variations of the sound velocity profile with range. It is simpler and requires less computational time. FACT is generally considered more appropriate than the PE model for frequencies above 800 Hz. The FACT model is widely used in acoustic transmission loss predictions provided to fleet users in the U. S. Navy. Both the PE model and FACT 9H are available at the Naval Postgraduate School, accessed through the IBM 3033 computer.

In 1984 Dosso and Chapman [Ref. 2] reported an experiment on propagation loss that they had conducted in the northeast Pacific Ocean. Sound velocity profiles indicated the presence of a shallow sound channel overlying a deep sound channel. They placed sources in the shallow sound channel, with receivers in the shallow sound channel and the deep sound channel. They measured propagation losses over ranges extending from zero to 35 km for propagation both within the SSC and across the boundary with the DSC. Using a split-step parabolic equation model, Dosso and Chapman were able to obtain good agreement between their experimental results and the predictions of the model. A full discussion of Dosso and Chapman's experiment is contained in Chapter III.

This study examines the Dosso and Chapman experiment by using the Naval Postgraduate School's PE and FACT 9H models. Chapter IV compares these predictions with the Dosso and Chapman's experimental results, supporting the use of the two models to predict the optimum frequency for sound propagation within a shallow sound channel. The models are then applied to two sound velocity profiles of interest to the Naval Postgraduate School's Environmental Acoustic Research Group. These profiles were obtained under summer conditions in a deep ocean basin (4000 meters) at high latitude. Chapter V describes the results of the NPS PE model as applied to these profiles. Chapter VI discusses the FACT 9H model and its predictions for the Dosso and Chapman profiles and the high-latitude summer profiles. Chapter VII then summarizes this study's results and conclusions and presents recommendations for further investigation.

II. THEORY

A. SOUND IN THE SEA

The manner in which sound is transmitted through a medium depends on the velocity with which it propagates. The velocity of sound at any given point in the ocean is calculated from the temperature, salinity and water depth. Since pressure varies linearly with water depth, these two quantities can be treated as interchangeable. In shallow depth temperature is generally the dominant factors affecting the speed of sound, but in the deep depth pressure is. Thus the velocity of sound in the ocean varies in all dimensions: horizontally, vertically and temporally [Ref. 3].

The ocean may be thought of as composed of many layers of water, in each of which sound has a different velocity. Where the sound velocity profile (SVP) shows a velocity minimum, sound is refracted toward that depth, resulting in a focusing of energy at that velocity minimum. This depth is often referred to as a sound channel axis.

A typical sound velocity profile like that of Figure 2.1 [Ref. 4] shows a surface layer of seawater which is subject to the actions of sun, wind and precipitation. This layer is often well-mixed, but its temperature, salinity and thickness may vary greatly from place to place and from day to day. Typically the surface layer shows a constant or slightly increasing sound velocity profile. The surface layer may extend to a depth of several tens of meters. At some point below the surface layer a strong thermal gradient may show up. Temperature and therefore sound velocity decrease sharply with depth, creating a seasonal thermo-

cline. Deeper still lies the main thermocline, formed by another strong negative thermal gradient. Below this is the deep isothermal layer, which extends to the sea floor. In this layer salinity is essentially constant, as is temperature. Pressure and velocity increase very nearly linearly with depth. The layers bounded above by the main thermocline and below by the increasing velocity gradient are called the deep sound channel (DSC). Sound can be trapped in this channel and refracted repeatedly toward the velocity minimum, which is called the DSC axis. This axis may occur at depths ranging from several hundred to over 1000 meters.

Certain environmental conditions can cause a sound velocity profile like that shown in Figure 2.2. A combination of winds, high precipitation and low evaporation such as is found in the northeastern Pacific Ocean can lead to the formation of a secondary or shallow sound channel (SSC) just below the seasonal thermocline. Just as sound can be trapped in the DSC sound can also be trapped in the SSC [Ref. 2].

B. ACOUSTIC WAVEGUIDES

Sound channels act as acoustic waveguides. The ray theory of sound propagation predicts that sound can be refracted and trapped in ducts. Trapping depends on the thickness of the duct and the wavelength of the sound; if the wavelength is "too large" to be contained within the vertical dimension of the duct, the sound will propagate poorly. Frequencies corresponding to those longer wavelengths will propagate poorly, if at all; higher frequencies with shorter wavelengths will propagate much better. Normal mode theory provides a tool for understanding these propagation effects [Ref. 4]. The transition from poor to good propagation is marked by the cutoff frequency. This

frequency does not mark an abrupt end to propagation below which sound cannot be transmitted at all; rather it is a lower boundary below which propagation is less effective.

Acoustic propagation in a sound channel is exactly analogous to the propagation of radio waves in a ground-based duct. Urick [Ref. 3] provides an equation from the theory of radio propagation for the maximum wavelength which will "fit" in such a duct. Dosso and Chapman [Ref. 2] use this equation to calculate the cutoff frequency for their 80-meter thick shallow sound channel as about 250 Hz.

Urick gives another equation derived from radio propagation theory to calculate the cutoff frequency: [Ref. 3]

$$\lambda_{max} = 4.7 \times 10^{-3} \cdot H^{3/2} \qquad (2.1)$$

where λ_{max} is the maximum wavelength of the trapped sound in feet, and H is the thickness of the duct in feet. Converted into metric units and using a sound velocity of 1483 m/s, this formula yields a cutoff frequency of about 243 Hz for Dosso and Chapman's 80-meter channel. A third formula is given by Kinsler, Frey, Coppens and Sanders [Ref. 4]

$$f_{co} \approx 2 \times 10^{5} / D^{3/2} \qquad (2.2)$$

for D in meters. This yields a cutoff frequency of about 280 Hz for this channel. All of these calculations agree within useful ranges, since the cutoff frequency does not mark an abrupt end to propagation.

C. TRANSMISSION LOSS

Several mechanisms act to decrease the energy of an acoustic wave as the wavefront moves farther away from its

source. The most obvious loss mechanism is spreading. Once an outwardly propagating wavefront reaches a reasonable distance from a sufficiently small source, the wavefront can be considered for all practical purposes to be spherical. Thus, the energy in the wave is spread out over an area that increases as the square of the range from the source. In decibels, spherical spreading alone would produce a transmission loss (TL) of

$$TL_{spher} = 20 \log_{10} R \qquad (2.3)$$

If the sound is somehow contained so that spreading may only take place horizontally, as is the case when the sound source is inside a channel or duct, the spreading is cylindrical rather than spherical and the loss is given by

$$TL_{cyl} = 10 \log_{10} R \qquad (2.4)$$

Other mechanisms cause additional energy to be lost. These attenuation mechanisms include scattering and absorption. The degree of attenuation is strongly dependent on the frequency of the sound, with higher frequencies experiencing greater attenuation. Thorp [Ref. 5] developed extensive tables to describe the attenuation of sound as a function of frequency.

Sound can be scattered from rough boundaries at the sea surface or bottom, or from discontinuities at the edges of the layers. Bubbles, marine organisms and suspended particulate matter will also scatter sound [Ref. 4]. Scattering is generally more important for higher frequencies than for lower ones.

Sound energy can also be lost through absorption. Viscosity effects in the interaction of water molecules as the sound wave passes account for one absorption mechanism.

Chemical reactions are also important sources of absorptive loss. Of the many chemical constituents of seawater, certain compounds appear to undergo continuous dissociation into ions and reassociation. This relaxation mechanism takes up acoustic energy. The most important absorption mechanism for frequencies near 1000 Hz appears to be the borate-boric acid relaxation mechanism [Ref. 6].

In general, attenuation increases logarithmically with frequency. The attenuation losses due to such mechanisms are so small at low frequencies that the measurements must be made over extremely long ranges to detect any losses. The precision with which the measurements must be made and the inhomogeneities in the ocean further complicate the task. Urick [Ref. 3] provides an excellent discussion of absorption and attenuation.

Two factors are operating with opposing effects on sound being propagated through sound channels. First, attenuation mechanisms tend to cause losses of acoustic energy. Second, the focusing effect of the channel tends to reduce the losses. In the ideal case, a sound channel bounded above and below by smooth interfaces between layers with no absorption or leakage should produce losses at about the rate due to cylindrical spreading alone. The minimum frequency which will be trapped well in a channel is the cutoff frequency. At frequencies near 1000 Hz, absorption mechanisms become important, and scattering losses also come into play. Therefore it should be possible to find some optimum frequency for transmission of sound in a channel of given thickness, lying somewhere above the cutoff frequency and below the frequency range where absorption and scattering losses become large.

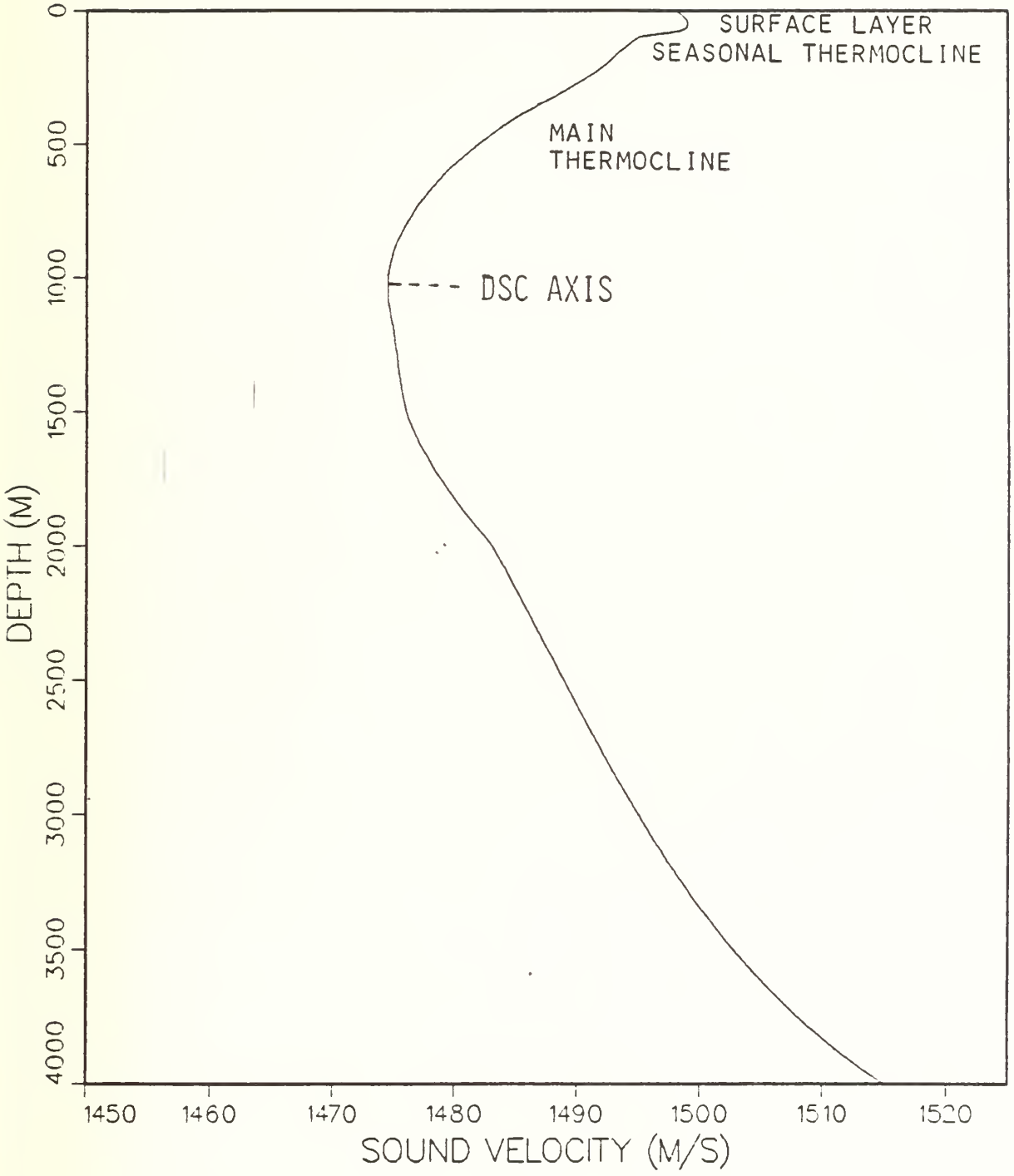

Figure 2.1 Typical mid-latitude sound velocity profile.

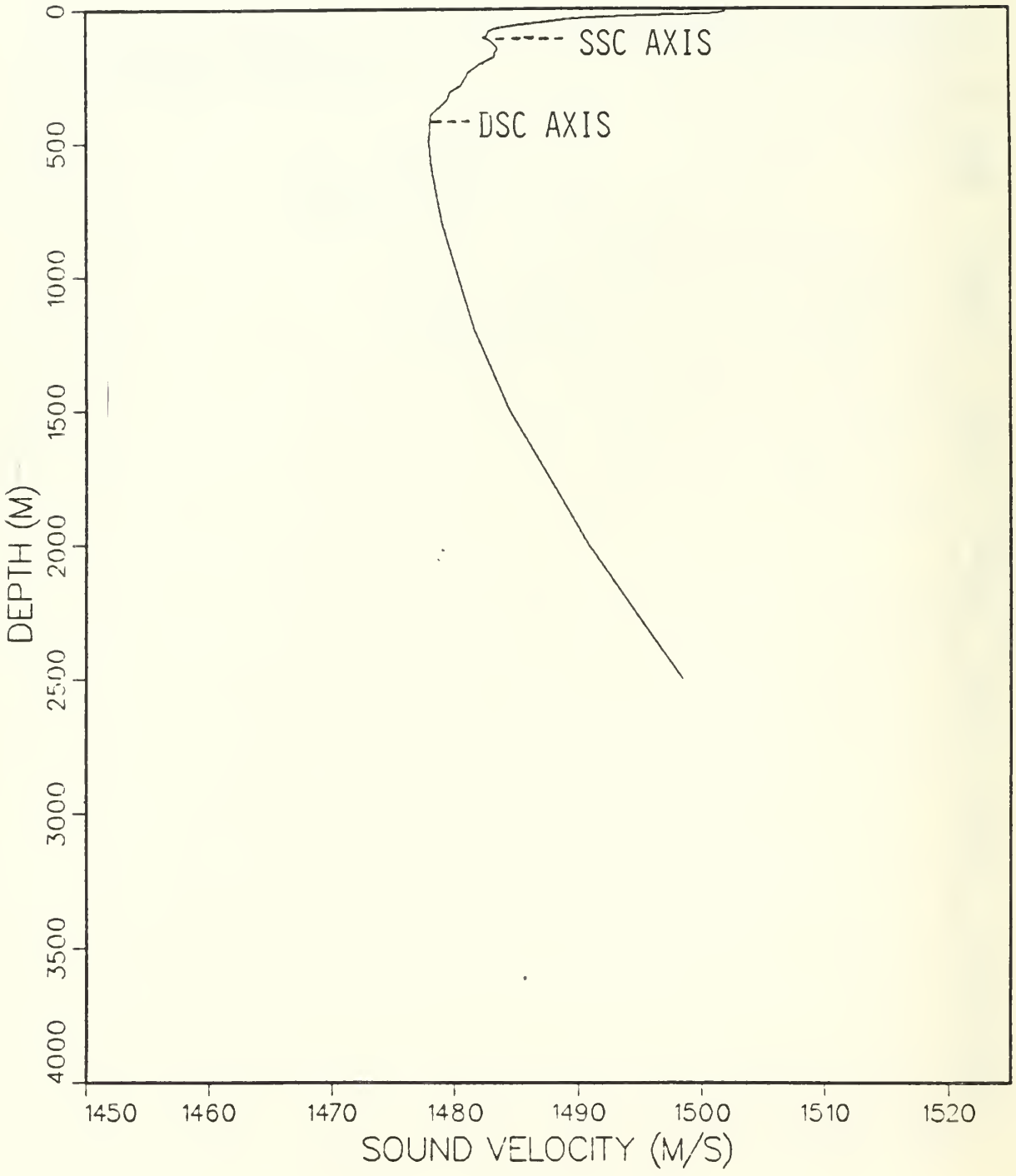

Figure 2.2 Sound velocity profile showing shallow sound channel.

III. THE DOSSO AND CHAPMAN EXPERIMENT

A. DATA COLLECTION

Dosso and Chapman [Ref. 2] conducted an experiment in sound propagation within and below the shallow sound channel. During summer conditions in the northeast Pacific Ocean off the west coast of Canada, CFAV ENDEAVOUR took up a station and monitored data collection equipment. A single calibrated hydrophone was suspended below the vessel at a depth of 101 meters, approximately the shallow sound channel axis. An array of hydrophones was suspended at 417 meters near the deep sound channel axis. A second vessel, CVAF PARIZEAU, opened range from CFAV ENDEAVOUR, dropping explosive charges every 1.8 km (approximately one nautical mile). The charges were set to detonate at 98 meters, near the shallow sound channel axis.

CFAV PARIZEAU also measured sound velocity profiles at 16-kilometer intervals over the track (Figures 3.1 through 3.3). Later analysis revealed that the sound channel deepened over the portion of the track between eight and twenty kilometers, so that the sources were not located within the SSC and sound trapping was greatly reduced for sources detonated between those ranges. Section D below discusses steps that Dosso and Chapman took to account for this deepening of the SSC.

The received acoustic energy was measured as 1/3 octave band averages for each shot for both the shallow and deep hydrophones. Dosso and Chapman were able to distinguish bottom-interacting propagation paths by the different arrival times for shots in the first 35 kilometers of the track, and these arrivals were subtracted from the resulting

energy levels. Bottom interactions could not be isolated from more distant signals. Propagation loss was calculated as known source level minus the received level measured at the hydrophones.

B. RESULTS AND DISCUSSION

For the shallow sound channel [Ref. 2], measured propagation loss was plotted as a function of range for the 1/3 octave bands. The propagation loss demonstrated strong dependence on range, as expected. An optimum frequency for propagation of about 800 Hz was observed.

Figure 3.4 shows the propagation loss measured by Dosso and Chapman for both source and receiver located within the shallow sound channel. The solid curve represents geometrical spreading loss, calculated from

$$H = 10 \log_{10} (R \cdot R_o) \qquad (3.1)$$

where range R and ocean depth R_o are measured in meters. Figure 3.4 (a) represents propagation loss below the optimum frequency of 800 Hz; Figure 3.4 (b) represents propagation loss above 800 Hz. The close agreement between the geometrical loss curve and the 800 Hz data over much of the range is noteworthy.

Figure 3.5 displays the propagation loss within the shallow sound channel for the optimum propagation frequency of 800 Hz, with the effects of chemical absorption removed. Again the solid line represents geometrical spreading for comparison. Note the abrupt increase in losses over the 8-20 km range. Over this range the sound channel axis deepened, so that the sources were no longer within the duct.

Figure 3.6 presents the same data plotted as a function of frequency for three-point range averages centered at 24

and 33 km. The solid circles represent actual measurements; the open circles represent values adjusted upward to remove the effects of chemical absorption. The dotted lines represent the expected loss from geometrical spreading alone at 800 Hz. This display shows more clearly the optimum frequency of 800 Hz and how closely the losses for this frequency approximate the losses due to geometrical spreading alone. It was clear that frequencies above and below 800 Hz experienced greater losses. Diffraction or "leakage" from the shallow sound channel accounted for the losses at lower frequencies. High frequencies experienced losses due to chemical absorption mechanisms and scattering.

C. COMPARISON BETWEEN SSC AND DSC PROPAGATION

The deep sound channel trapped lower frequencies (longer wavelengths) than the shallow sound channel because the DSC is much thicker. Figure 3.7 demonstrates the effects of receiver depth on propagation loss. The sources were located at 98 meters, near the shallow sound channel axis. One receiver was also near the shallow sound channel axis at 101 meters. The other receiver was positioned at 417 meters, near the deep sound channel axis. At 160 Hz sound leaked easily out of the shallow sound channel but was well trapped within the deep sound channel. At 315 Hz, just above the cutoff frequency for the shallow sound channel, propagation in the channel improved. At 630 Hz sound was effectively trapped in the shallow sound channel, and propagation loss at the deep receiver was significantly greater than at the shallow receiver.

Dosso and Chapman plotted relative gain between the two receivers according to the relationship

$$\text{Relative Gain} = TL_{deep} - TL_{shallow} \qquad (3.2)$$

Figure 3.8 displays the results for a four-point range average centered at 24 km. The cutoff frequency of 250 Hz is clearly demonstrated. Below 250 Hz the SSC fails to trap the sound effectively, giving larger transmission losses than the DSC and a negative relative gain. Above 250 Hz the SSC traps the sound better, producing smaller transmission losses than the DSC and a positive relative gain. Larger propagation losses in the SSC below 25 Hz result from surface decoupling effects.

D. MODELING PROPAGATION LOSS IN THE SSC

Geometrical spreading is a simple model, but it is not able to predict the frequency and range dependence that Dosso and Chapman observed. A split-step parabolic equation (PE) model was used to calculate propagation loss based on the sound velocity profiles measured at ranges of zero, 16 and 33 km along the track. [Ref. 2]. Attempts to model propagation using only these three profiles, however, were unsatisfactory. The 16 km profile indicated that the axis of the SSC had deepened, so that the sources were no longer contained in the channel. This is reflected in the increased propagation loss over the 5-20 km range in Figure 3.5. The improved propagation at and beyond 20 km indicated to Dosso and Chapman that the axis of the SSC must have risen to about 100 meters again. For this reason they used the profile recorded at 33 km for the 20 km range also. Dosso and Chapman also truncated their four sound velocity profiles at a depth of 600 meters, introducing an acoustically transparent bottom at that depth [Ref. 8]. This step had the practical effects of limiting the Fourier transform matrix to a manageable size and shortening computational time somewhat. It may also have had some effect on the predicted losses.

With these four sound velocity profiles Dosso and Chapman's model predicted losses with an acceptable degree of accuracy at 25 Hz and 630 Hz (the practical lower and upper limits of their model). But near the cutoff frequency of 250 Hz, the predicted losses were not in such good agreement with observed losses. The model did, however, predict strong dependence on both frequency and range as Dosso and Chapman observed. Figure 3.9 shows the model results compared to actual measurements.

E. SUMMARY OF DOSSO AND CHAPMAN'S EXPERIMENT

Dosso and Chapman point out that the shallow sound channel behaved like an acoustic waveguide with optimum propagation at 800 Hz, with increased losses at lower frequencies due to diffraction and at higher frequencies due to absorption and scattering [Ref. 2]. The propagation was found to be very sensitive to changes in the environment. The PE model that Dosso and Chapman used was able to account for these range-dependent effects with good agreement with experimental results at low and near-optimum frequencies. At intermediate frequencies the model showed range and frequency dependent effects, but the predicted losses were greater than experimental results indicated. Dosso and Chapman emphasize that more accurate modeling of propagation losses requires a much finer sampling of the environment; that is, sound velocity profiles at much closer intervals than 16 kilometers.

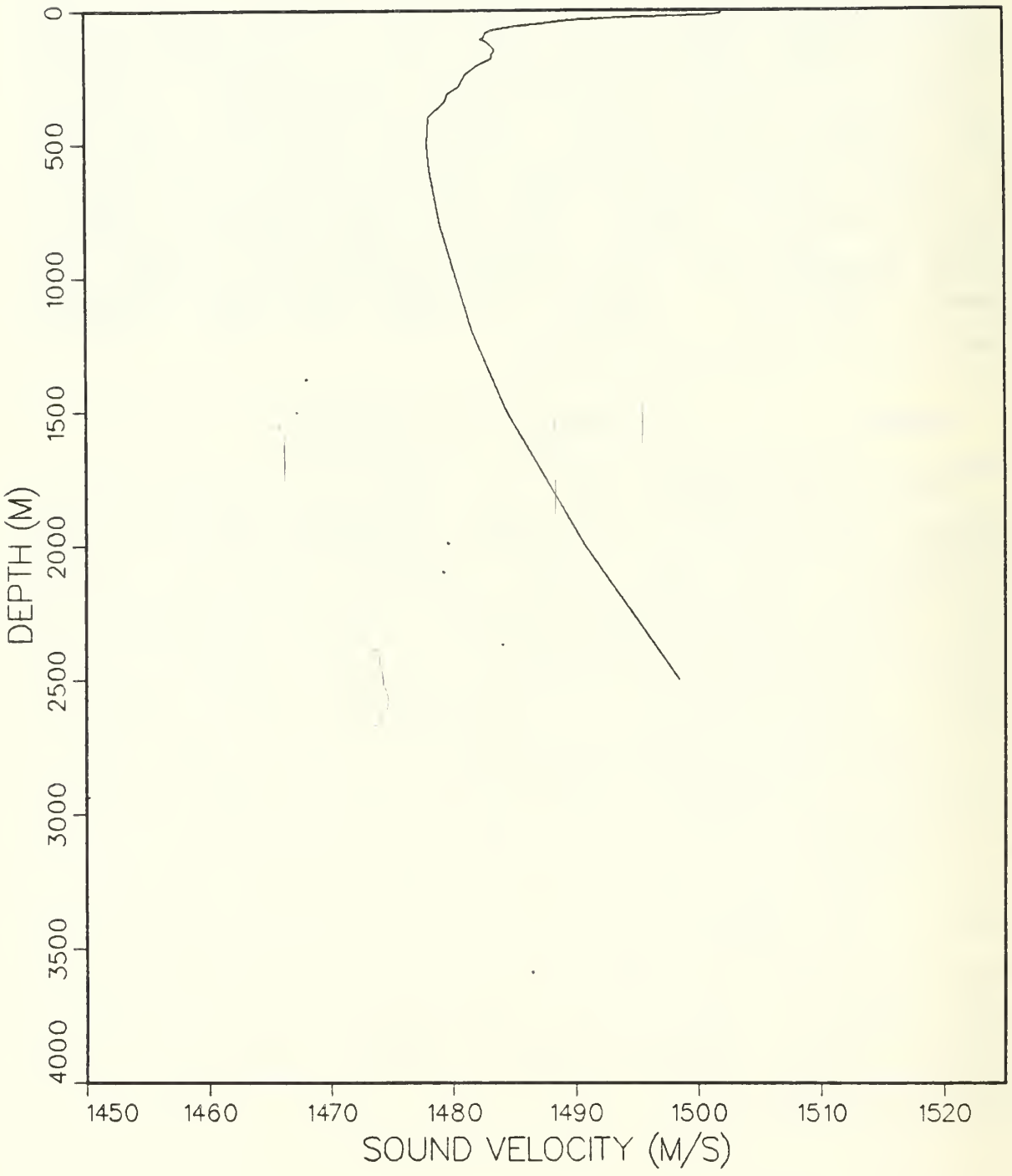

Figure 3.1 Dosso and Chapman's sound velocity profile at 0 km.

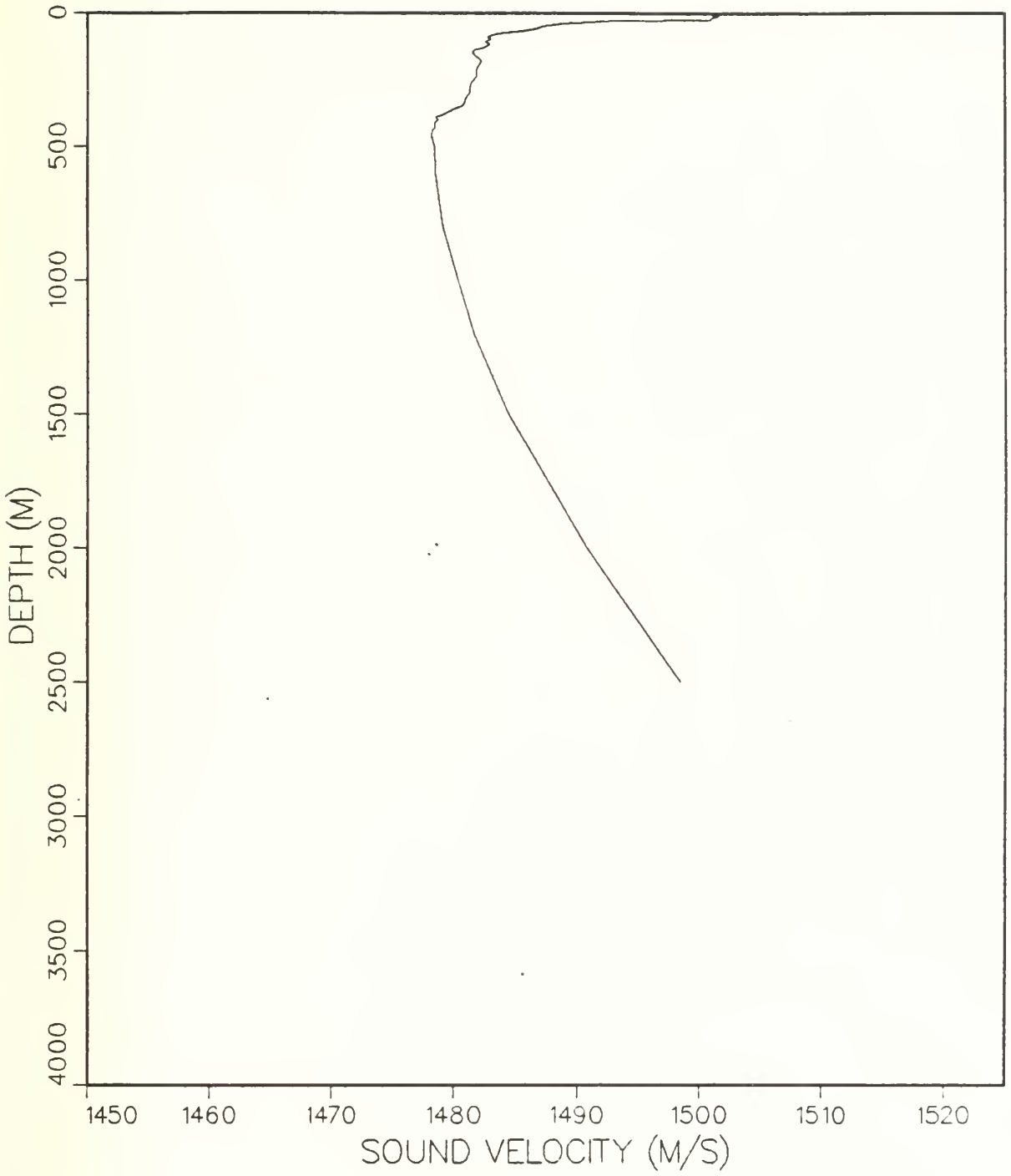

Figure 3.2 Dosso and Chapman's sound velocity profile at 16 km.

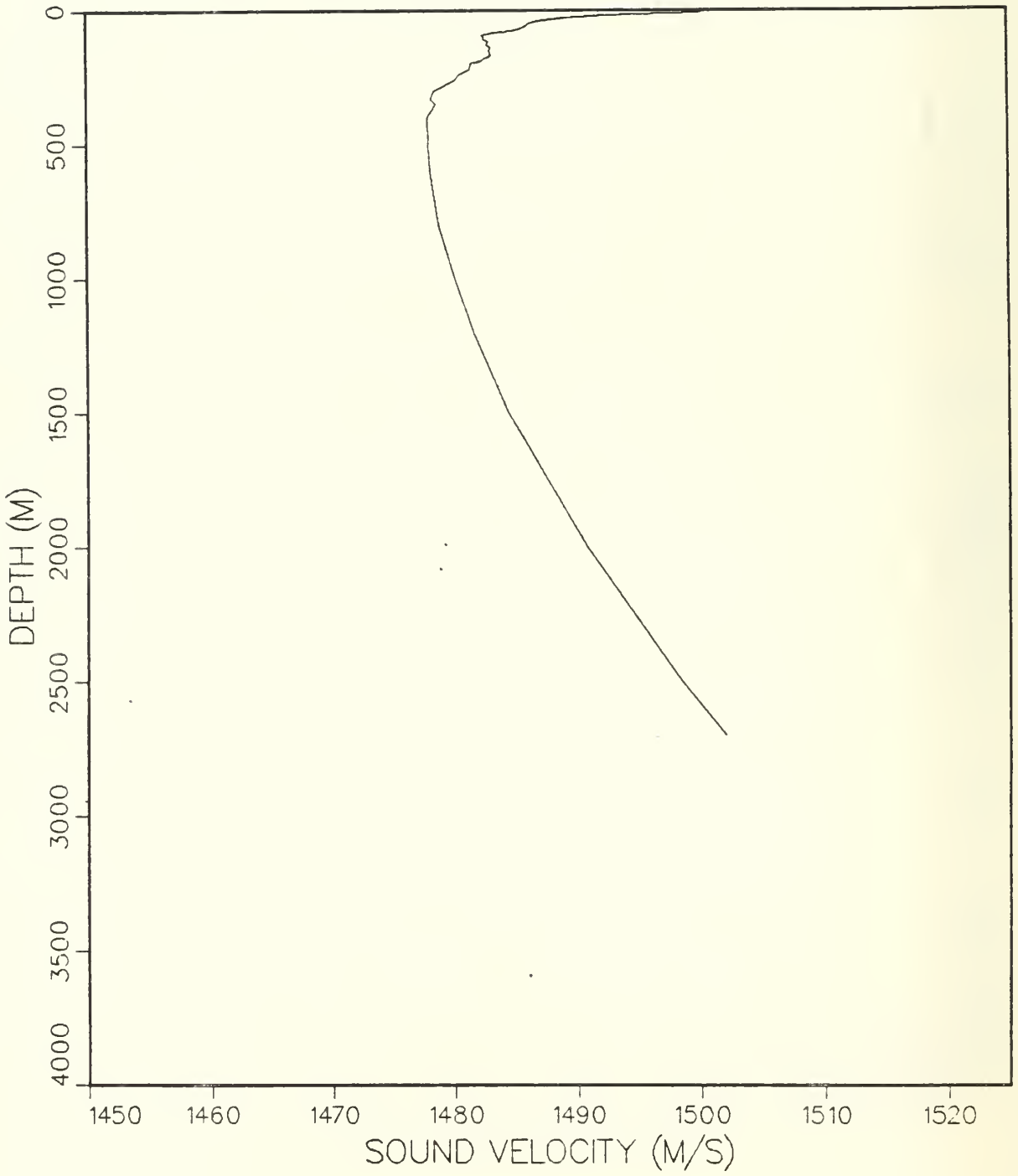

Figure 3.3 Dosso and Chapman's sound velocity profile at 20 and 33 km.

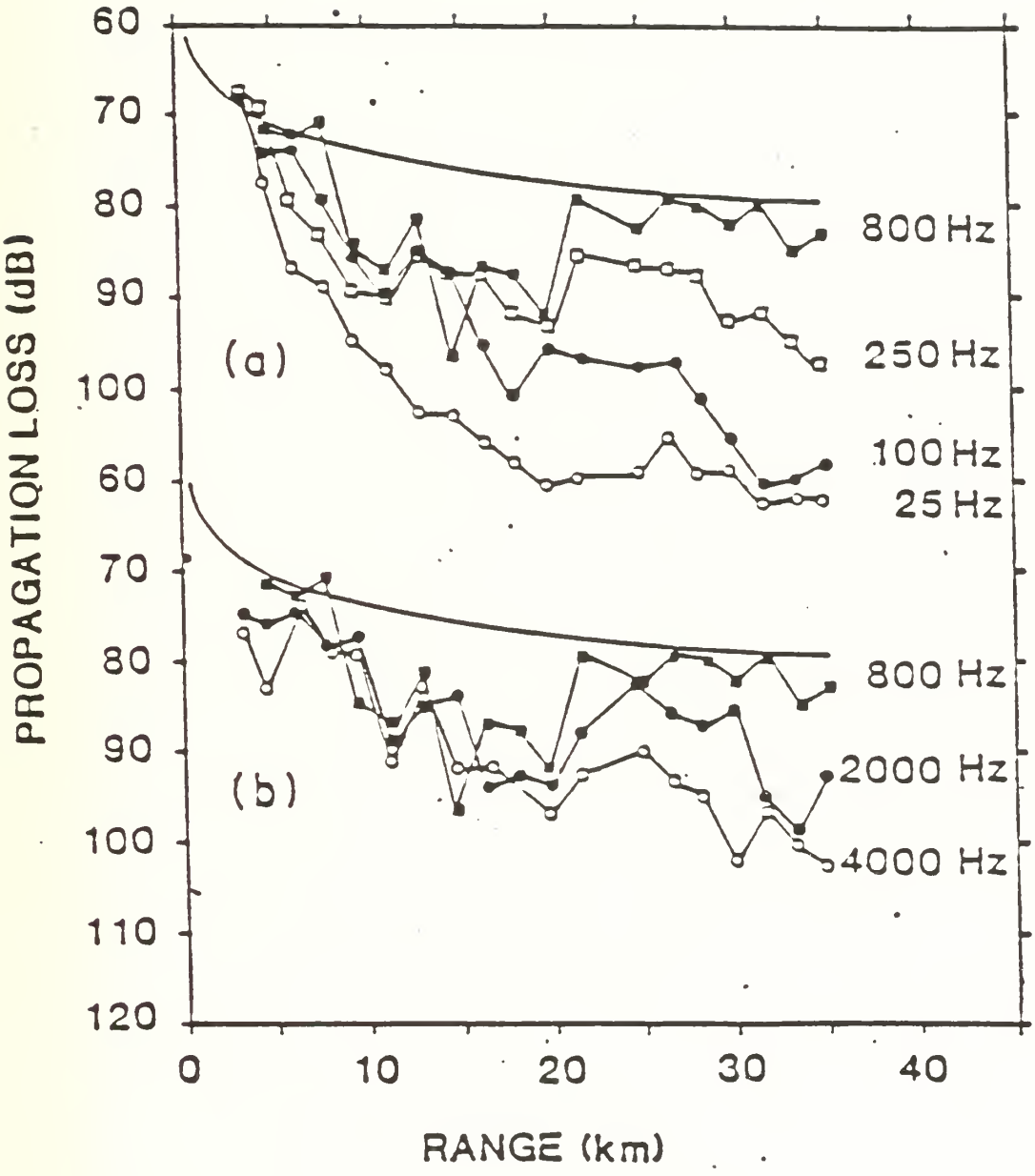

Figure 3.4 Propagation loss vs range (Dosso and Chapman).

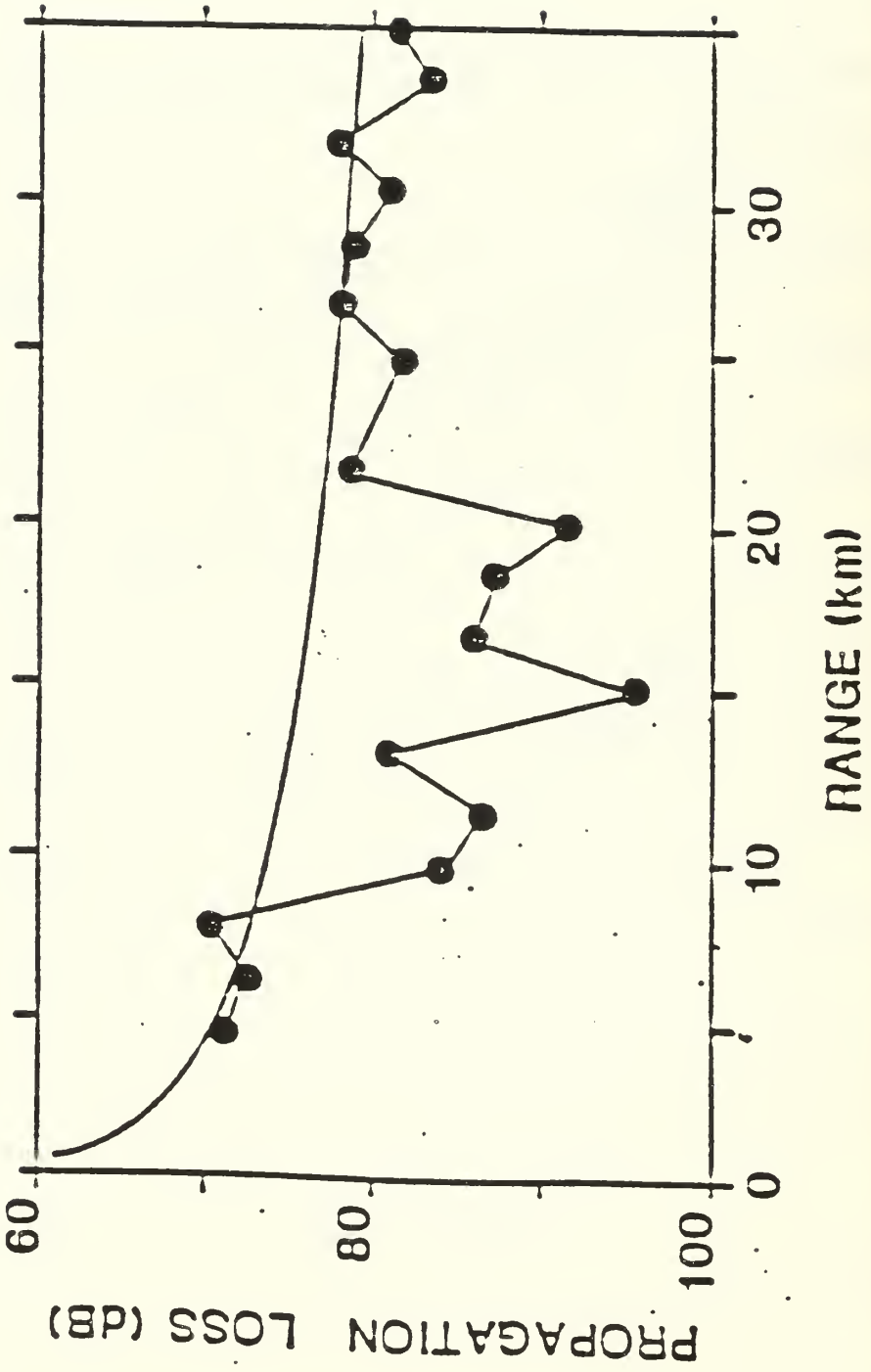

Figure 3.5 Propagation loss for 800 Hz, absorption removed (Dosso and Chapman).

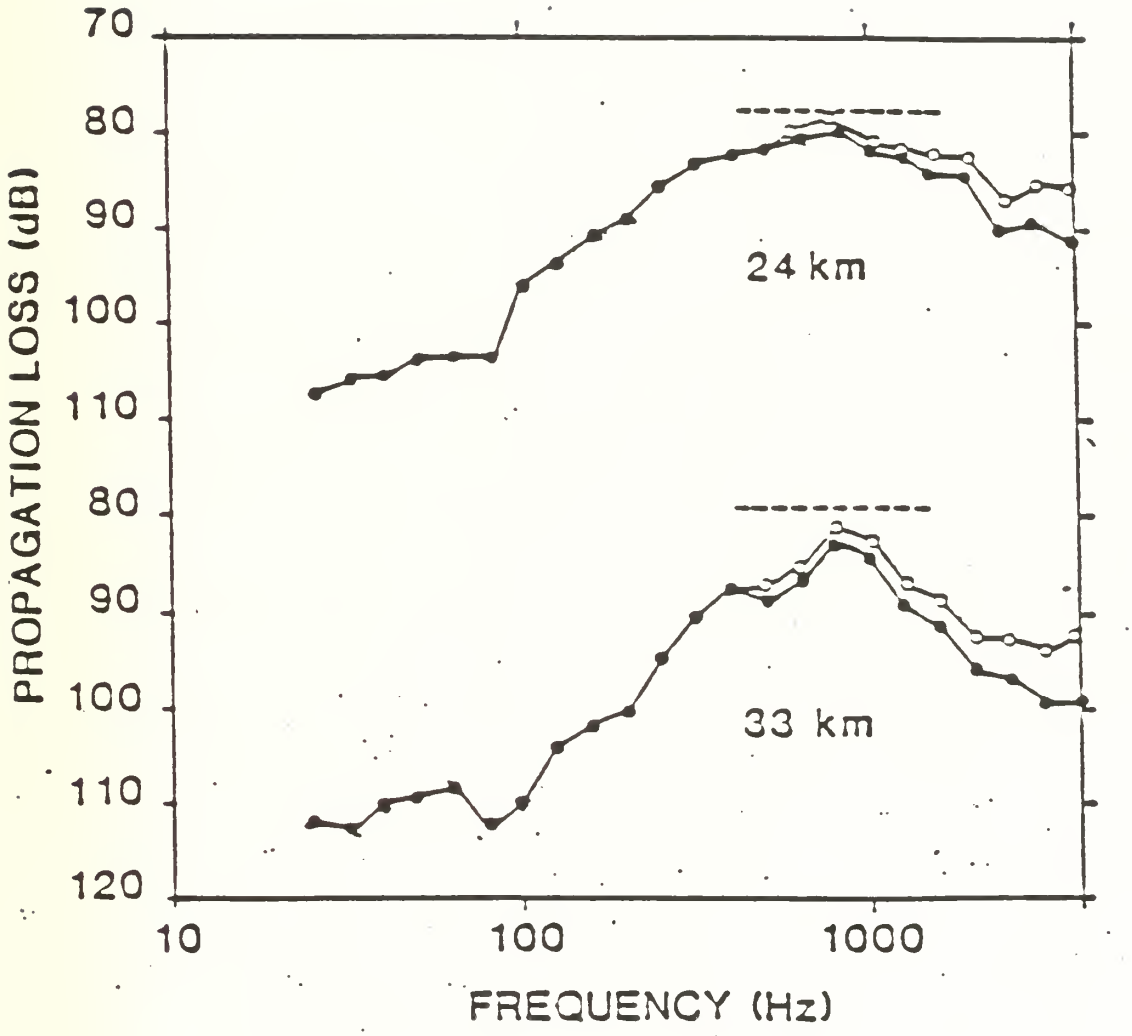

Figure 3.6 Measured loss vs frequency for three-point range averages (Dosso and Chapman).

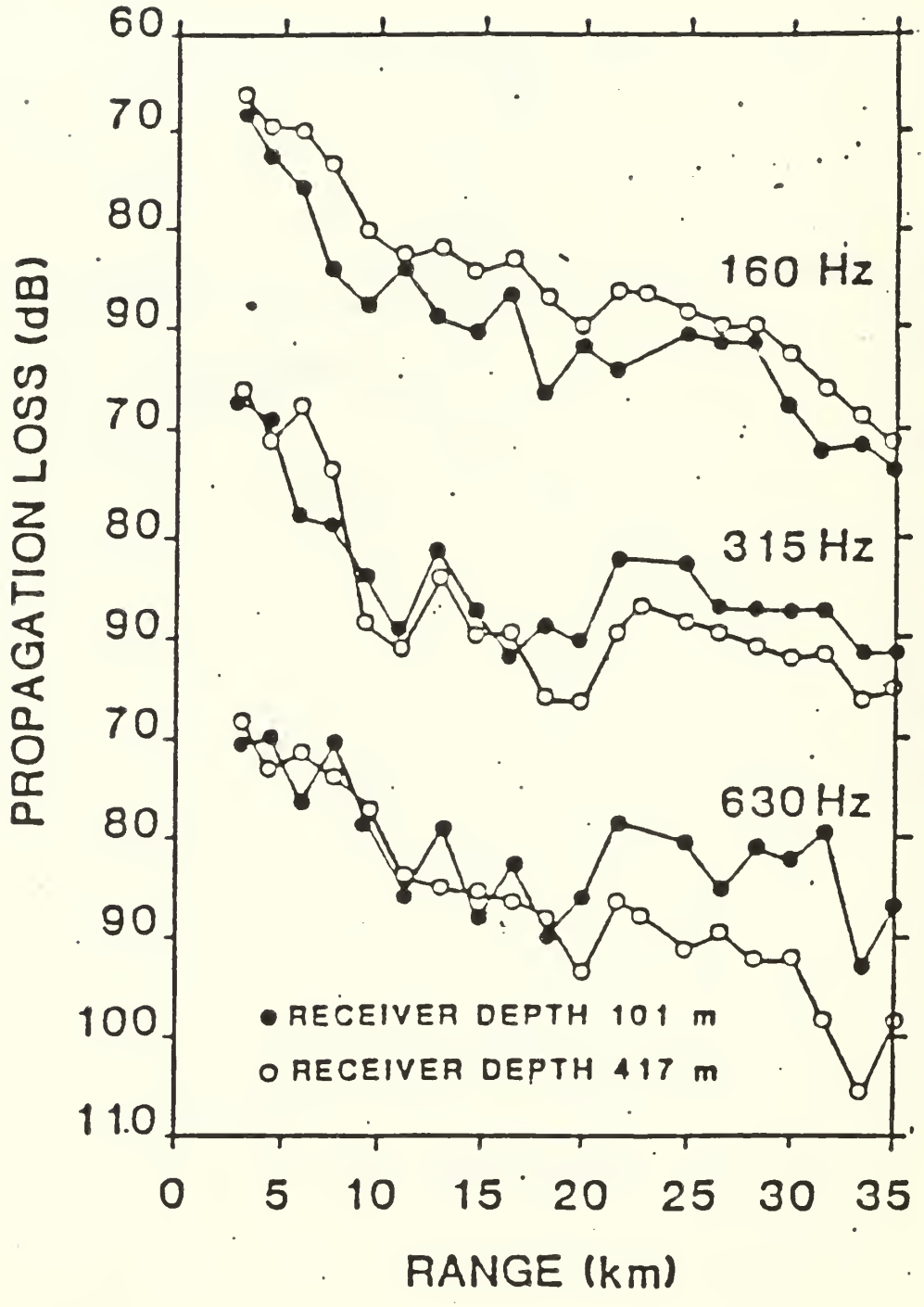

Figure 3.7 Propagation loss vs range for deep and shallow receivers (Dosso and Chapman).

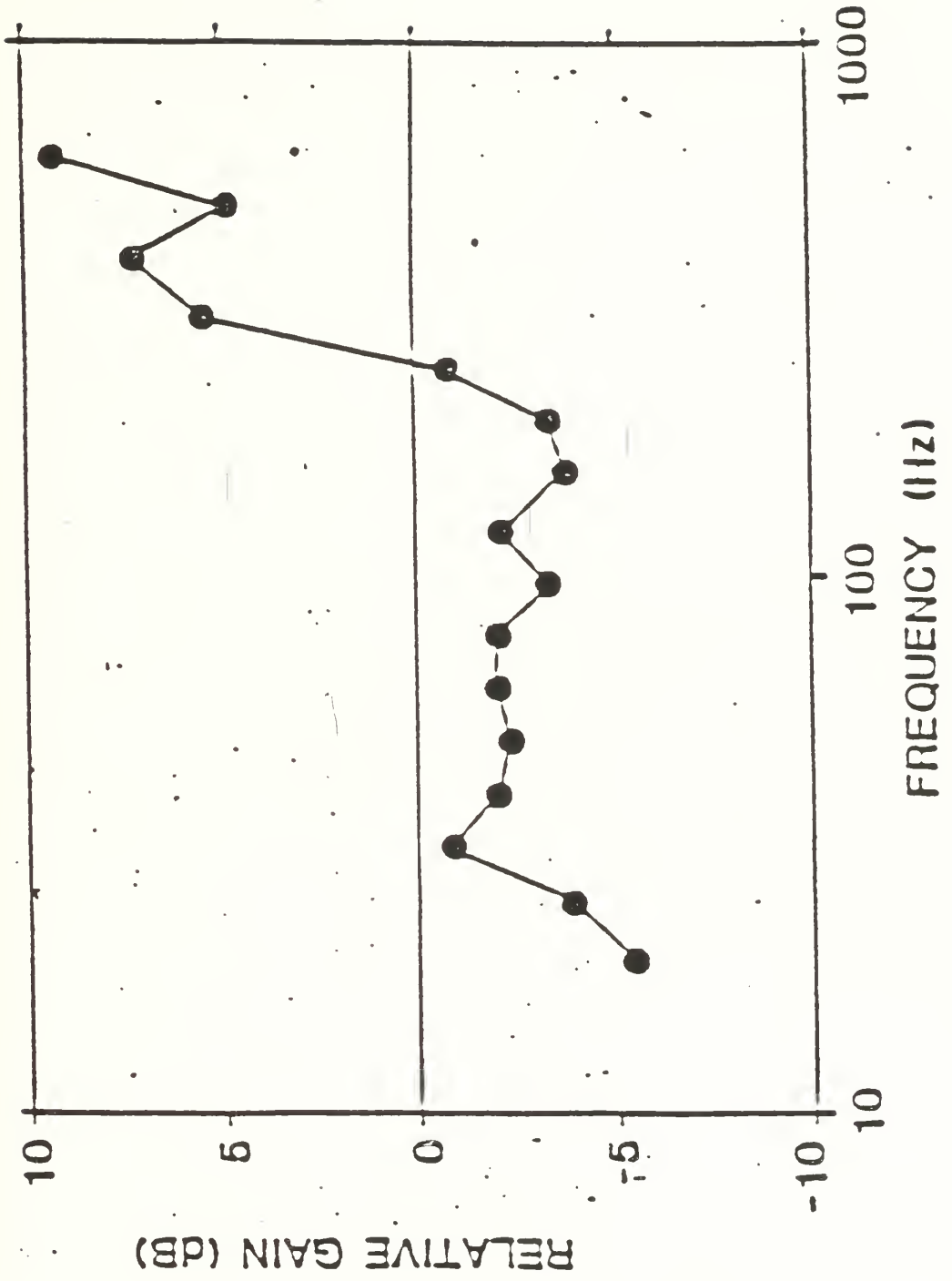

Figure 3.8 Relative gain between deep and shallow receivers (Dosso and Chapman).

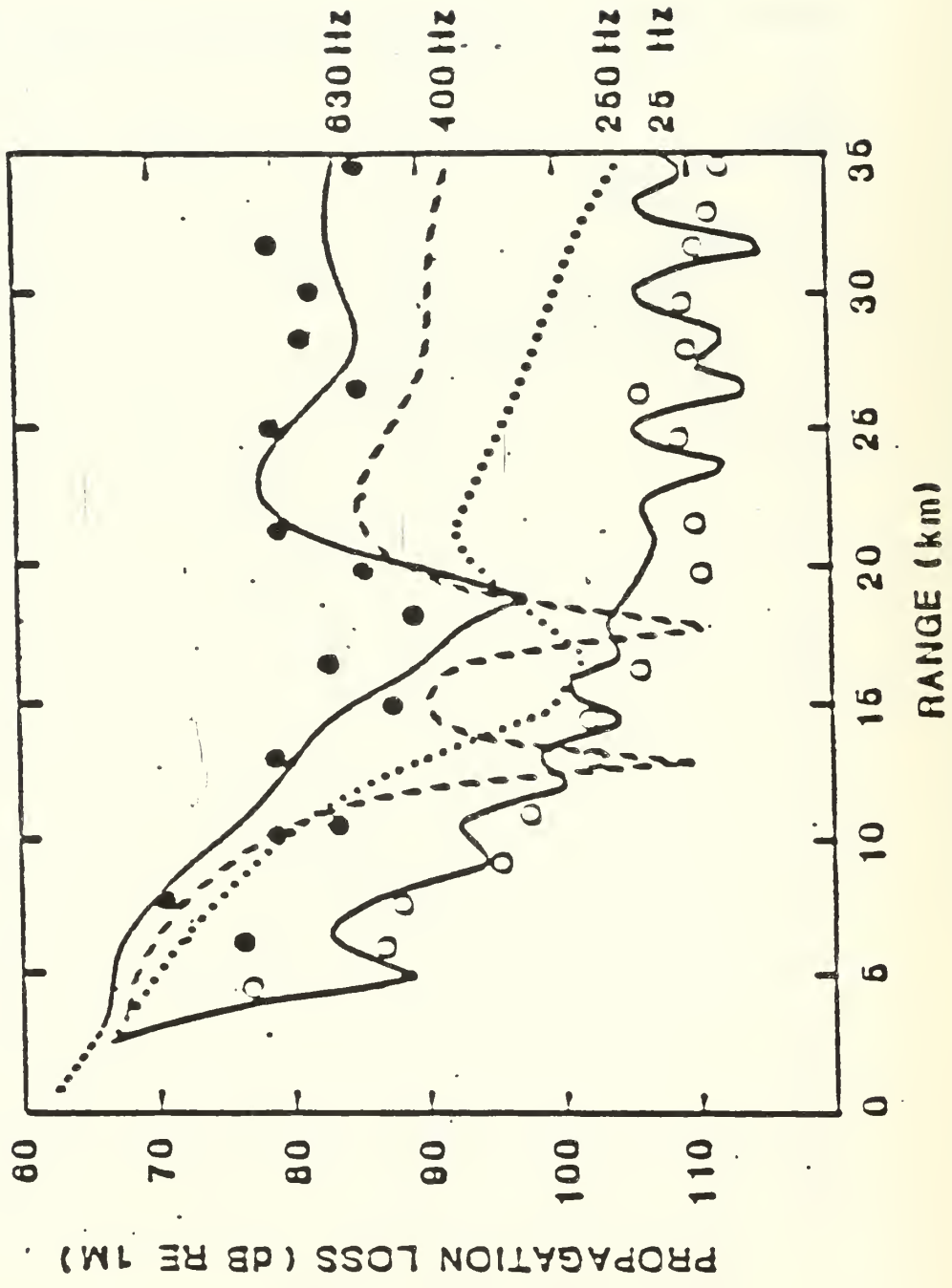

Figure 3.9 PE model results with observations for 630 and 25 Hz (Dosso and Chapman).

IV. THE NPS PARABOLIC EQUATION MODEL

Dosso and Chapman reported good results [Ref. 2] using their split-step Parabolic Equation (PE) model to predict propagation loss in a range-dependent environment where both a shallow sound channel and a deep sound channel existed. The first step in this study was to attempt to reproduce those results using the PE model available at Naval Postgraduate School Monterey.

A. MODEL DESCRIPTION

The split-step Parabolic Equation (PE) acoustic transmission loss model was chosen for study because it produces a numerical solution for an approximation to the wave equation and is generally considered to provide one of the most accurate tools for predicting transmission loss. It can deal with range-dependent environments (multiple sound velocity profiles) and with some interaction of sound with the sea floor. Its drawbacks are its relatively low-frequency capability, inability to handle all bottom loss conditions, and lack of flexibility in dealing with boundary conditions at the sea surface (the model uses a flat pressure-release boundary which does not account for the effects of wind and waves). This PE model is implemented on the IBM 3033 computer at the Naval Postgraduate School (NPS) and is accessed through an interactive program developed and managed by the School's Oceanography Department.

The FORTRAN source code for this PE model was written by the Acoustic Environmental Support Detachment (AESD) of the Naval Ocean Research and Development Activity (NORDA) during the 1970's. A complete description of the physics and algo-

rithms for this model are given in [Ref. 7]. The wave equation

$$[\nabla^2 + K_o^2 n^2(r,z)]\, p(r,z) = 0 \qquad (4.1)$$

is an elliptic equation which describes acoustic pressure as a function of range r and depth z. It can be approximated by a parabolic partial differential equation of the form

$$\frac{\partial \Psi}{\partial r} = i\,(A + B)\,\Psi \qquad (4.2)$$

where

$$A = -\frac{1}{2K_o}\,\frac{\partial^2}{\partial z^2} \qquad (4.3)$$

and

$$B = \frac{k_o}{2}\,(n^2-1) \qquad (4.4)$$

This solution makes the assumptions that the sound is propagating radially outward from a source in a cylindrically symmetric medium and that the range r is very large compared to the size of the source and the wavelength of the sound: these are the cylindrical symmetry and the far-field assumptions. The source is further considered to be oscillating harmonically at a discrete frequency. The ocean surface is considered to be a flat pressure-release boundary, and the acoustic field vanishes in the bottom at the maximum depth of the Fourier transform [Ref. 7].

The parabolic equation accounts for diffraction and other full-wave effects; it also allows solution for range-dependent environments. The parabolic equation can be solved numerically using the Tappert-Hardin split-step Fourier algorithm to yield a solution for the entire

acoustic pressure field as a function of range and depth [Ref. 7].

The PE solution is best where the source and receiver are arranged so that the path between the two makes a small angle with the horizontal. At larger angles, the group and phase velocities of the computed solution become subject to errors and produce inaccurate representations in the interference pattern. This affects the accuracy of the predicted transmission loss for a given range. Computing time increases quickly with frequency. The numerical solution is limited by the practical Fourier transform size, which means that the input environment governs the extent to which the model can handle higher frequencies. For practical purposes the PE model should be used to predict propagation loss for frequencies below 200 Hz along waterborne or shallow bottom-bounce paths [Ref. 7].

The PE model becomes inappropriate for situations where the bottom slopes steeply and where large sound speed gradients occur [Ref. 7].

B. VALIDATION AGAINST DOSSO AND CHAPMAN'S DATA

This study is concerned with waterborne paths and shallow angles. We are not specifically interested in bottom interactions. Even though the frequencies in which we are interested may be as high as 800 Hz [Ref. 2], we are willing to use computational time to examine a full-wave solution. Especially important for comparison with Dosso and Chapman's experimental data is the fact that the PE model can utilize a range-dependent environment. The input parameters described in Appendix A are derived from [Ref. 2] and [Ref. 8]. The resulting information and displays show reasonable agreement with Dosso and Chapman's work.

Compare Figures 4.1 through 4.5 with Figure 3.4. The smooth, downward trending curve represents transmission loss due to geometric spreading alone, calculated from equation 3.1. The measured 1/3 octave band levels of Figure 3.4 show signs of smoothing because many frequencies have been added together, lessening the multipath interference effects that become apparent for discrete frequencies [Ref. 2].

It is apparent, however, that frequencies below the cutoff frequency of 250 Hz propagate poorly within the shallow sound channel and that higher frequencies propagate better. An interesting outcome here is that the 2000 Hz experiences less transmission loss than the experimentally determined optimum frequency of 800 Hz at ranges greater than 17.5 km. Note also that the three highest frequencies all show sudden steep increases in transmission loss in the 17-20 km range and that the levels never really recover. This is the range at which Dosso and Chapman noted a change in their sound speed profiles so that their sources were no longer within the shallow sound channel.

Dosso and Chapman observed an increase in transmission loss over roughly the same ranges (Figure 3.4), followed by better propagation at ranges beyond 20 km. They were able to model these results successfully by adding another sound velocity profile at 20 km, using the same profile they had measured at 33 km. With the same input parameters the NPS PE model yielded a much steeper drop and did not indicate a return to levels expected from the experimental data.

Dosso and Chapman's Figure 3.5 compares to Figure 4.6. For Figure 3.5 Dosso and Chapman plotted measured data, with losses due to chemical absorption removed. This figure clearly shows the close correspondence between the measurements for the optimum frequency of 800 Hz and the losses predicted for geometrical spreading alone. The only anomalies arise over the 8-20 km range, as discussed above.

The NPS model allows the user to select whether attenuation will be considered. Figure 4.6 represents the NPS PE model prediction for 800 Hz without attenuation. Again the steep drop in transmission occurs between 15 and 20 km. A comparison with Figure 4.2 shows that the two curves are essentially similar, but attenuation accounts for a 1-2 dB greater loss in Figure 4.2.

Dosso and Chapman's experimental data yielded good results when propagation loss was plotted as a function of frequency for 24 and 33 km (Figure 3.6). Recall that Dosso and Chapman measured 1/3 octave band levels and then calculated three-point range averages to obtain each curve. The NPS PE model produces transmission loss predictions for discrete frequencies. To obtain transmission loss for the desired ranges, values were read from the computer-generated PE model graphic output at the appropriate ranges and at one kilometer on either side. The three values for each range were averaged to produce the values used in plotting Figure 4.7. Again multipath interference effects can account for the fluctuations with range and frequency. While an optimum frequency of 800 Hz is easy to read from Figure 3.6, it is more difficult to state an optimum frequency from Figure 4.7. Frequencies in the 500-700 Hz range seem to have propagated best.

Dosso and Chapman compared results from shallow sound channel and deep sound channel receivers in Figure 3.7. Figures 4.8 through 4.10 present the corresponding results from the NPS PE model. As expected for a frequency well above cutoff, the 630 Hz curves (Figure 4.8) show better propagation where both source and receiver were within the shallow sound channel, but much greater loss (up to 10-20 dB) where the receiver was in the deep sound channel. The two curves are in closer agreement for 315 Hz (Figure 4.9) as would be expected for a frequency near cutoff, where

trapping and leaking are better balanced. There is still a 10 dB better propagation for the 15-17.5 km range when both source and receiver are in the channel. Figure 4.10 demonstrates significant transmission loss for 160 Hz, which is well below cutoff. In this case the deep receiver experiences better propagation by 5-10 dB over almost the entire range, indicating that the shallow sound channel failed to trap this frequency effectively.

It should especially be noted in Figures 4.8 and 4.9 that anomalous propagation is occurring in the 17-25 km range. This may be due to the change in depth of the shallow sound channel that Dosso and Chapman noted and tried to correct by adding the sound velocity profile at 20 km. This compensation was apparently much less successful with the NPS PE model than with Dosso and Chapman's model.

Figure 4.11 corresponds to Figure 3.8. Relative gain is calculated according to equation 3.2, following Dosso and Chapman's procedure. Their results were good for 24 km, showing a sudden improvement above the 250 Hz cutoff frequency when both source and receiver were in the SSC. The curve for the NPS PE model at the 24 km range does not produce good results, probably due to the failure of the added profile at 20 km to compensate for the changing depth of the SSC. The 15 km curve, however, is taken before the SSC deepened and indicates better results. The 250 Hz cutoff frequency is clearly indicated. The NPS results, however, show unexpected peaks at 40-50 Hz and at 100 Hz, where the shallow sound channel receiver should not be doing as well as the deep receiver. Other frequencies below cutoff behave as expected.

Together Figures 4.12 through 4.15 correspond to Figure 3.9, where Dosso and Chapman plotted their PE model predictions along with experimentally measured data. Note that Dosso and Chapman's 630 Hz curve shows a minimum at

about 18 km, followed by better propagation at longer ranges. Their predictions correspond rather well to the measurements. On the other hand, Figure 4.12 predicts several dB better propagation for 630 Hz than was observed for ranges less than 15 km and several dB worse than observed at ranges beyond 20 km. Again the compensation using the 20 km profile was less successful for the NPS PE model than for Dosso and Chapman's model. The steep drop and failure to recover in the transmission loss curves are even more apparent in Figure 4.13 for 400 Hz and Figure 4.14 for 250 Hz. In Figure 4.15 for 25 Hz the observed values match quite well with predicted values out to about 15 km. At that point the prediction goes wrong again and predicted values fall 10-15 dB below measured values.

C. DISCUSSION OF NPS PE RESULTS

Discounting the multipath effects on transmission loss which produce extreme fluctuations in transmission loss with both range and frequency, it appears valid to use the NPS Parabolic Equation model to estimate optimum frequency for sound propagation in a shallow sound channel. The plot of transmission loss versus frequency (Figure 4.7) shows an optimum frequency range of 500-700 Hz. This is acceptable in comparison with Dosso and Chapman's measured optimum frequency of 800 Hz for the same set of sound velocity profiles. This is also good enough for active and passive sonar operators to use in selecting the best frequency ranges for their equipment.

The NPS PE model was not, however, a good estimator for absolute levels of transmission loss. The NPS PE curves showed large differences in transmission loss levels when compared to Dosso and Chapman's measurements. For relative gain between deep and shallow receivers the NPS PE model

demonstrated an appropriate cutoff frequency around 250 Hz, but with unexpected peaks at frequencies well below cutoff.

Some of these anomalous results from the NPS PE model may arise from using full-depth sound velocity profiles. Reasoning from ray-tracing theory, a fully absorbing bottom placed at 2500-2900 meters may have allowed sufficient depth for some deep propagation paths to be refracted back toward the receiver. The fully absorbing bottom at 600 meters which Dosso and Chapman used in their modeling may have eliminated propagation by these paths. Interference effects between these paths and the ducted propagation may account for some of the differences between Dosso and Chapman's results and the NPS PE results.

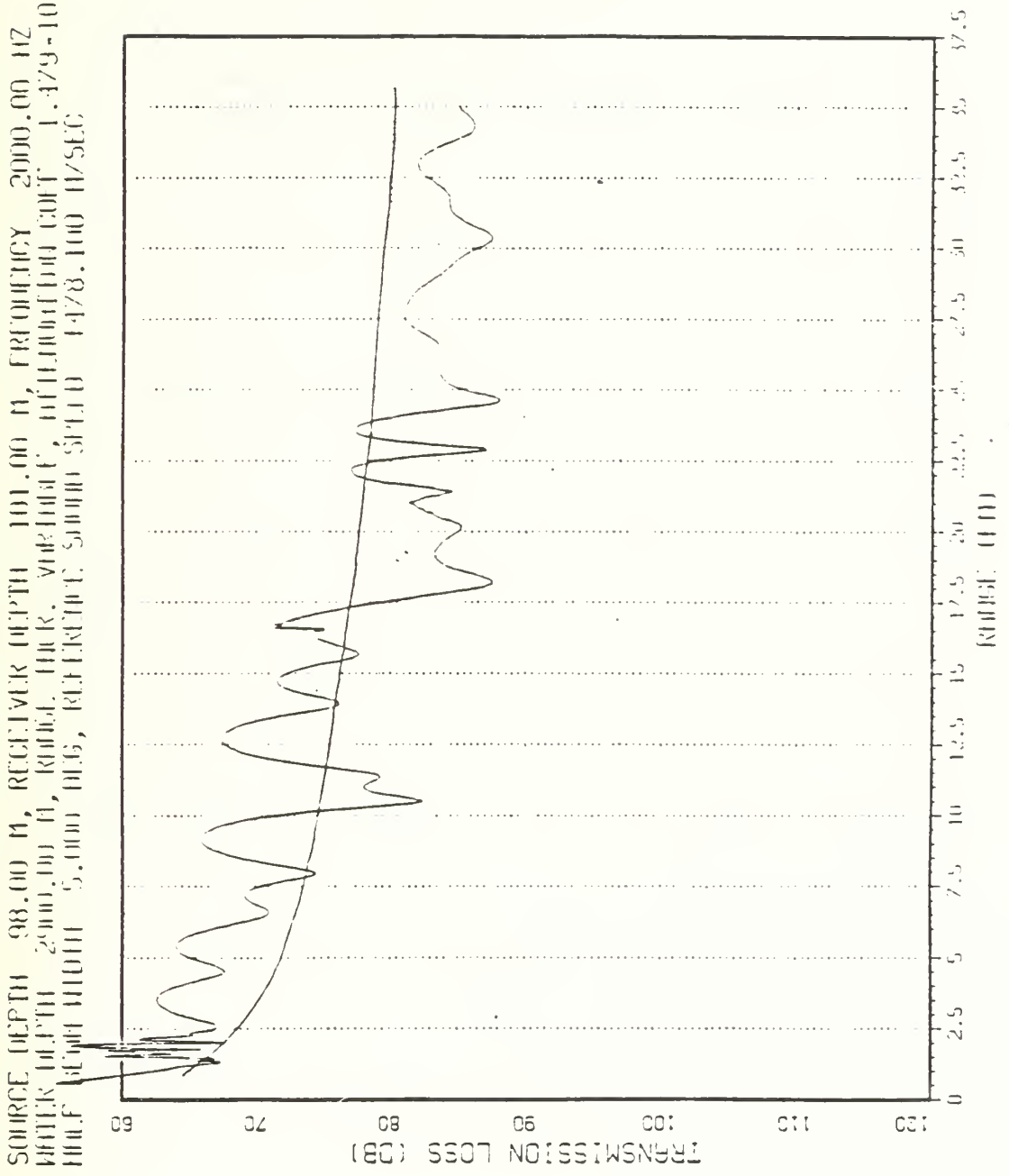

Figure 4.1 Transmission loss vs range, 2000 Hz (NPS PE model).

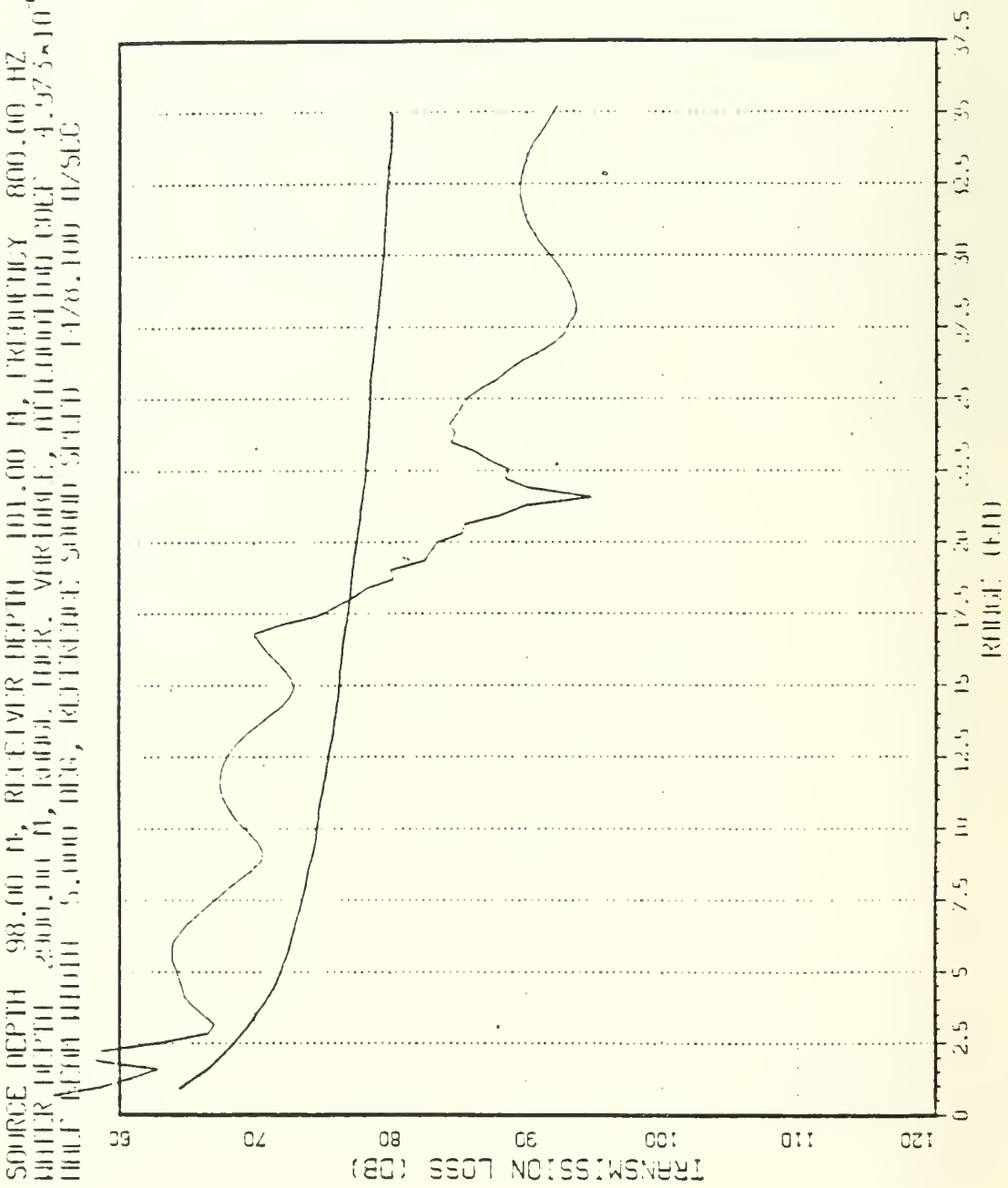

Figure 4.2 Transmission loss vs range, 800 Hz (NPS PE model).

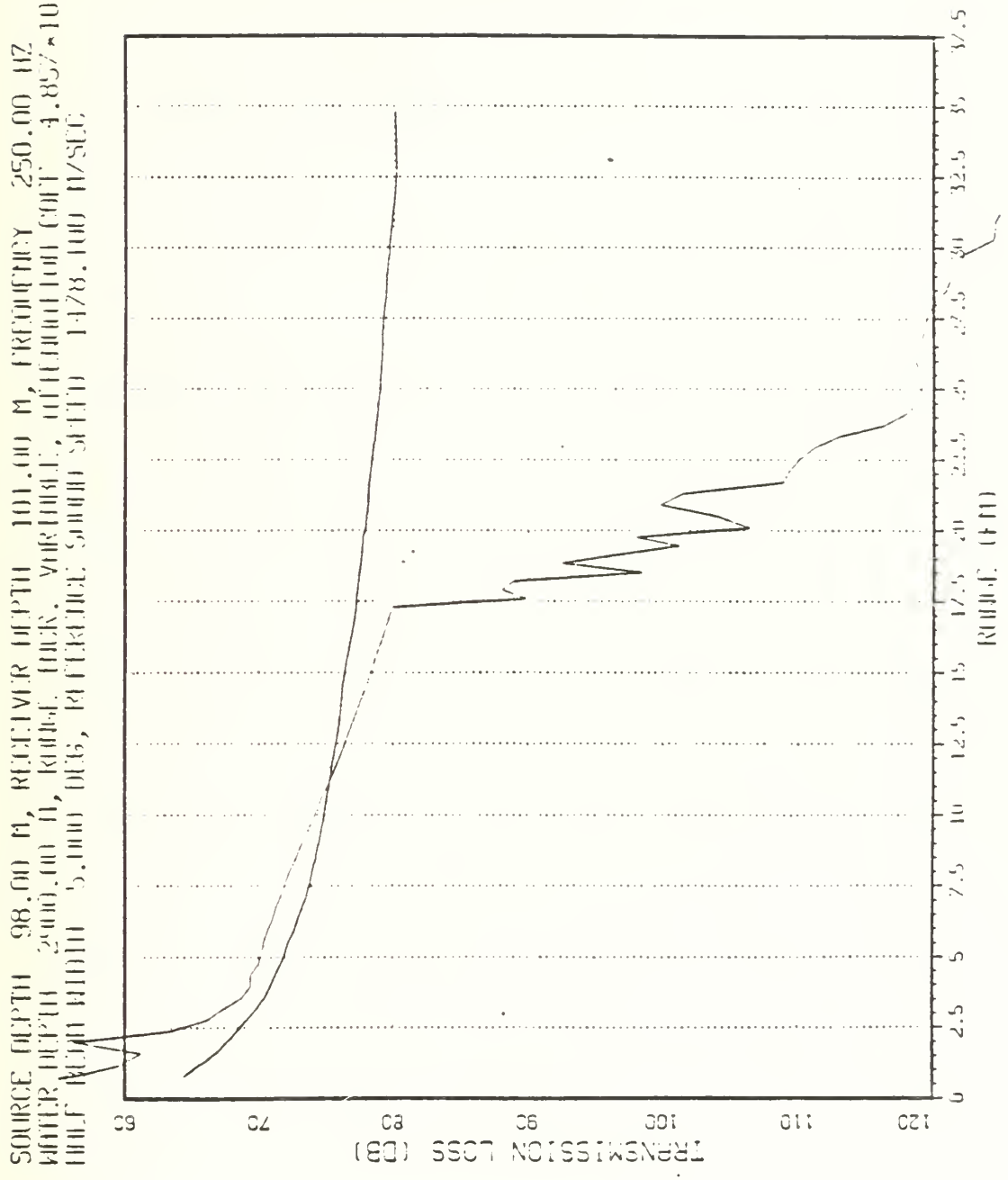

Figure 4.3 Transmission loss vs range, 250 Hz (NPS PE model).

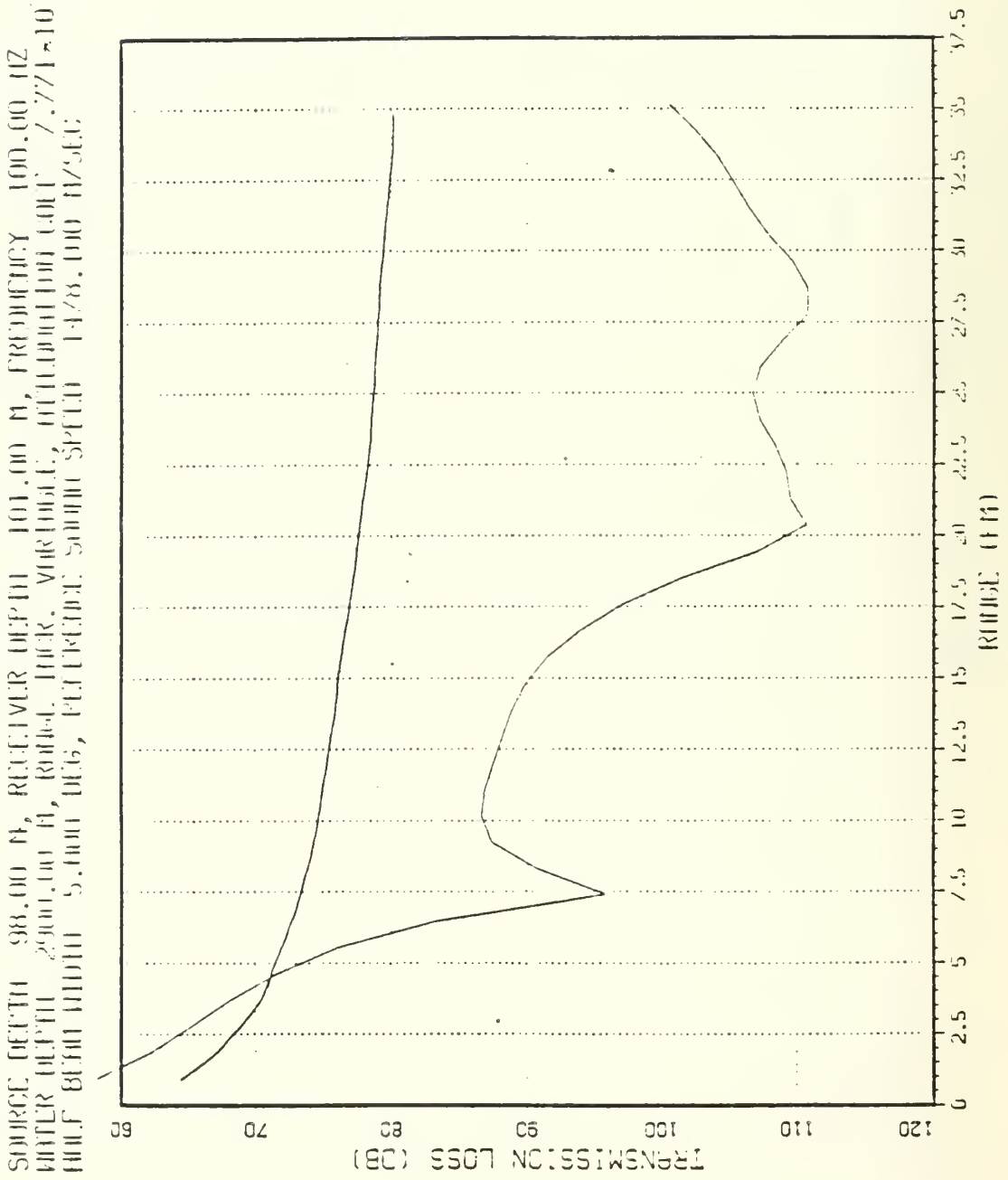

Figure 4.4 Transmission loss vs range, 100 Hz (NPS PE model).

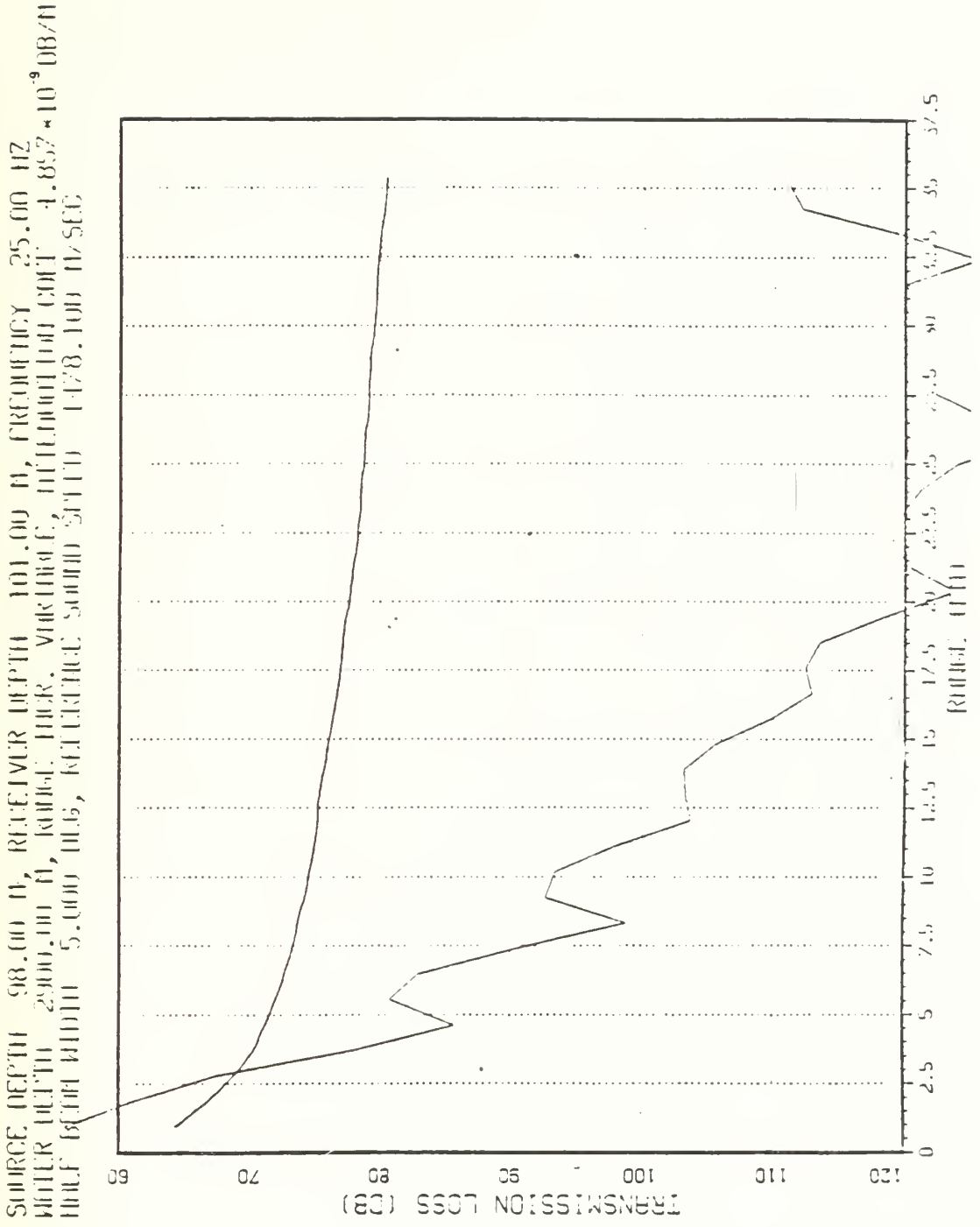

Figure 4.5 Transmission loss vs range, 25 Hz (NPS PE model).

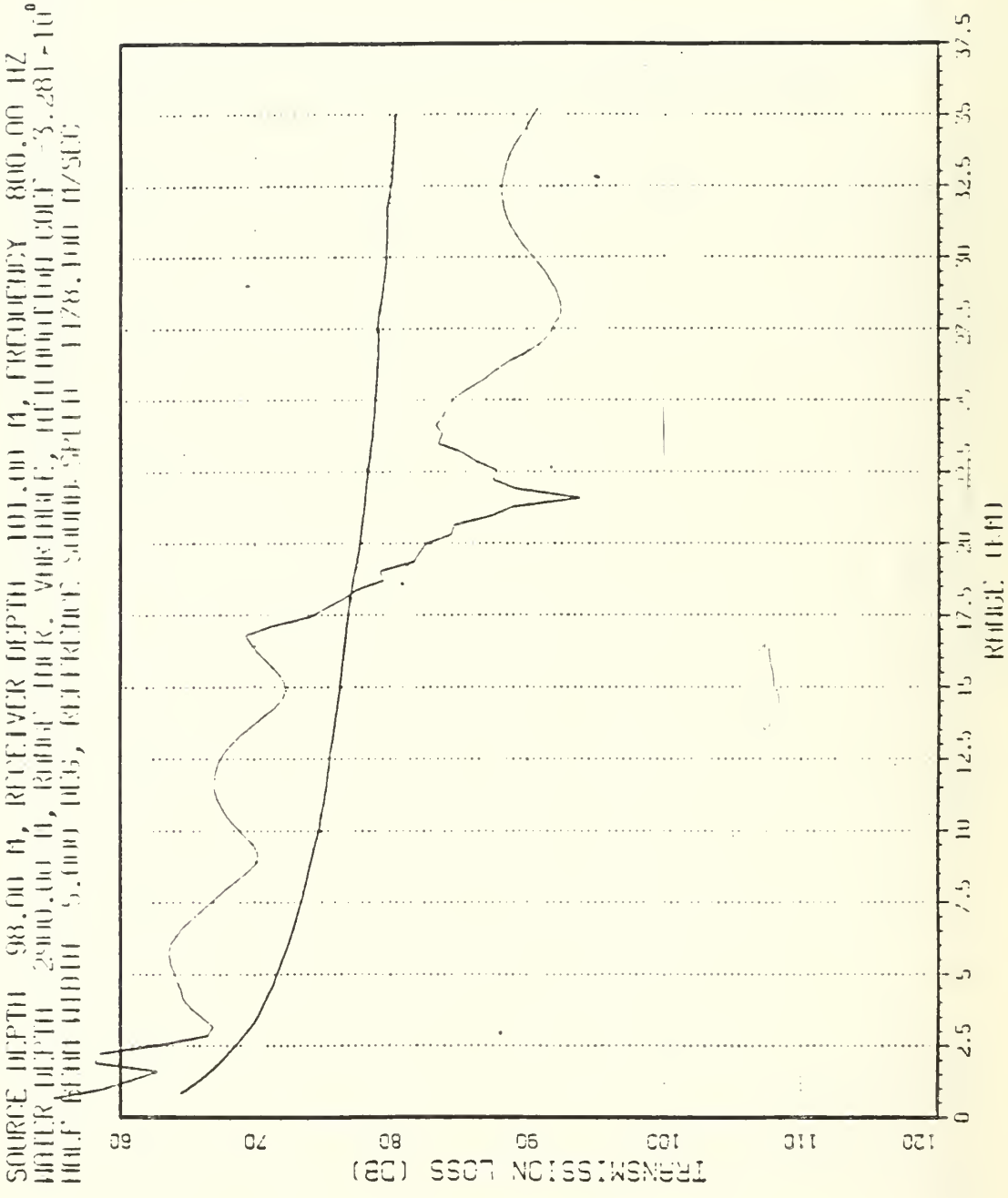

Figure 4.6 Transmission loss for 800 Hz, absorption removed (NPS PE model).

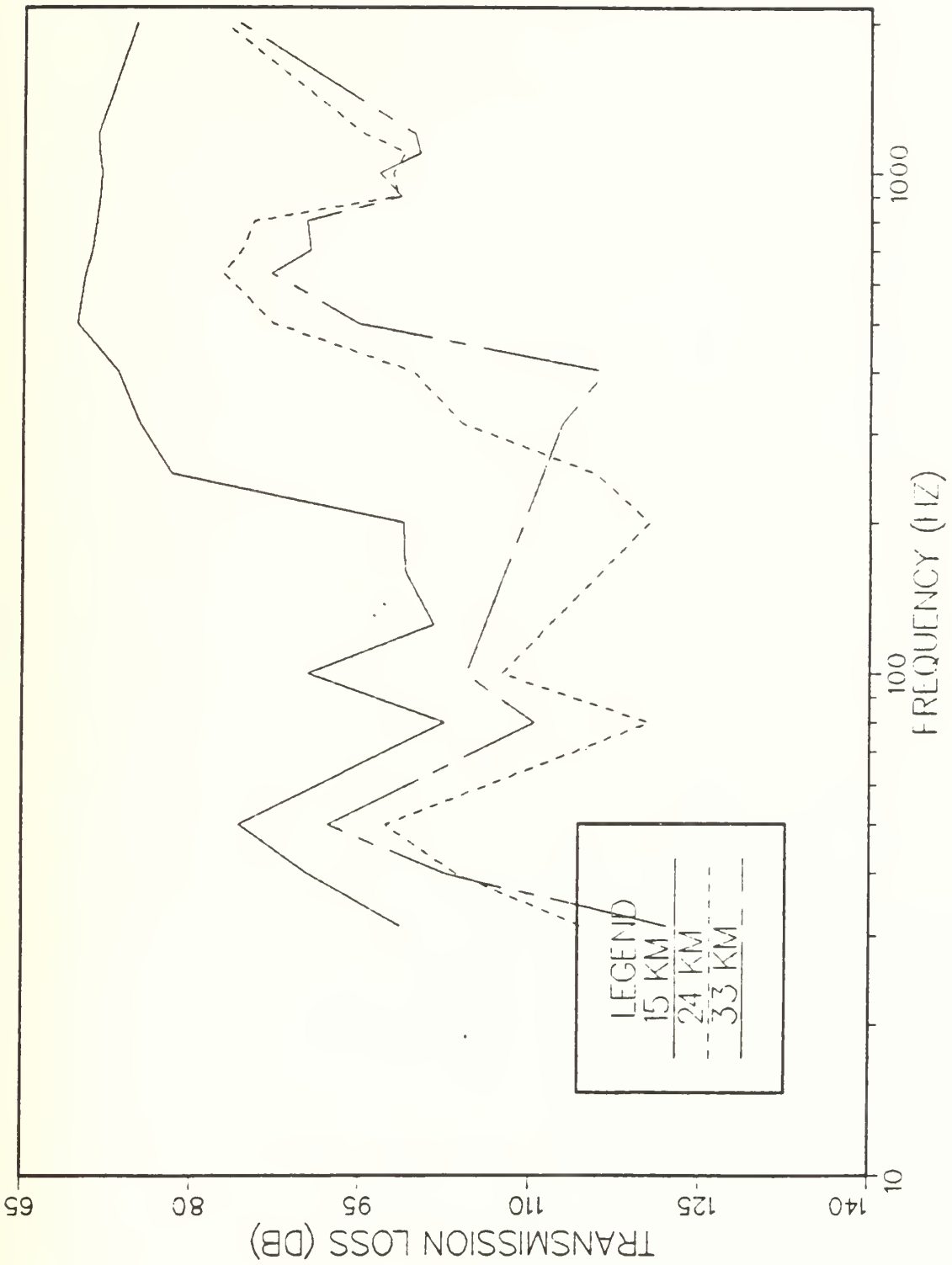

Figure 4.7 Transmission loss vs frequency (NPS PE model).

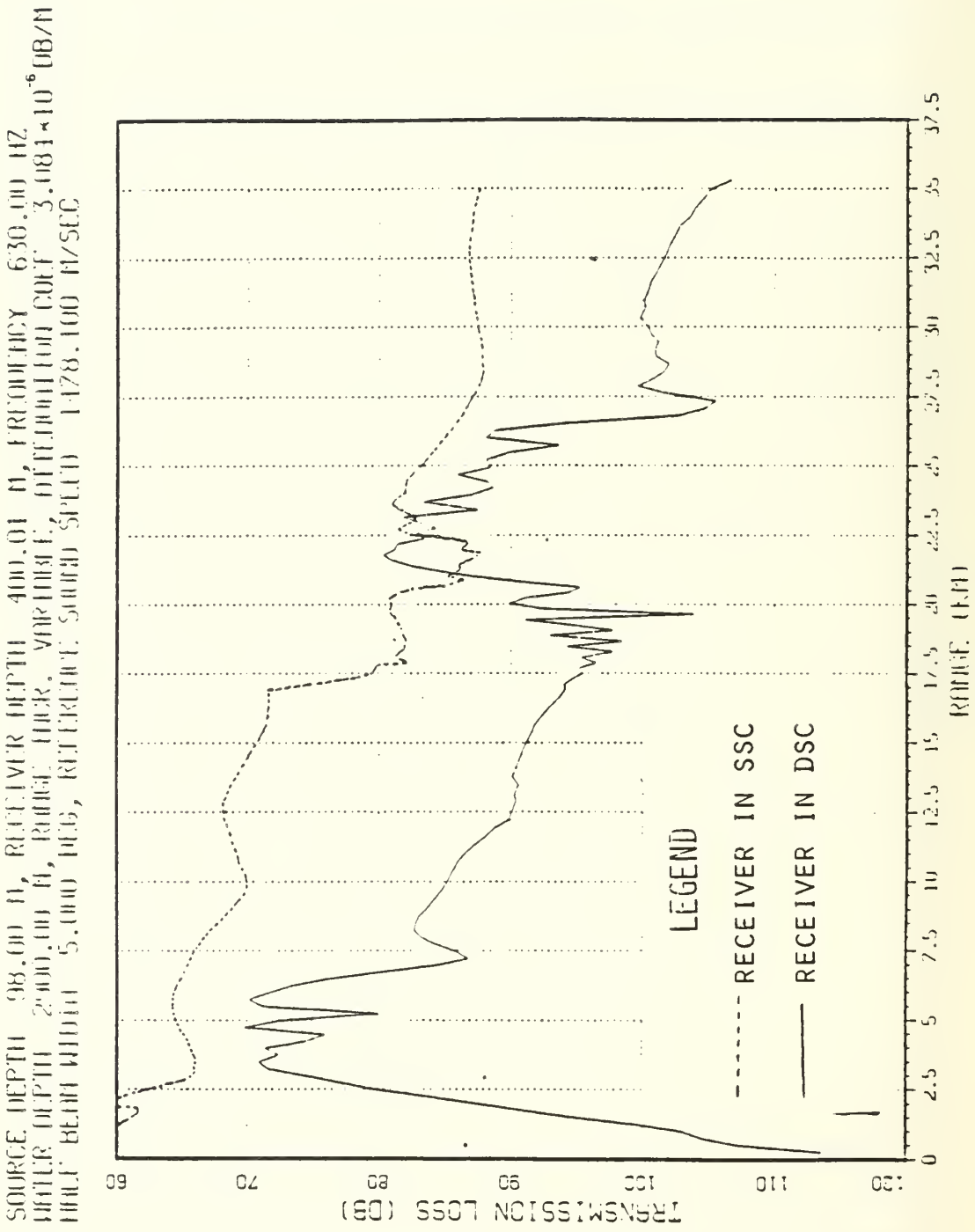

Figure 4.8 Shallow vs deep receiver, 630 Hz (NPS PE model).

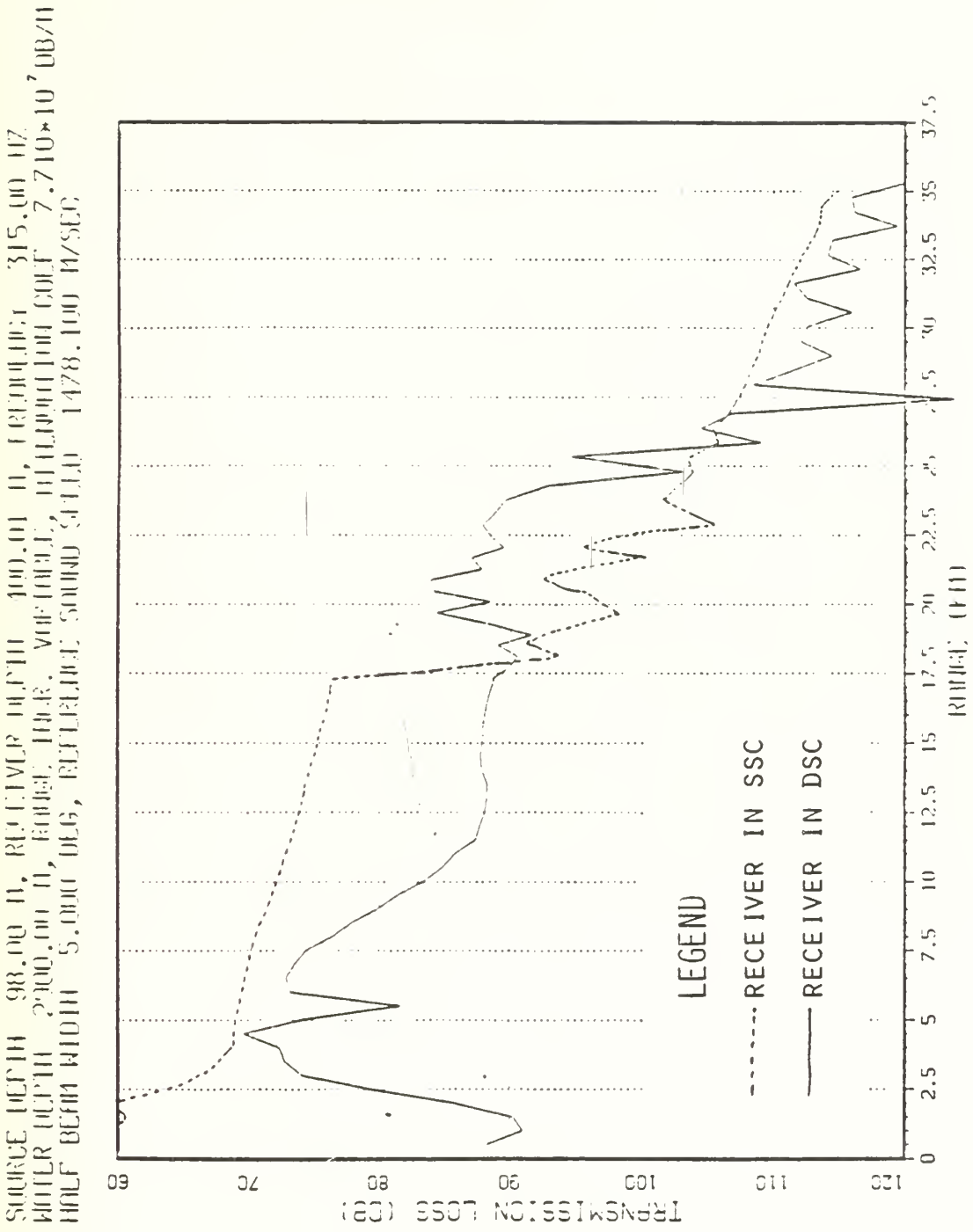

Figure 4.9 Shallow vs deep receiver, 315 Hz (NPS PE model).

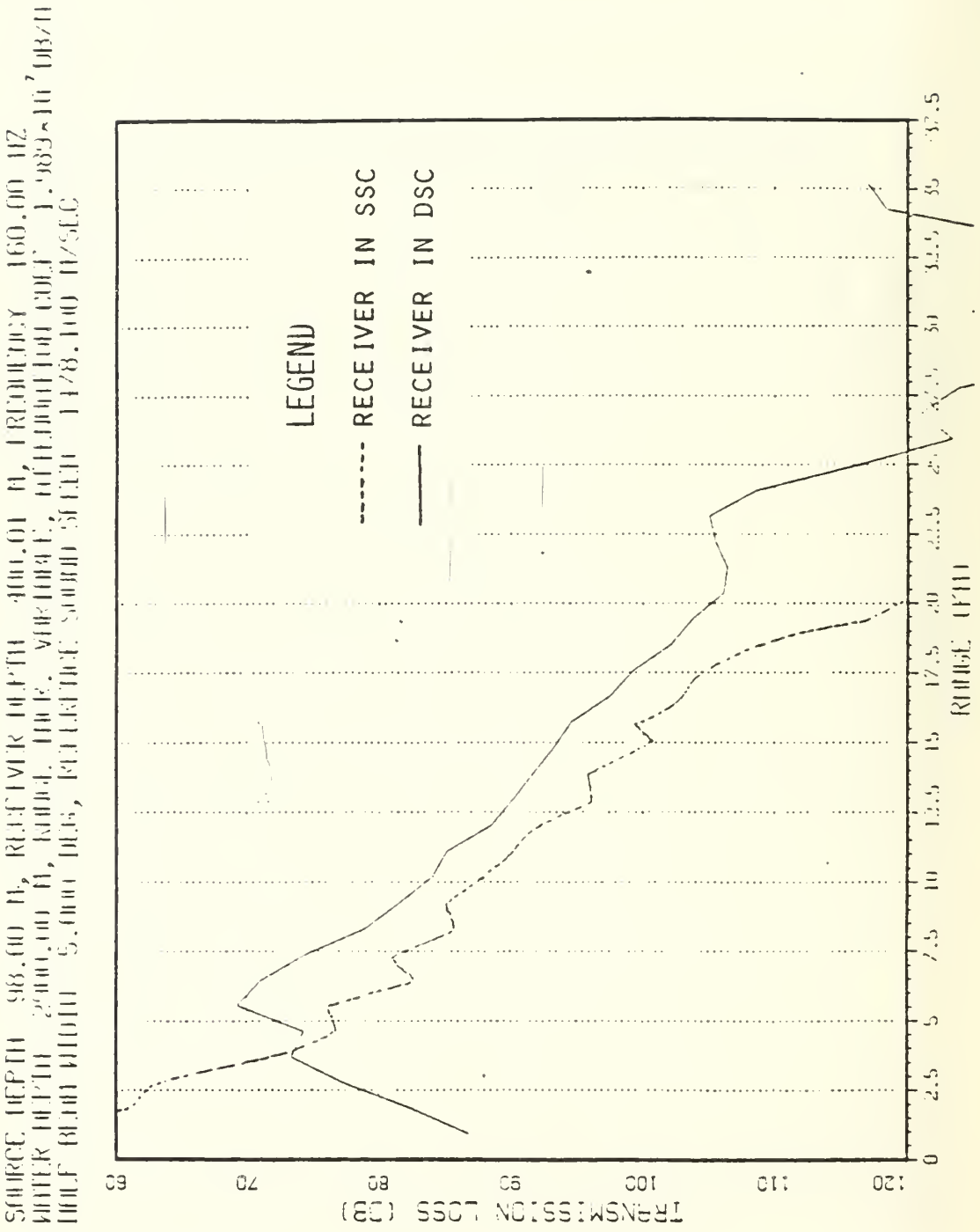

Figure 4.10 Shallow vs deep receiver, 160 Hz (NPS PE model).

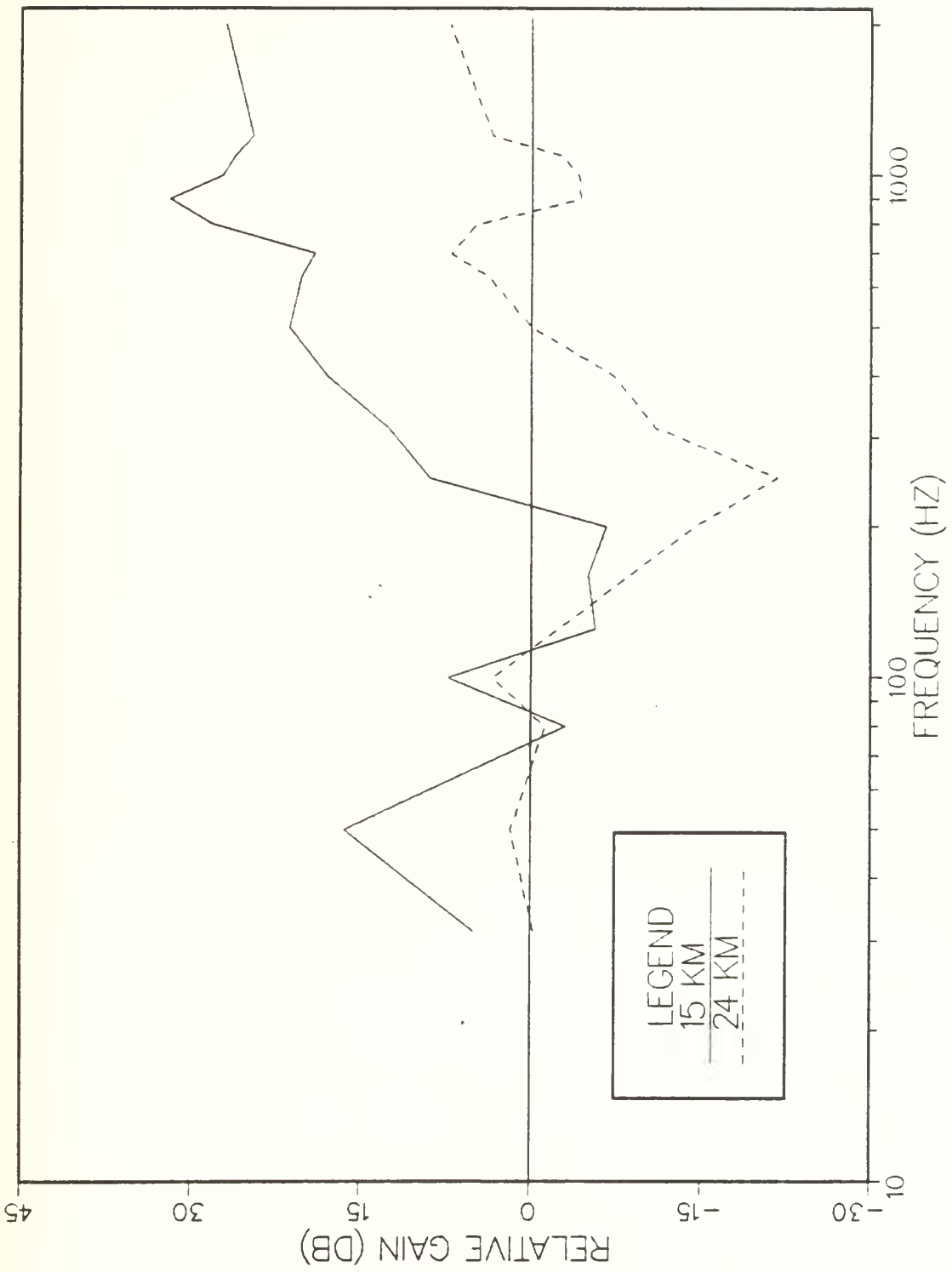

Figure 4.11 Relative gain between deep and shallow receivers (NPS PE model).

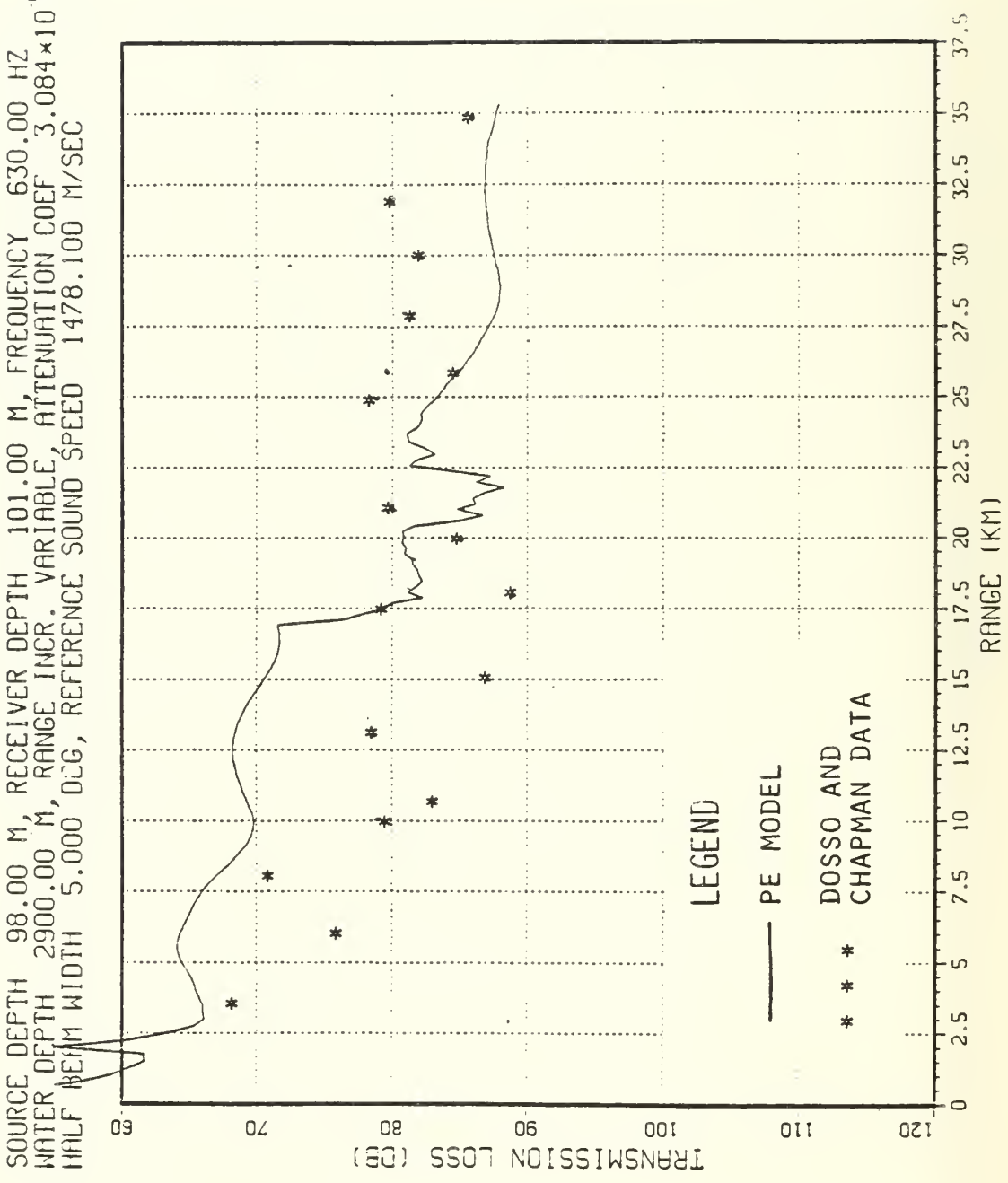

Figure 4.12 Transmission loss vs range, 630 Hz (NPS PE model).

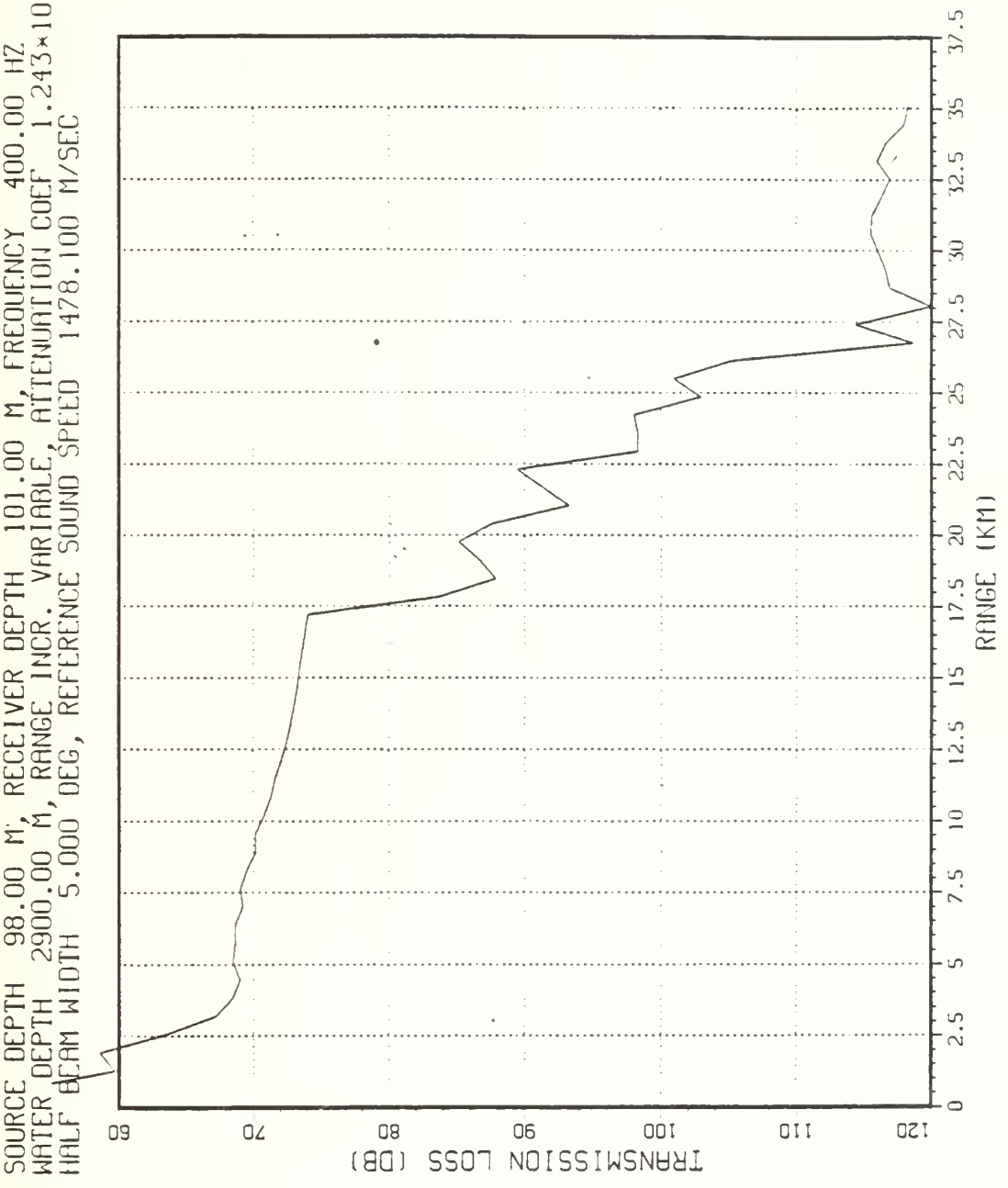

Figure 4.13 Transmission loss vs range, 400 Hz (NPS PE model).

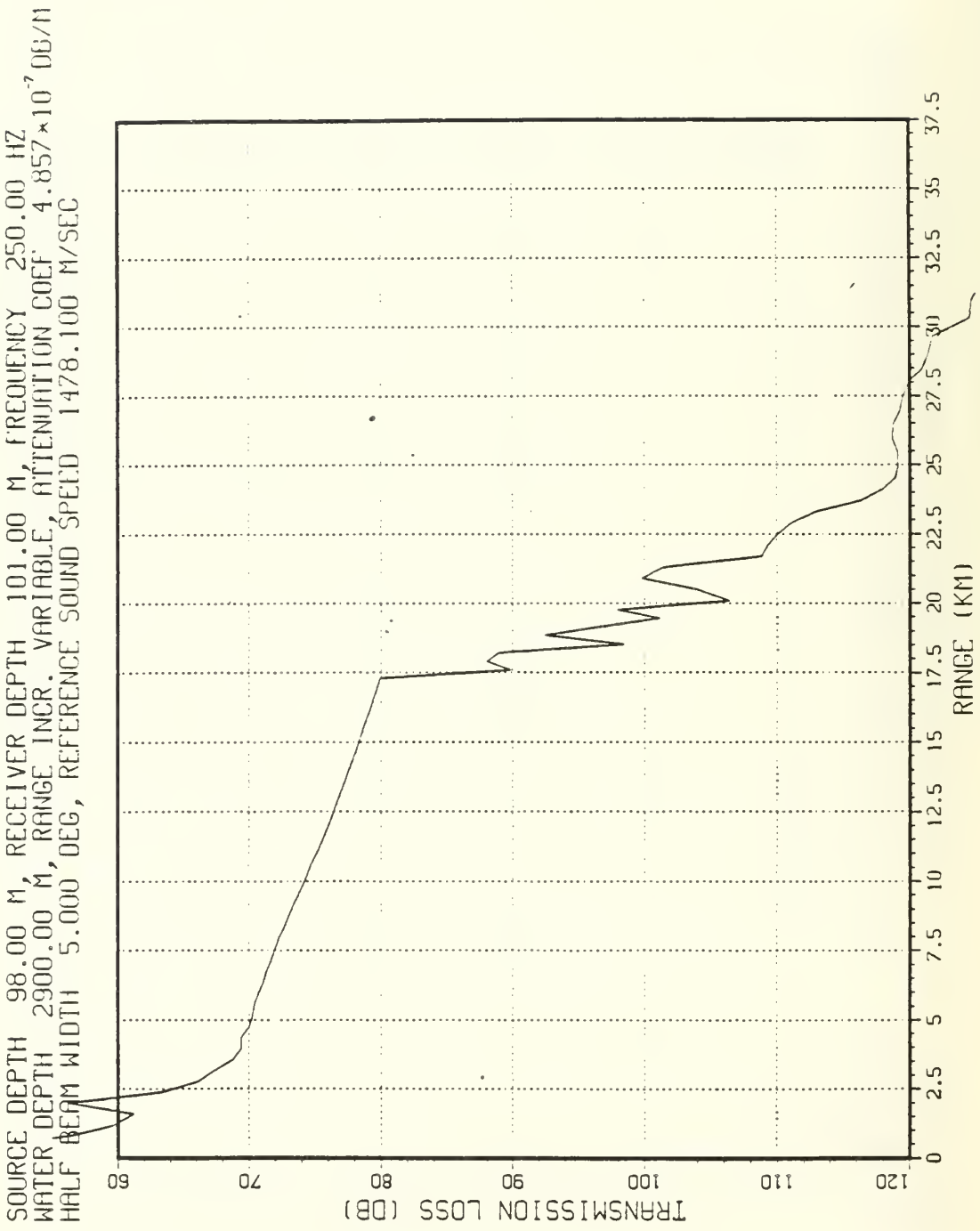

Figure 4.14 Transmission loss vs range, 250 Hz (NPS PE model).

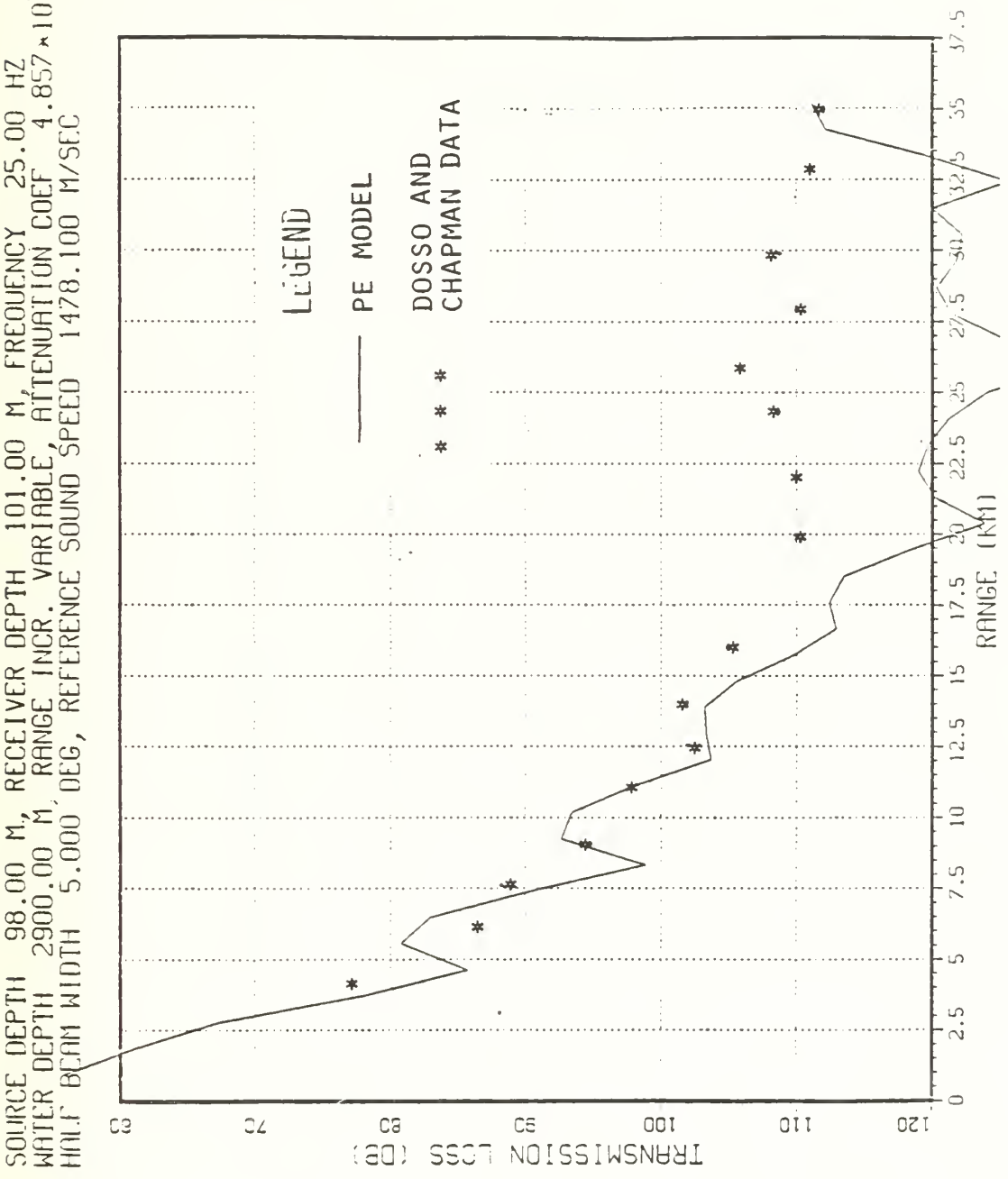

Figure 4.15 Transmission loss vs range, 25 Hz (NPS PE model).

V. TWO HIGH-LATITUDE SHALLOW SOUND CHANNELS

A. OPTIMUM FREQUENCIES IN THE SHALLOW SOUND CHANNELS

Since the NPS PE model yielded acceptable estimates of the optimum frequency for Dosso and Chapman's shallow sound channel, the next step in this study was to apply the model to some other shallow sound channels. Appendix A contains the NPS PE model input information for two sound velocity profiles taken in a deep, high-latitude ocean basin during summer conditions (10 and 28 June). Figures 5.1 and 5.2 show the SVPs. Note the presence of a surface layer and the absence of a deep sound channel.

The SSC for 10 June is 110 meters thick. Using equations 2.1 and 2.2 we would expect cutoff frequencies of 148 and 173 Hz for this channel. The SSC for 28 June is 105 meters thick, yielding cutoff frequencies of 159 and 186 Hz.

A plot of transmission loss versus frequency is the best tool for determining optimum frequency. For these two profiles the source was modeled at 98 meters and the receiver at 100 meters depth, providing for propagation within the shallow sound channel. Again the transmission loss levels at each range were calculated from the NPS PE model output graphics, by reading levels at the center ranges and one kilometer on either side, then computing a straight arithmetic average of the three readings. In Figures 5.3 and 5.4 it is much more difficult to identify an optimum frequency for the two shallow sound channels.

For the 28 June case (Figure 5.3) the transmission losses improve gradually and show optimum frequencies in the 600-900 Hz range, but no readily identifiable effect in the vicinity of the cutoff frequency. Propagation at

frequencies below cutoff is much better than would have been expected from Dosso and Chapman's results. Figures 5.5 through 5.8 are the NPS PE model results for several frequencies in the optimum range. Note that there is little difference in the overall transmission loss levels.

The 10 June case (Figure 5.4) is even more difficult to analyze. Again there is no clear indication of cutoff frequency in the graph. Note also that the curves for 15 and 24 km are virtually flat for frequencies below 200 Hz. The two curves show that transmission loss is highly dependent upon frequency, with improved transmission at 315-400 Hz and at several frequencies in the 600-1100 Hz range. Surprisingly, the transmission loss for 800 Hz on the 24 km curve is some 3 dB greater than for 315 Hz. Figures 5.9 and 5.10 are the NPS PE model results for the frequencies near optimum, and again there is not much apparent difference in the overall transmission loss levels.

In an attempt to identify the optimum frequency for the 10 June case more clearly, the investigator then introduced an artificially shallow bottom in hopes that this would simplify the propagation paths. The 10 June sound velocity profile was truncated at the lower boundary of the shallow sound channel, with a fully absorbing bottom placed at 150 meters. Source and receiver remained at 98 meters and 100 meters respectively; no other input parameters were changed. Figure 5.11 displays the results. There is still no indication of cutoff frequency, but two of the curves do show gradual improvement in transmission with increasing frequency. The 15 and 24 km curves show smallest transmission losses in the 700-900 Hz range. Unfortunately the 33 km curve shows smallest transmission loss at 600 Hz and large loss at 700 Hz. Figures 5.12 through 5.14 are NPS PE model results for frequencies near optimum. Using an artifically introduced shallow bottom appears to have improved

the optimum frequency prediction somewhat for the 10 June case.

Putting all three cases together and looking for a trend, we can tentatively identify a range of optimum frequencies around 600-900 Hz. The results for these shallow sound channels are not as clear or conclusive as Dosso and Chapman's results, but they should be adequate for the fleet sonar operator to use in setting up search plans.

B. OPTIMUM FREQUENCY FOR PROPAGATION ACROSS THE LAYER

The second part of this investigation involved the same sound velocity profiles with the source still located at 98 meters near the SSC axis, but with the receiver modeled at 20 meters, well within the surface layer. Figures 5.15 through 5.17 show the results.

Figure 5.15 for 28 June shows peaks at 125 and 600 Hz in the transmission loss versus frequency curves for 15, 24 and 33 km. Again the concept of cutoff frequency does not appear to have much meaning in these cases. Figure 5.16 shows peaks at 160-200 Hz and at 700 Hz. For the truncated 10 June profile, Figure 5.17 shows a peak at 75-100 Hz but not at higher frequencies.

Figures 5.18 through 5.20 show relative gain for our three cases, calculated according to the equation

$$\text{Relative Gain} = TL_{layer} - TL_{ssc} \qquad (5.1)$$

These high-latitude summer profiles do not show a cutoff frequency between the SSC and the surface layer. Propagation is always better when both source and receiver are contained within the shallow sound channel than when the source is in the SSC and the receiver is in the surface layer.

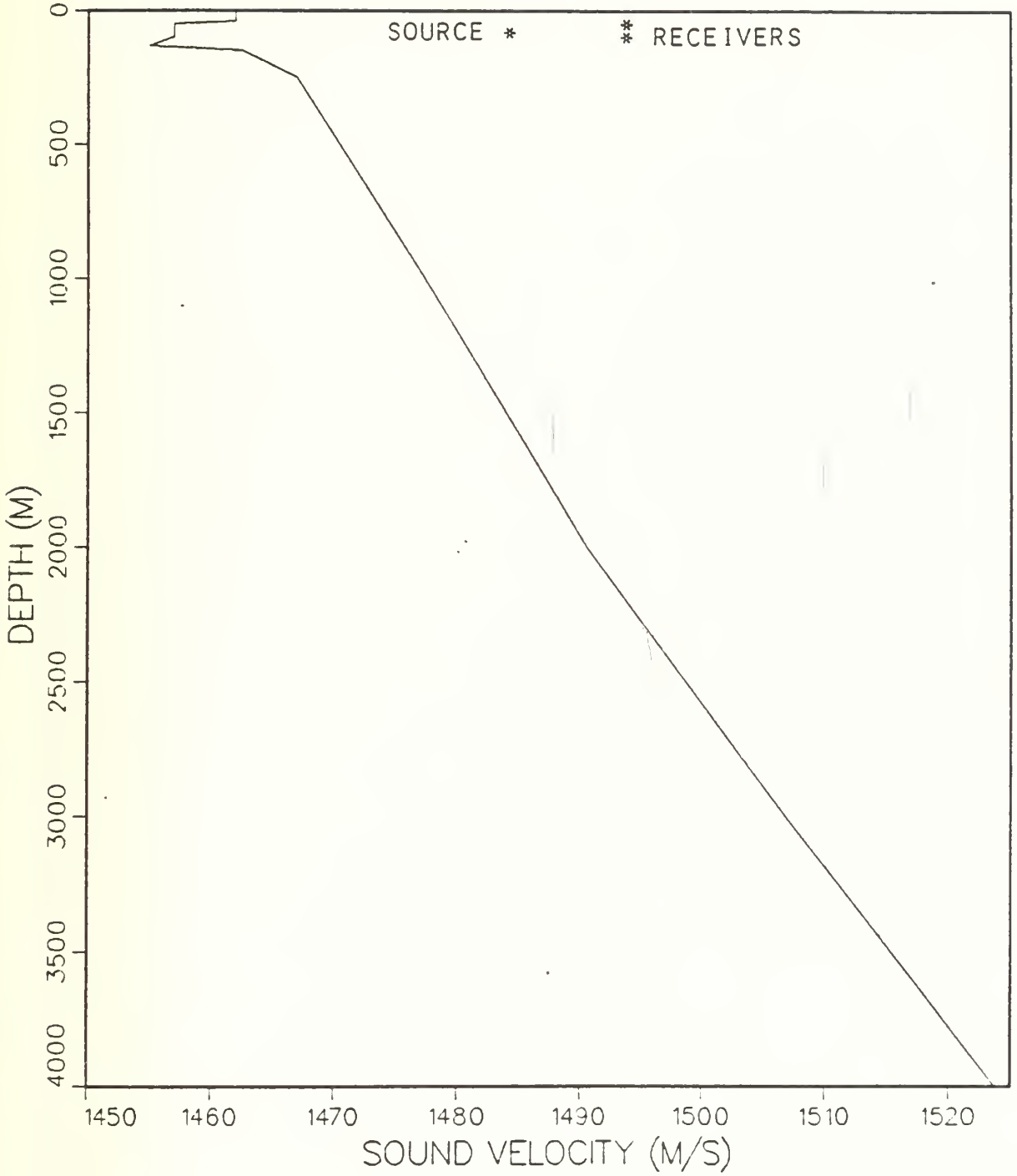

Figure 5.1 High-latitude sound velocity profile, 10 June.

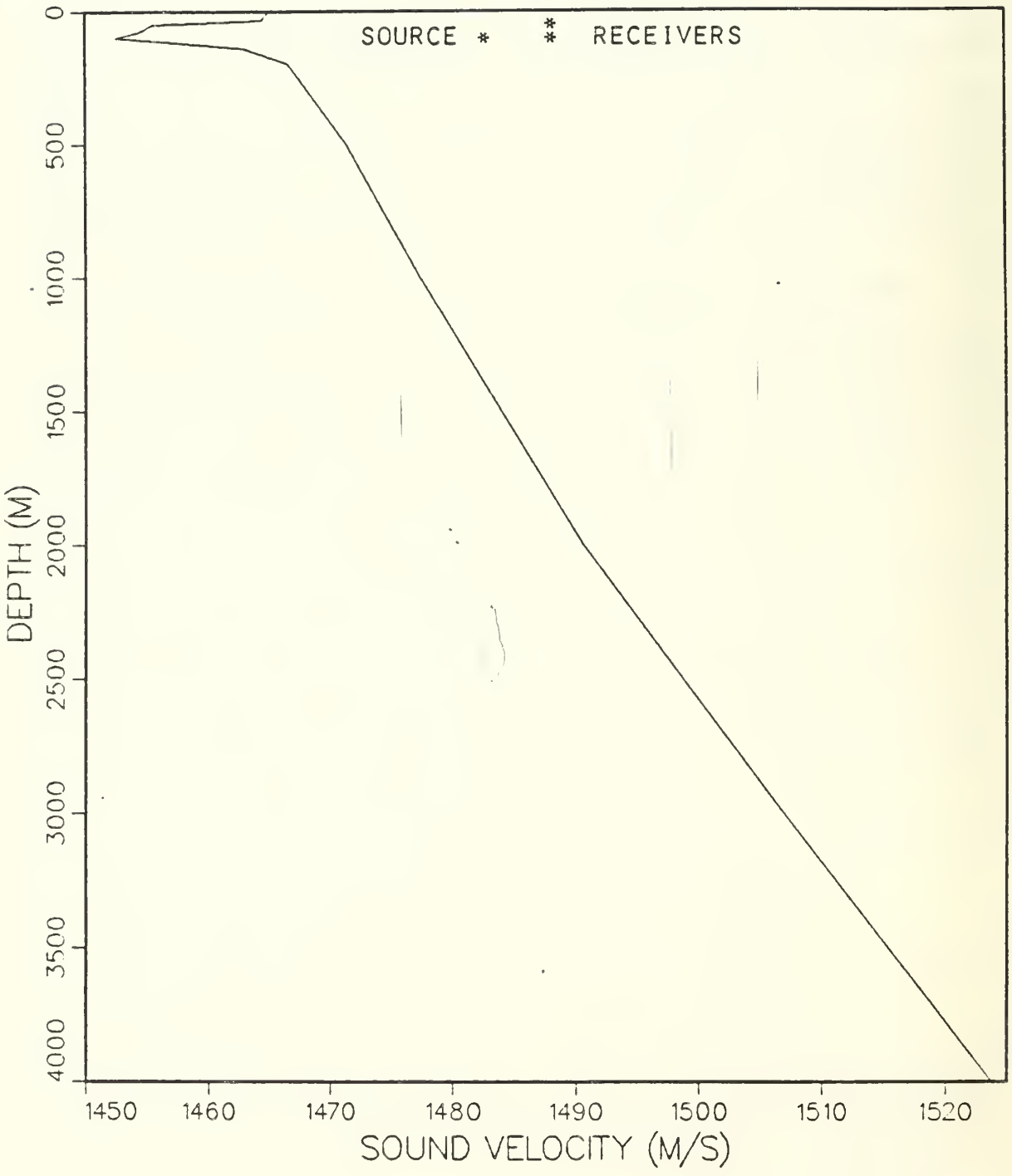

Figure 5.2 High-latitude sound velocity profile, 28 June.

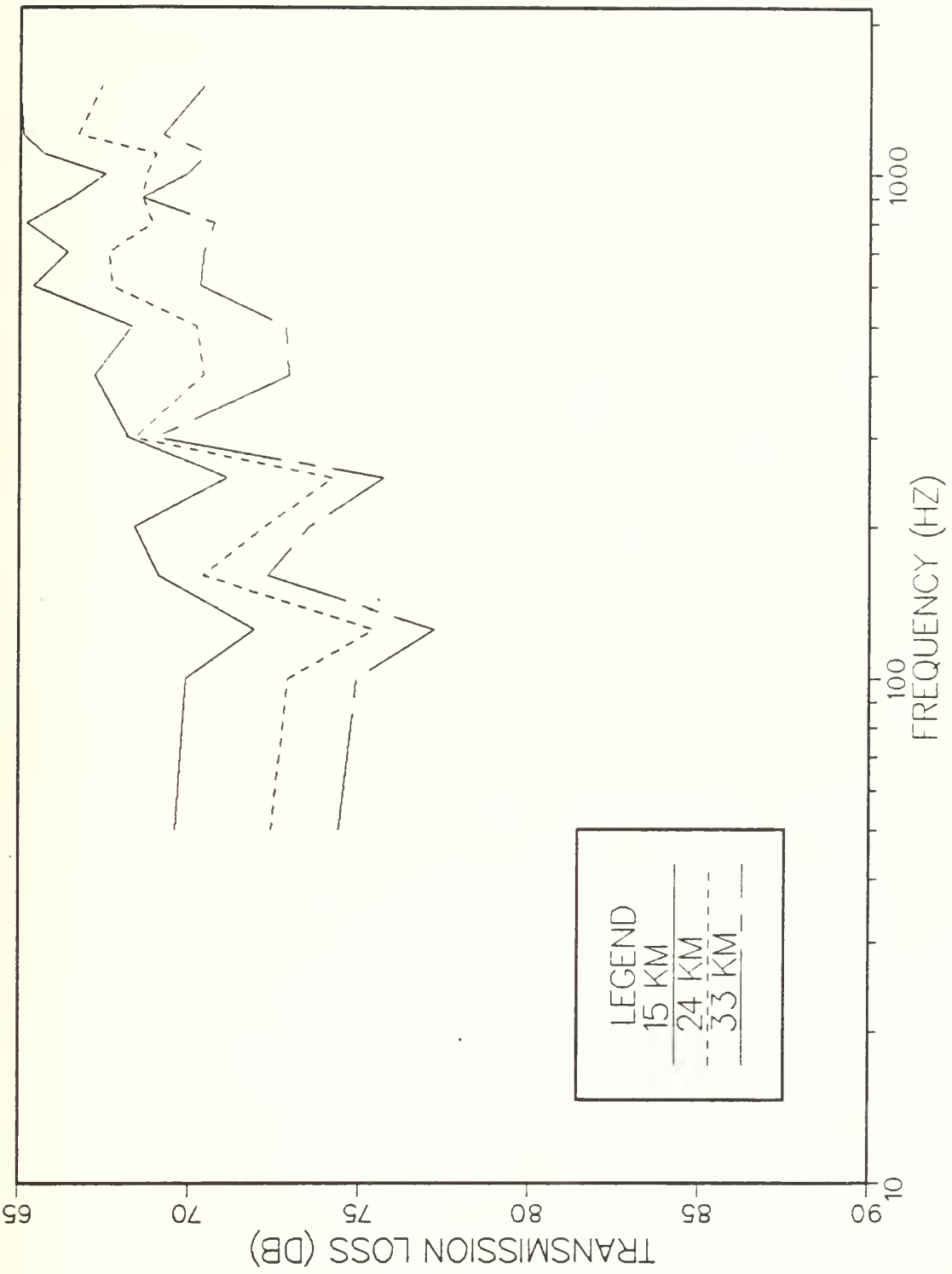

Figure 5.3 Transmission loss versus frequency, 28 June (NPS PE model).

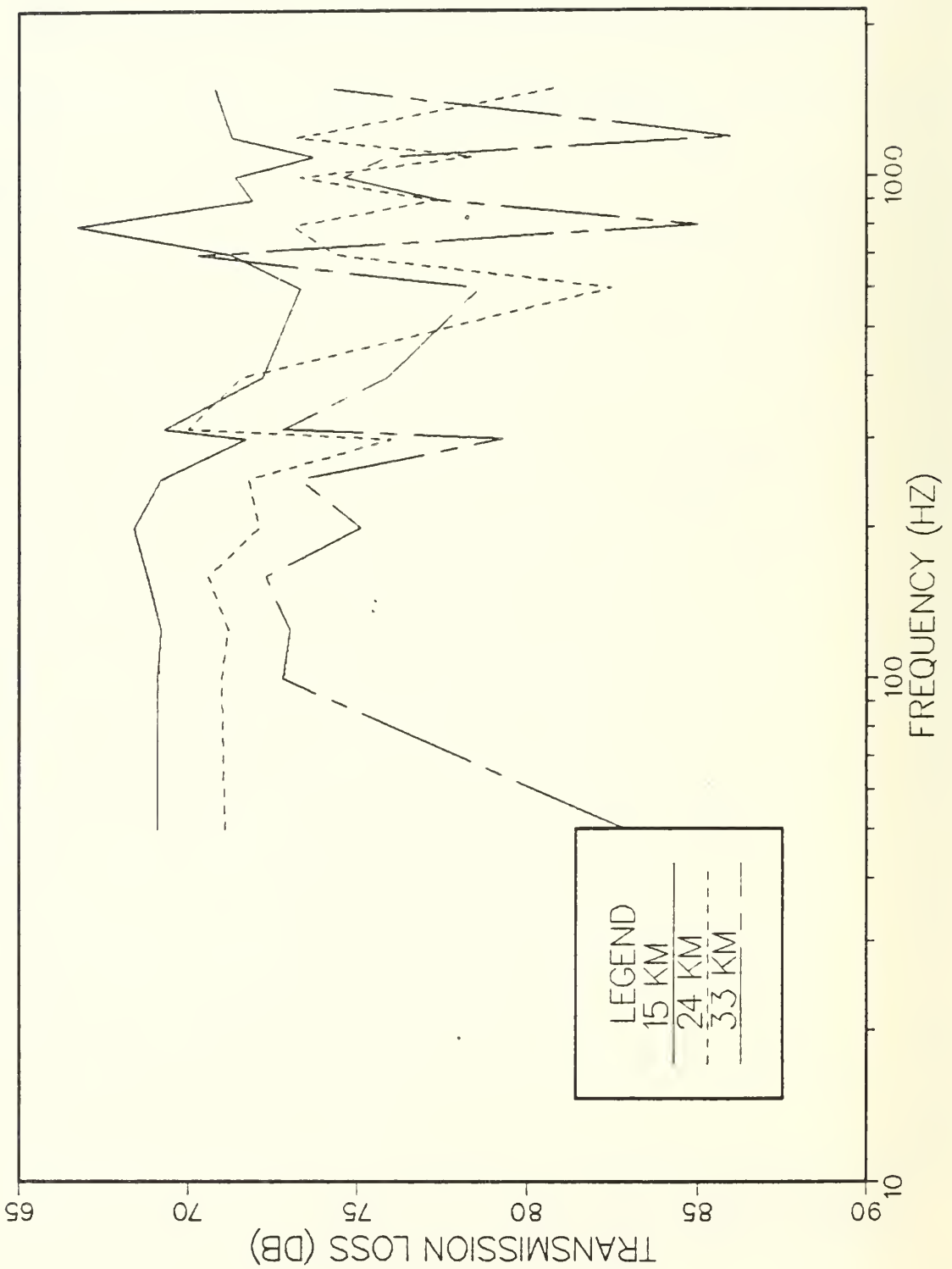

Figure 5.4 Transmission loss versus frequency, 10 June (NPS PE model).

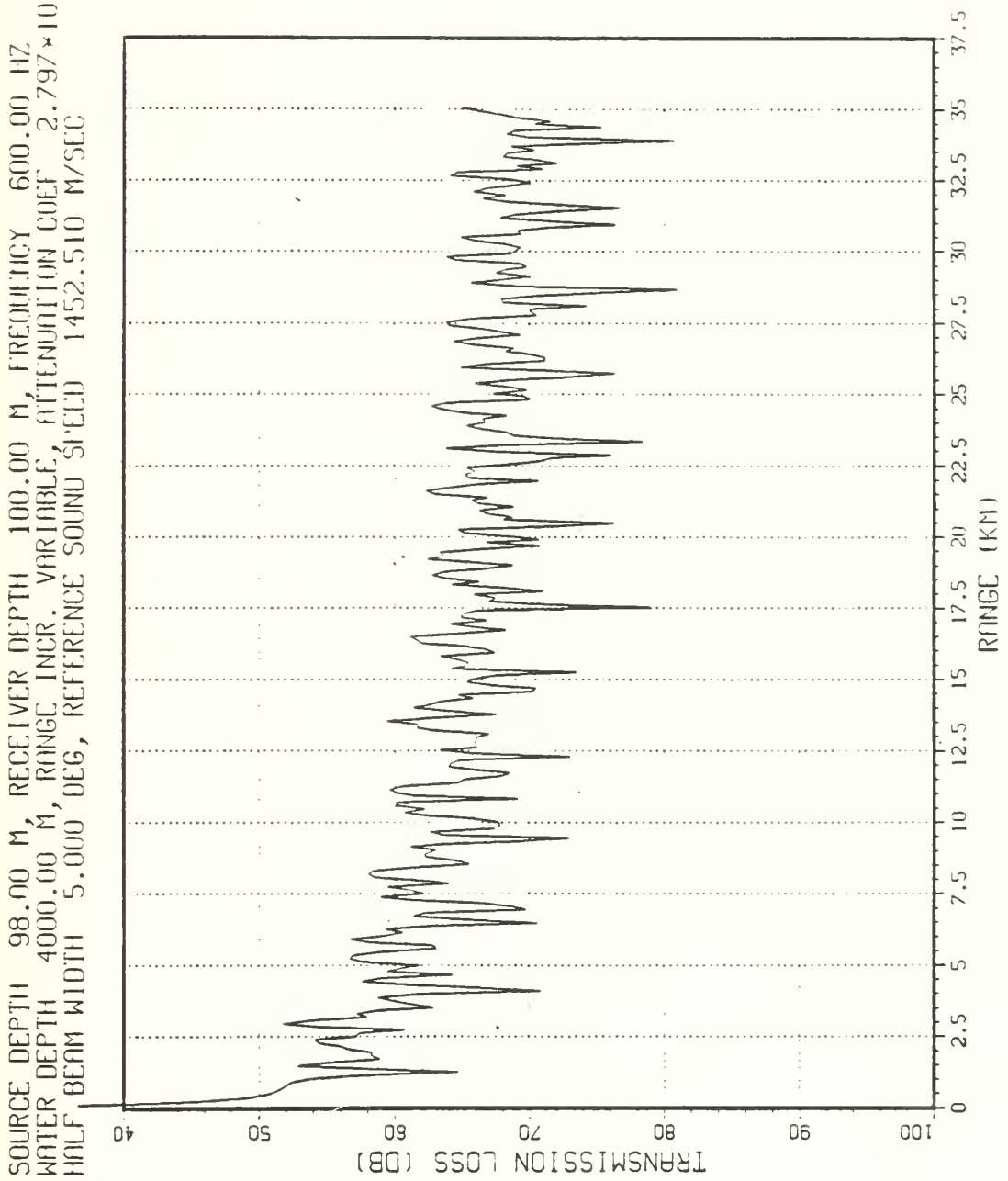

Figure 5.5 Transmission loss versus range, 28 June, 600 Hz (NPS PE model).

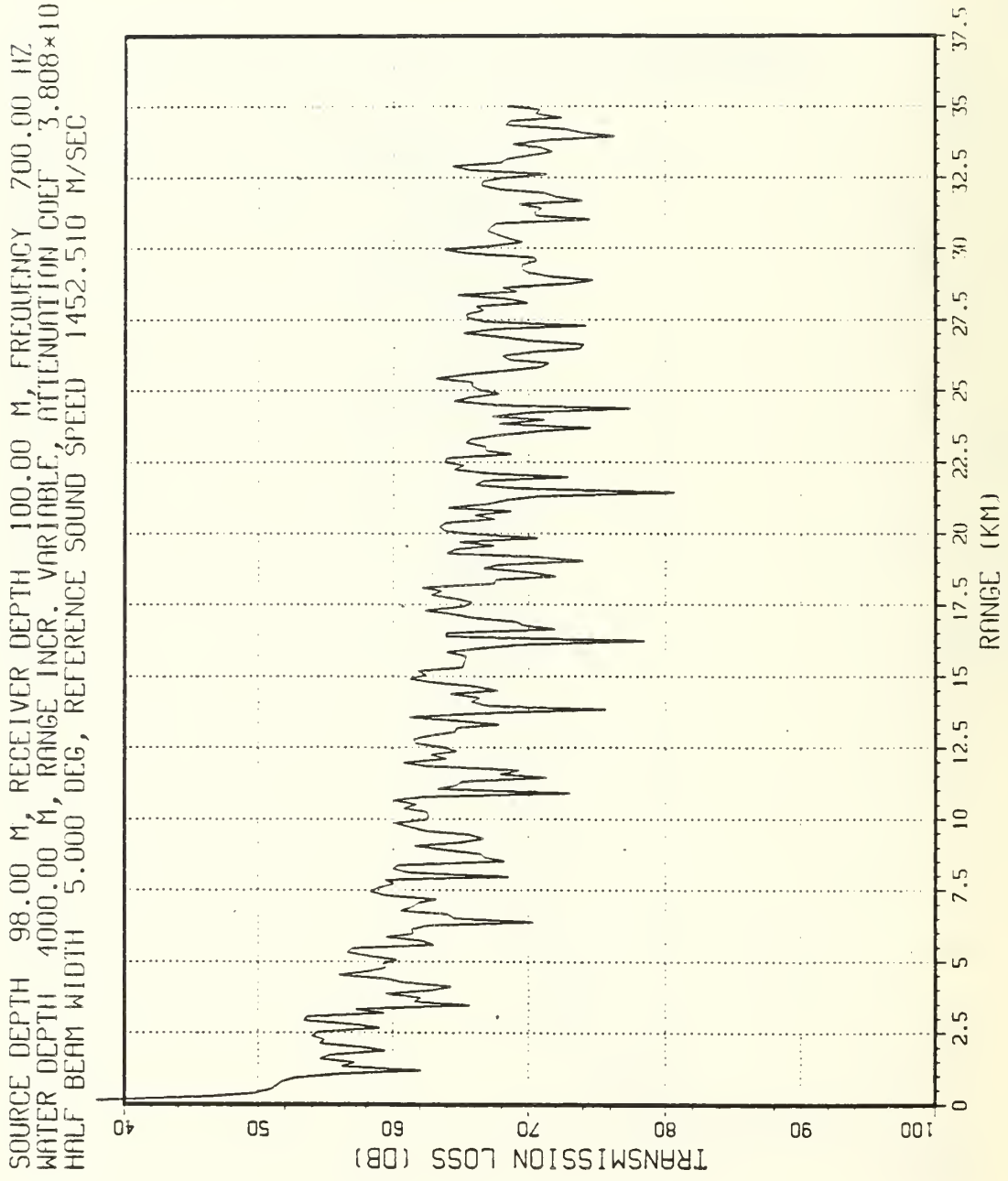

Figure 5.6 Transmission loss versus range, 28 June, 700 Hz (NPS PE model).

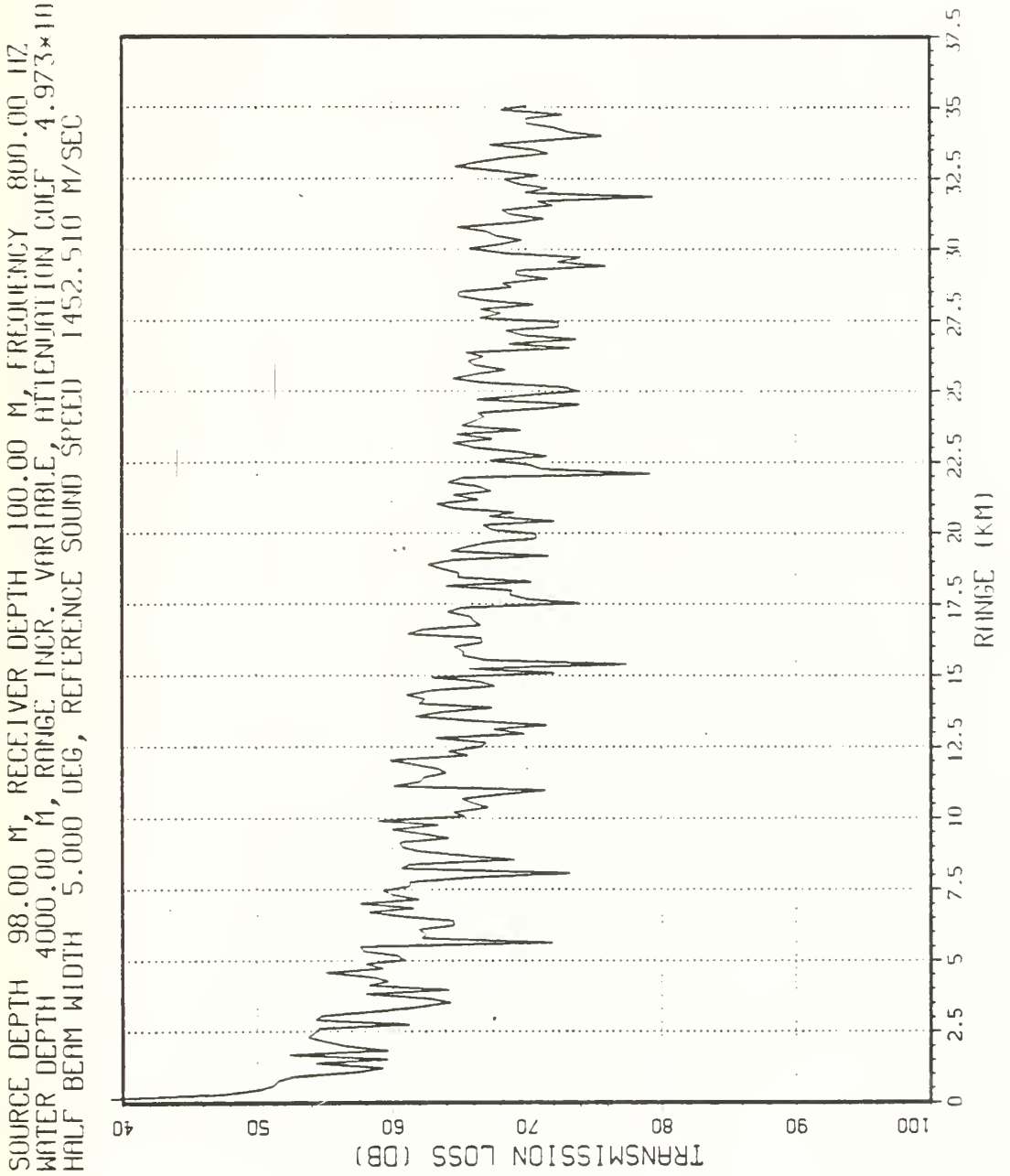

Figure 5.7 Transmission loss versus range, 28 June, 800 Hz (NPS PE model).

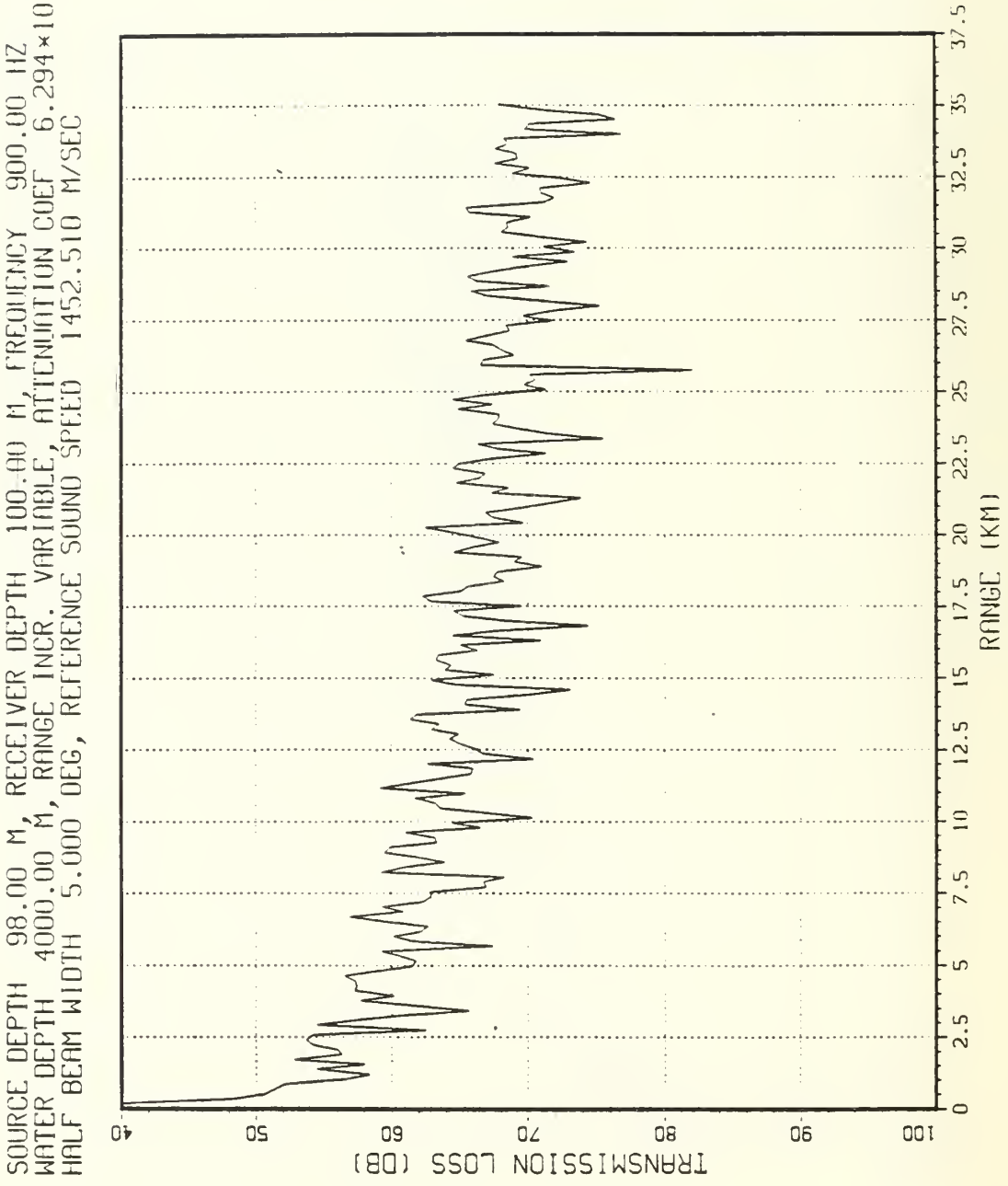

Figure 5.8 Transmission loss versus range, 28 June, 900 Hz (NPS PE model).

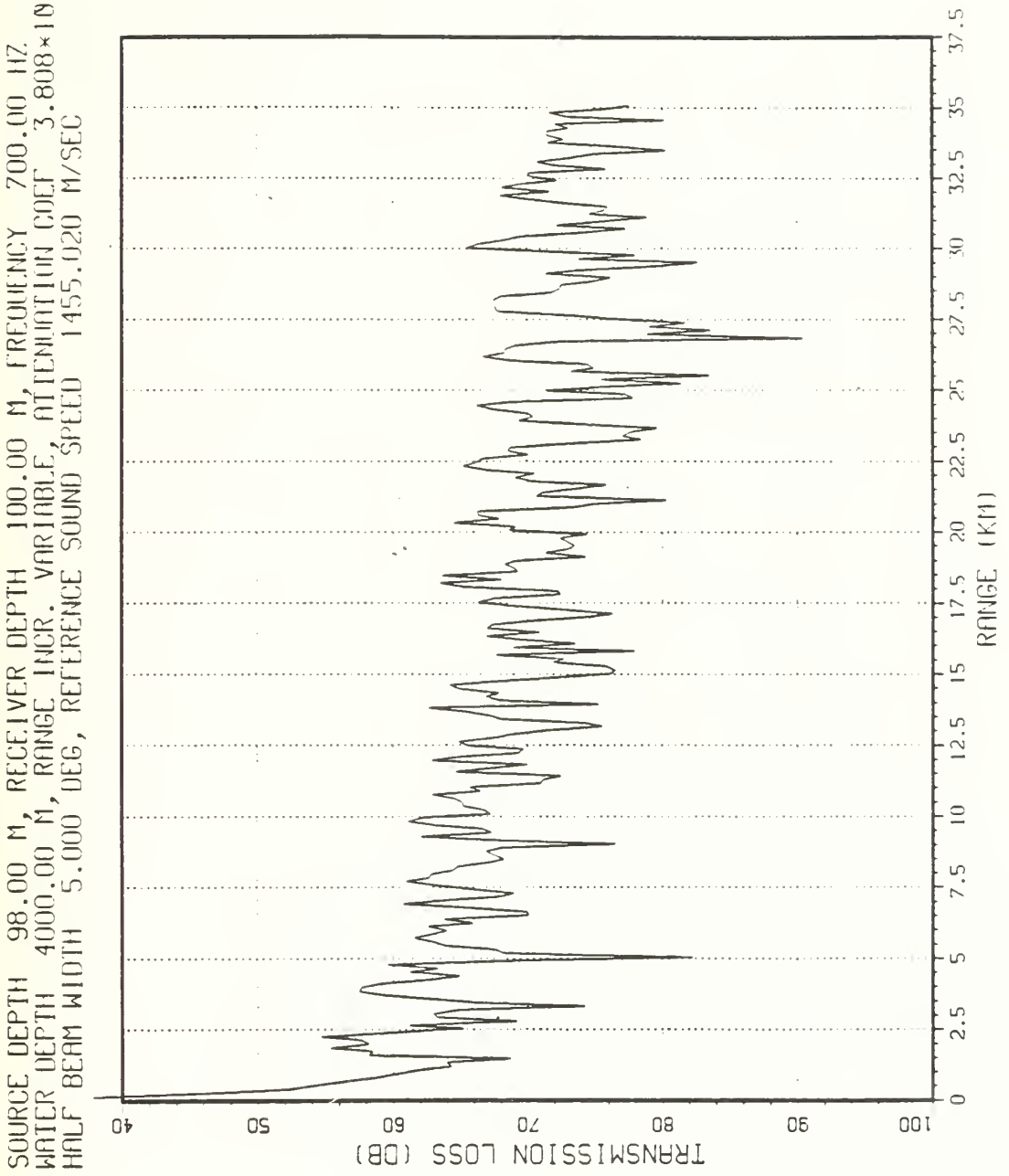

Figure 5.9 Transmission loss versus range, 10 June, 700 Hz (NPS PE model).

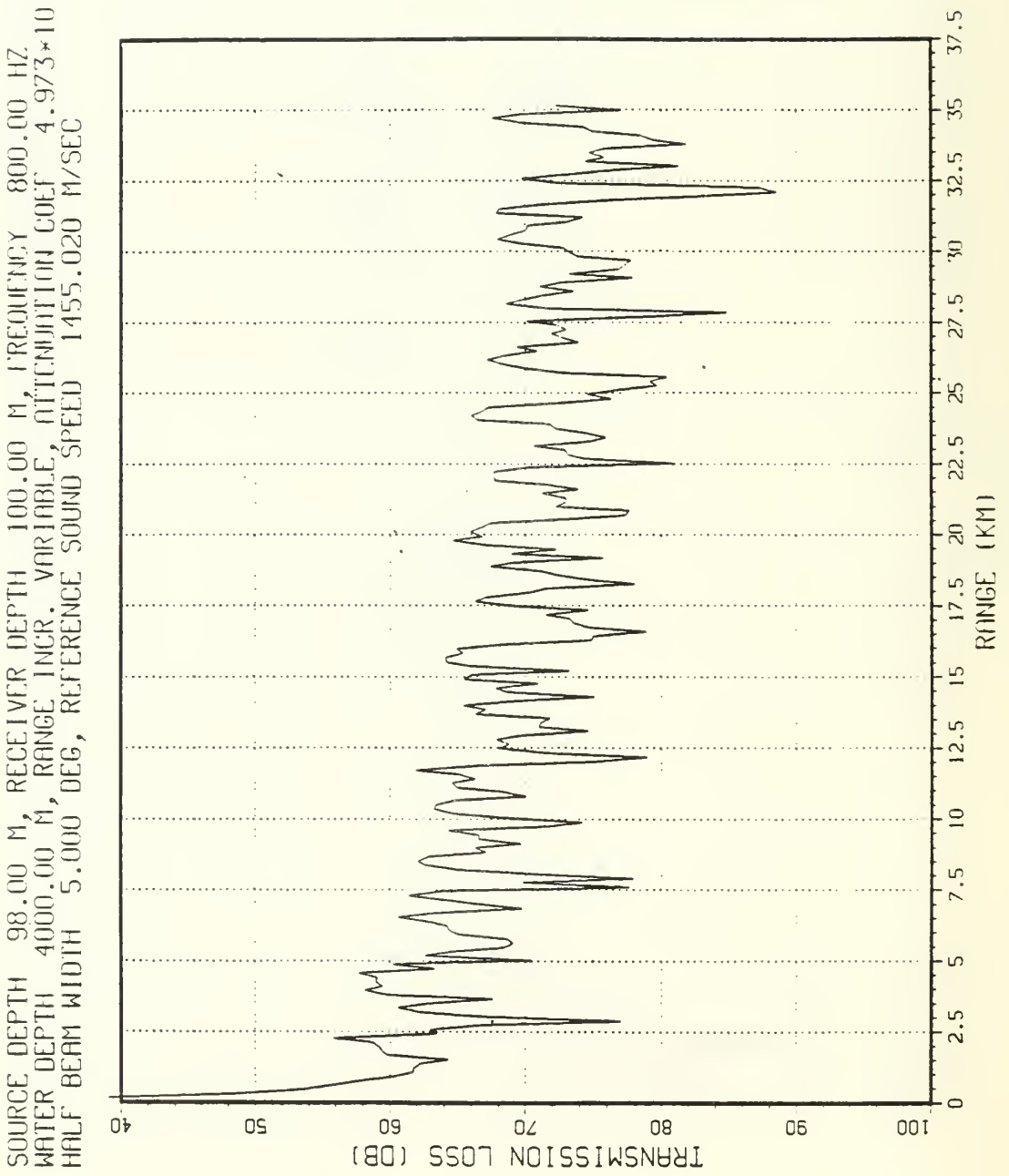

Figure 5.10 Transmission loss versus range, 10 June, 800 Hz (NPS PE model).

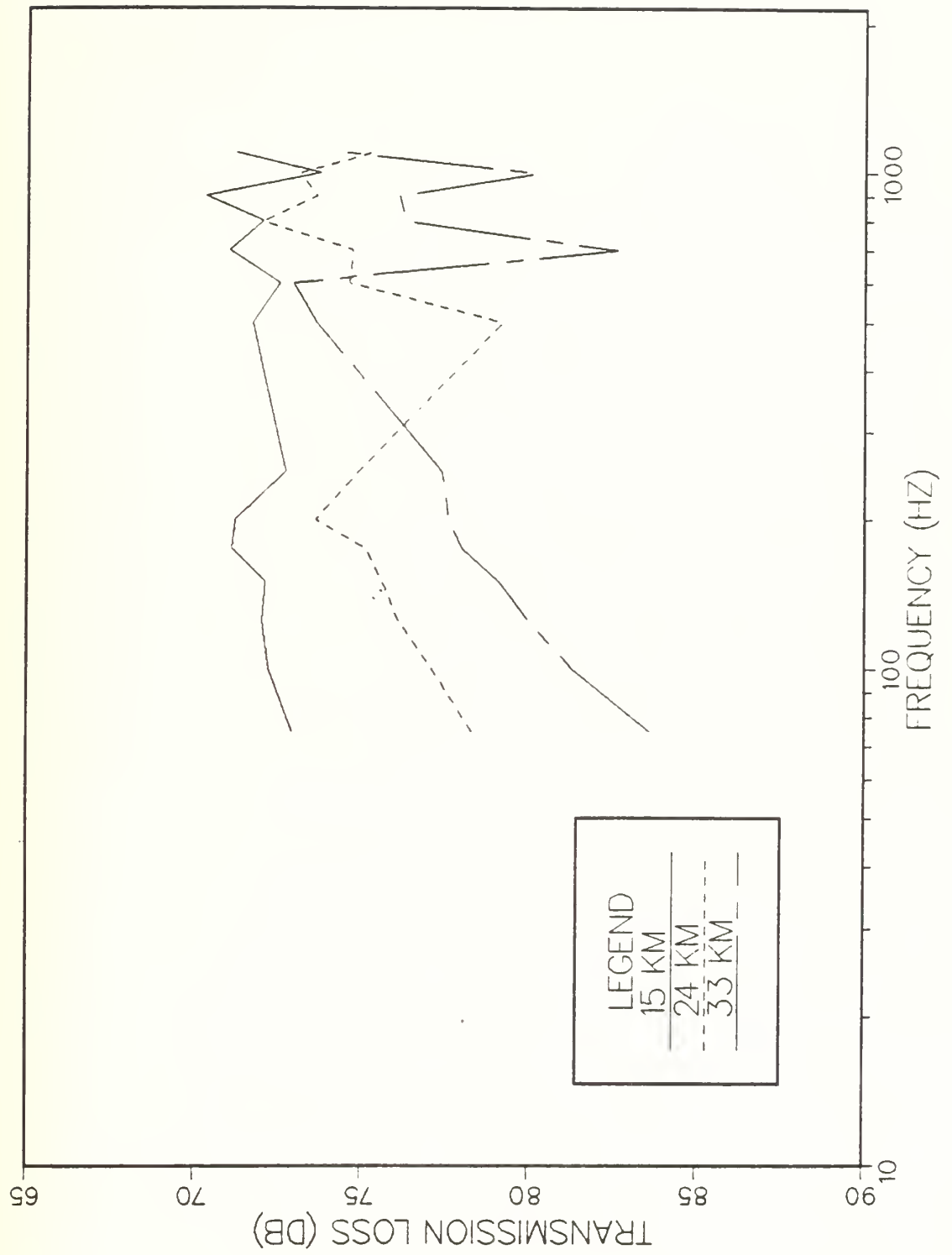

Figure 5.11 Transmission loss versus frequency, truncated profile (NPS PE model).

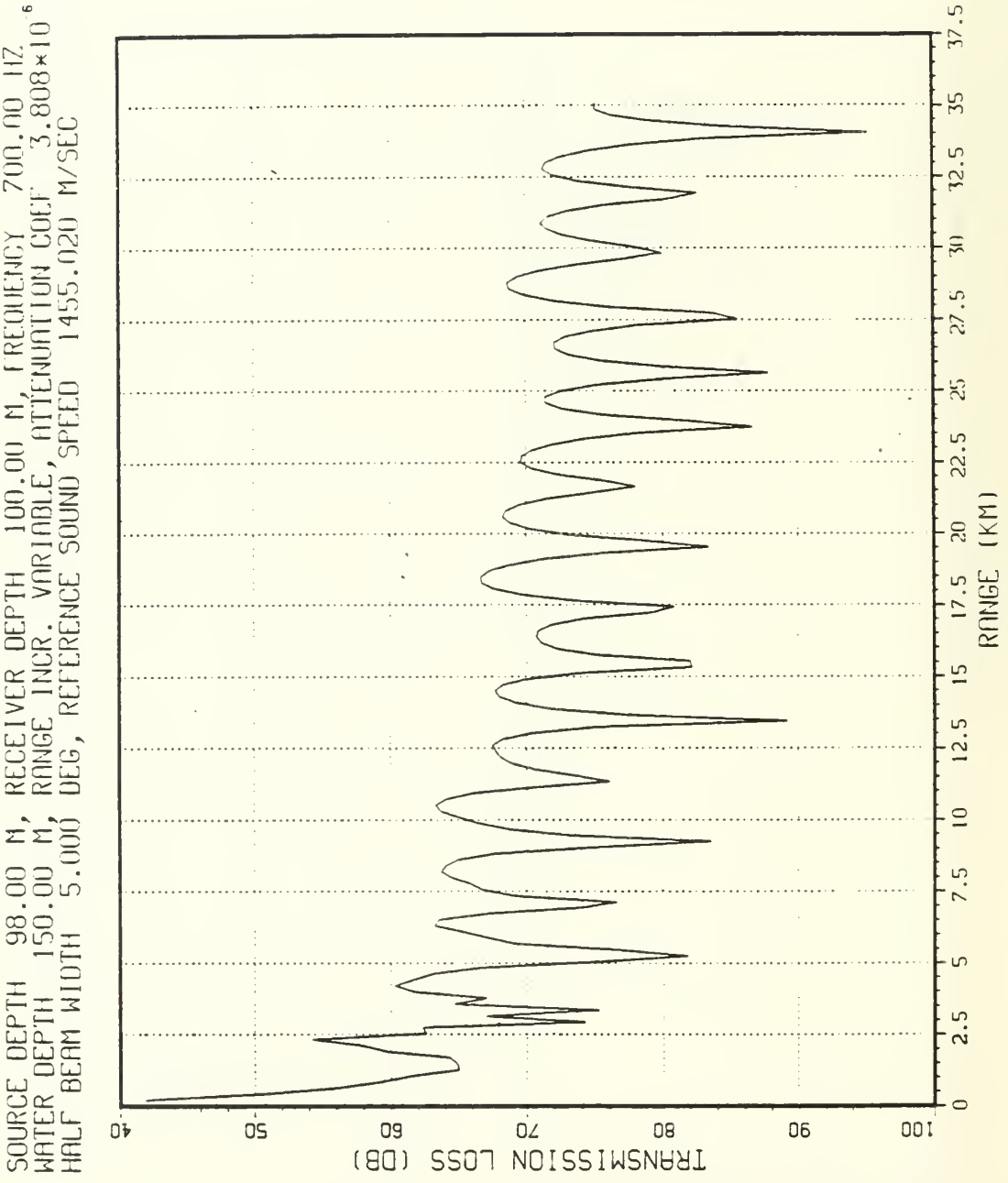

Figure 5.12 Transmission loss versus range, truncated profile, 700 Hz (NPS PE model).

Figure 5.13 Transmission loss versus range, truncated profile, 800 Hz (NPS PE model).

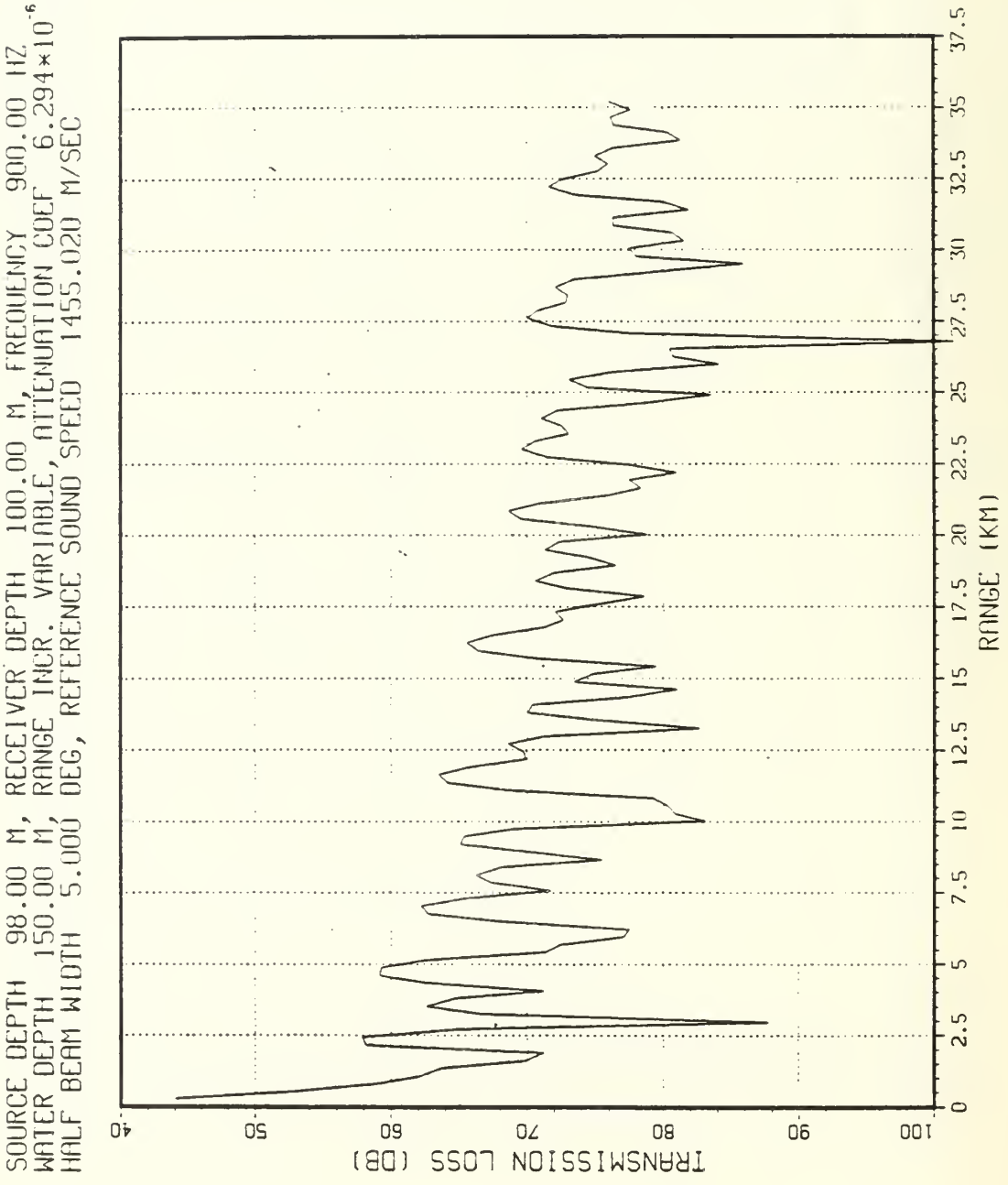

Figure 5.14 Transmission loss versus range, truncated profile, 900 Hz (NPS PE model).

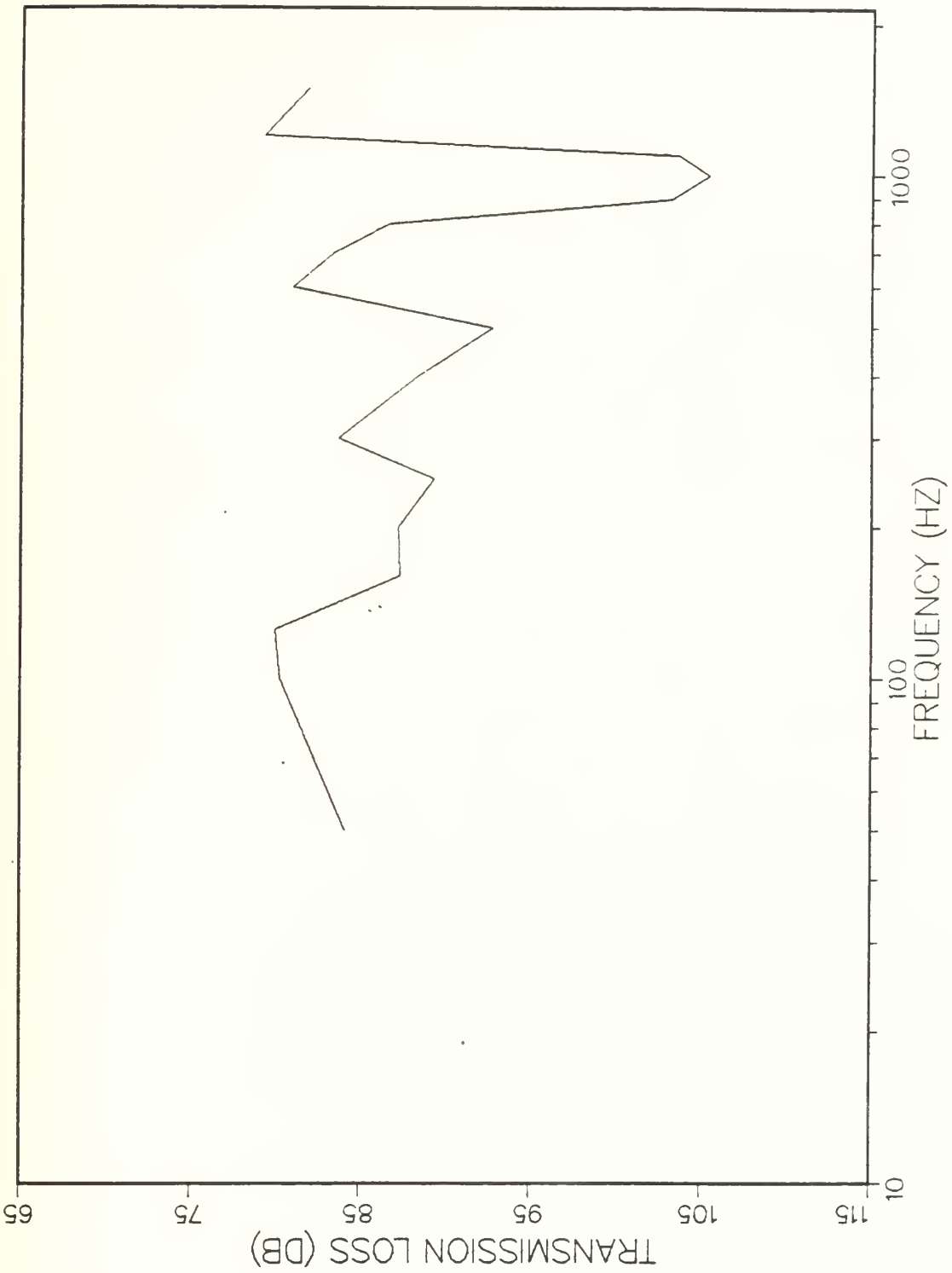

Figure 5.15 Transmission loss between surface layer and SSC, 28 June (NPS PE model).

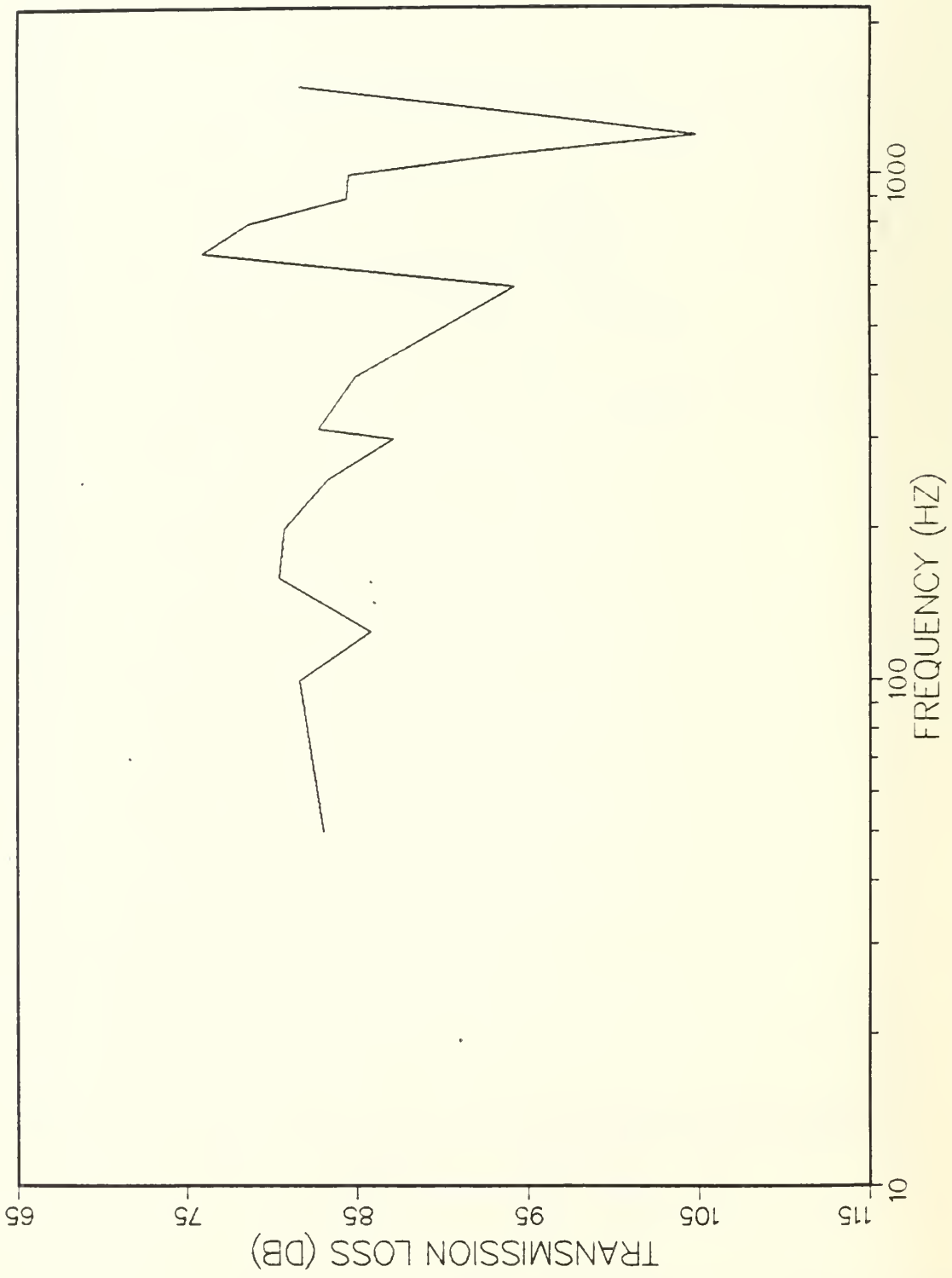

Figure 5.16 Transmission loss between surface layer and SSC, 10 June (NPS PE model).

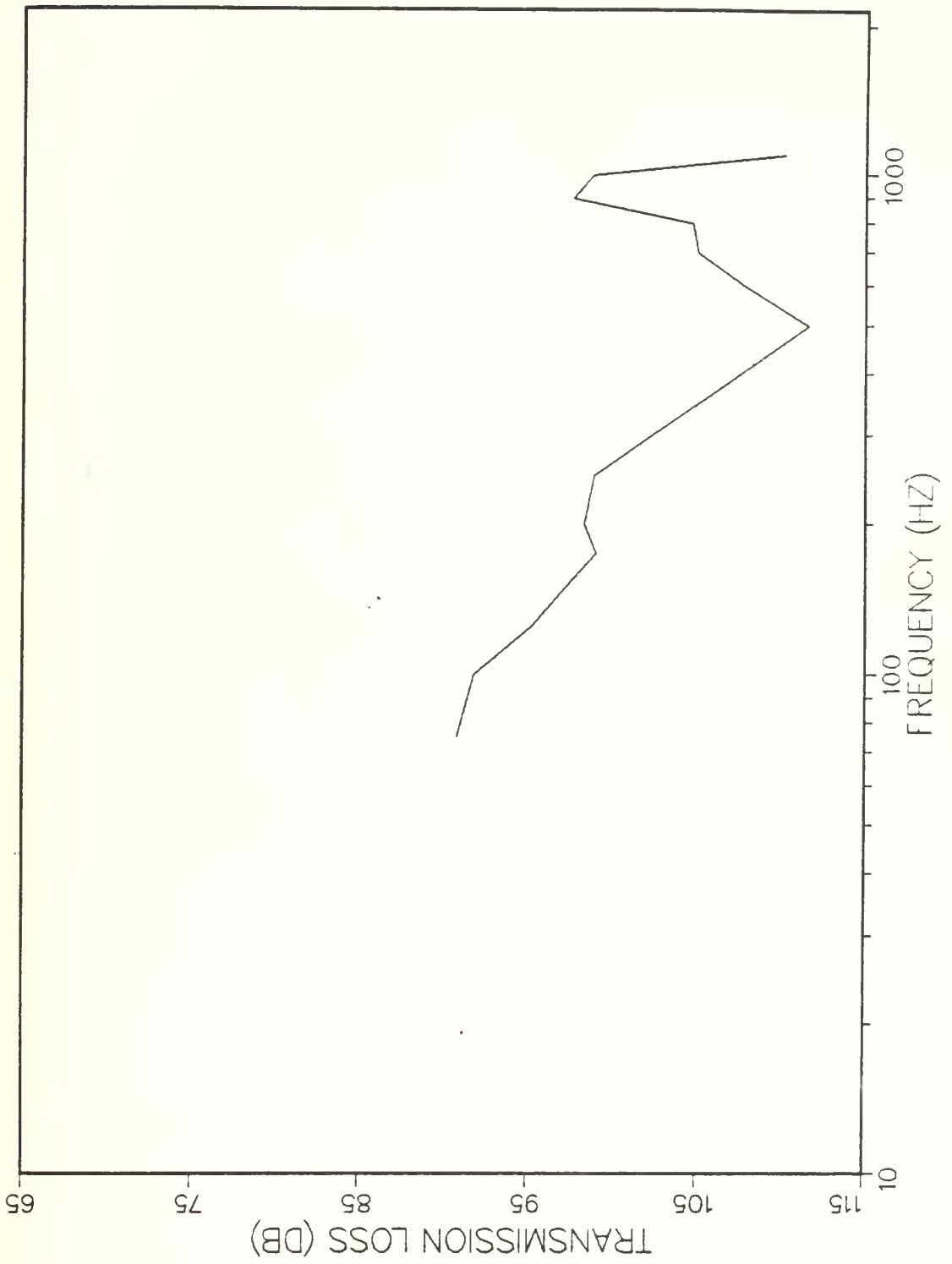

Figure 5.17 Transmission loss between surface layer and SSC, truncated profile (NPS PE model).

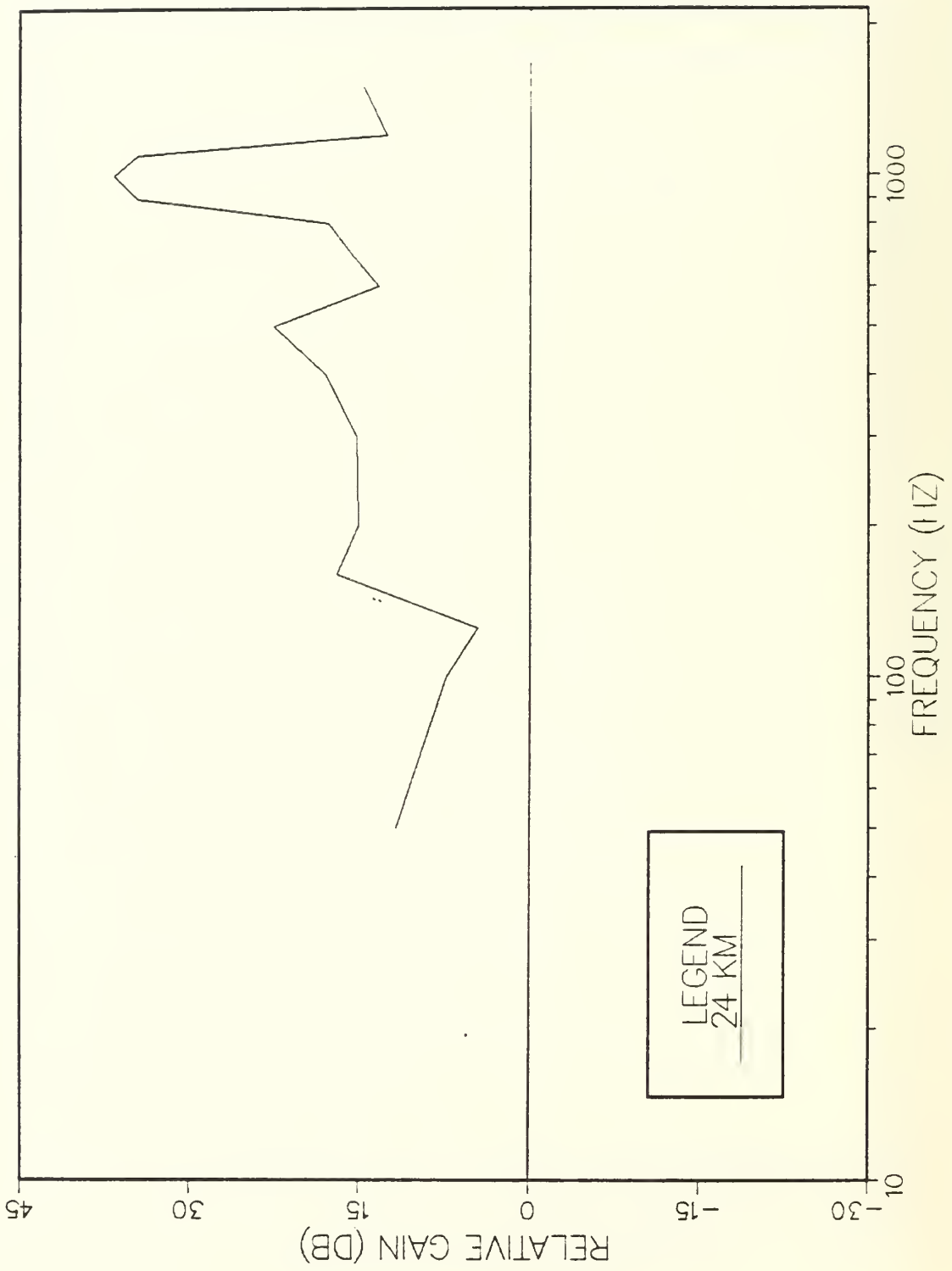

Figure 5.18 Relative gain between surface layer and SSC, 28 June (NPS PE model).

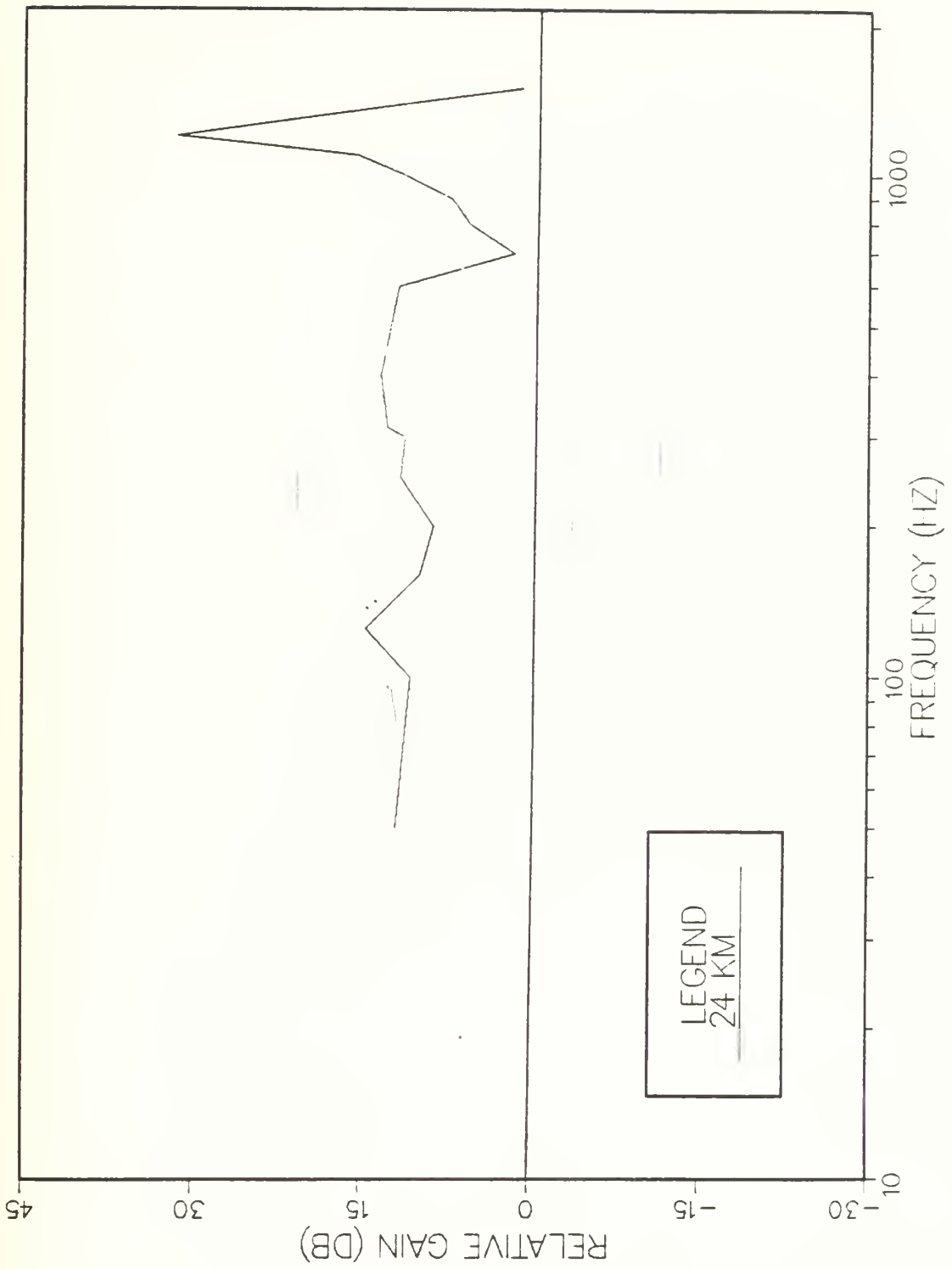

Figure 5.19 Relative gain between surface layer and SSC, 10 June (NPS PE model).

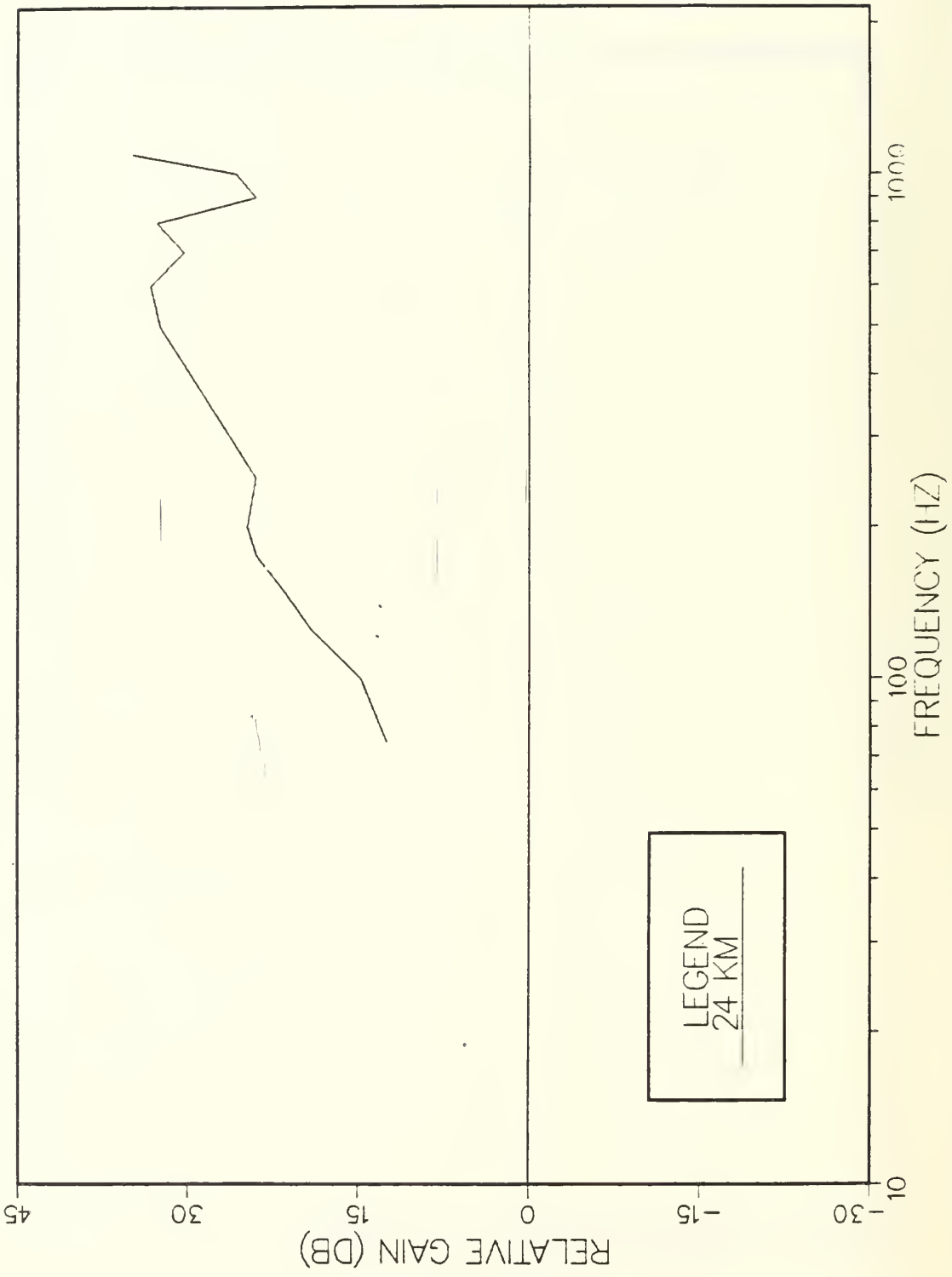

Figure 5.20 Relative gain between surface layer and SSC, truncated profile (NPS PE model).

VI. THE NPS FACT 9H MODEL

A. MODEL DESCRIPTION

The Fast Asymptotic Coherent Transmission loss model, version 9H (FACT 9H), like the split-step Parabolic Equation model, is accessed through the Naval Postgraduate School's IBM 3033 computer. FACT currently provides the acoustic predictions for the Integrated Command ASW Prediction System (ICAPS) on board U. S. Navy aircraft carriers and ASW Operations Centers (ASWOCs) worldwide. It is also the basis for a number of acoustic products routinely provided by the Fleet Numerical Oceanography Center, Monterey, to fleet users. Since the FACT model and its products are so widely distributed in the fleet, it is of interest to know how well FACT performs for the shallow sound channel case.

The FACT 9H model as installed at the Naval Postgraduate School was developed for the Naval Ocean Research and Development Activity (NORDA) [Ref. 9]. It uses ray tracing theory with special corrections to improve the treatment of caustics, which would produce calculations indicating excessive acoustic energy at certain ranges if not corrected. Unlike the PE model, FACT 9H accepts only one sound velocity profile, located at range zero. It makes no allowance for bottom topography changing over the length of a track. The user may indicate the absorption characteristics of the bottom, or specify a table of values for bottom loss versus grazing angle.

In addition, a semi-empirical expression is used to account for propagation in a surface duct. In this module the user may indicate the wave height, unlike the NPS PE model which makes no provisions for boundary conditions at

the surface. As a ray-tracing model, FACT 9H is not expected to deal with waveguide phenomena such as diffraction and leakage as successfully as the PE model does. The surface duct module is intended to remedy this problem somewhat and to improve the acoustic prediction in the case of surface ducts. No correction has yet been applied for shallow sound channels.

The investigation of the FACT 9H model proceeded along essentially the same lines as that of the PE model. The FACT 9H model was first tested against the experimental results of Dosso and Chapman. Then the model was applied to the 10 June and 28 June sound velocity profiles. Input parameters are described in Appendix A.

B. VALIDATION AGAINST DOSSO AND CHAPMAN'S DATA

Since FACT 9H does not allow for a range-dependent environment or for wave effects like diffraction and leakage, it was not expected to perform very well for the shallow sound channel observed by Dosso and Chapman. Again the first test applied to the FACT 9H output was a plot of transmission loss versus frequency (Figure 6.1). As for the PE model, the levels were obtained by taking three-point range averages centered at 24 km. Since only the zero range sound velocity profile was used, there was no need to be concerned about the effects of the shallow sound channel axis deepening over the eight to twenty kilometer range.

Surprisingly, the transmission loss when both source and receiver were within the SSC showed a gradual decrease and optimum values at 800-900 Hz, consistent with Dosso and Chapman's actual measurements. Over the entire frequency band tested the FACT 9H model predicted losses between 70 and 78 dB, while Dosso and Chapman observed losses between about 80 and 110 dB. The transmission loss in the optimum

frequency range is some 10 dB less than Dosso and Chapman's measurements, but at least the optimum occurred at the proper frequencies. The transmission loss curve for the deep sound channel receiver showed only a fairly consistent increase with higher frequencies.

Figures 6.2 and 6.3 are the FACT 9H transmission loss curves for the three frequencies near optimum. The shallow receiver curves (Figure 6.2) show more fluctuations, probably due to multipath arrivals of sound reflecting from the flat ocean surface. The deep receiver curves (Figure 6.3) are smoothed by the partial absorption of sound in the ocean bottom.

The plot of relative gain (Figure 6.4) reiterates the information in Figure 6.1 in a way that should indicate the presence of a cutoff frequency. We already know that the channel should exhibit a cutoff frequency at about 250 Hz, but there is no evidence for this in Figure 6.4. The shallow receiver always shows better propagation than the deep receiver. This result is not surprising in that the FACT 9H model is not designed to handle such wave effects.

C. THE HIGH-LATITUDE SHALLOW SOUND CHANNELS

With good predictions for optimum frequency in the Dosso and Chapman case, the investigation proceeded to the 10 June and 28 June high-latitude, deep ocean sound velocity profiles. For the 28 June case (Figure 6.5) transmission loss in the shallow sound channel did indeed show a gradual rise and fall. The best frequency, however, was in the vicinity of 400 Hz, much lower than the 600-900 Hz predicted by the PE model (Chapter 5, Section A). As one might expect, transmission losses between the SSC and the surface layer are always significantly greater than when the source and receiver are both contained in the SSC.

As for the 10 June case, FACT 9H results showed a slight but steady increase in transmission loss over the entire frequency range (Figure 6.6). The best frequency was, in fact, the lowest tested: 75 Hz. The transmission loss curve for the receiver located in the surface layer is only a few dB greater than the SSC curve. Recall that the NPS PE model also failed to produce satisfactory results for the 10 June case. Truncating the sound velocity profile at 150 meters with a fully absorbing bottom seemed to improve the PE model prediction somewhat, but Figure 6.7 does not present much of a difference for the FACT 9H model.

Perhaps the 10 June case is a "weaker" shallow sound channel for modeling purposes. Dosso and Chapman's sound velocity profiles show a velocity gradient between 0.1436/s and 0.2071/s between the bottom of the surface layer and the axis of the shallow sound channel. The 28 June sound velocity profile has a velocity gradient of 0.1871/s. The 10 June sound velocity profile, however, has a velocity gradient of only 0.0737/s. There may be a critical value for the velocity gradient between the surface layer and the SSC axis that will produce good results in the models.

For now, however, it does not appear that the FACT 9H model is successful in predicting optimum frequencies for propagation of sound in shallow sound channels. In view of the extensive usage of the FACT model to provide acoustic transmission loss products to fleet operations, this problem warrants further attention.

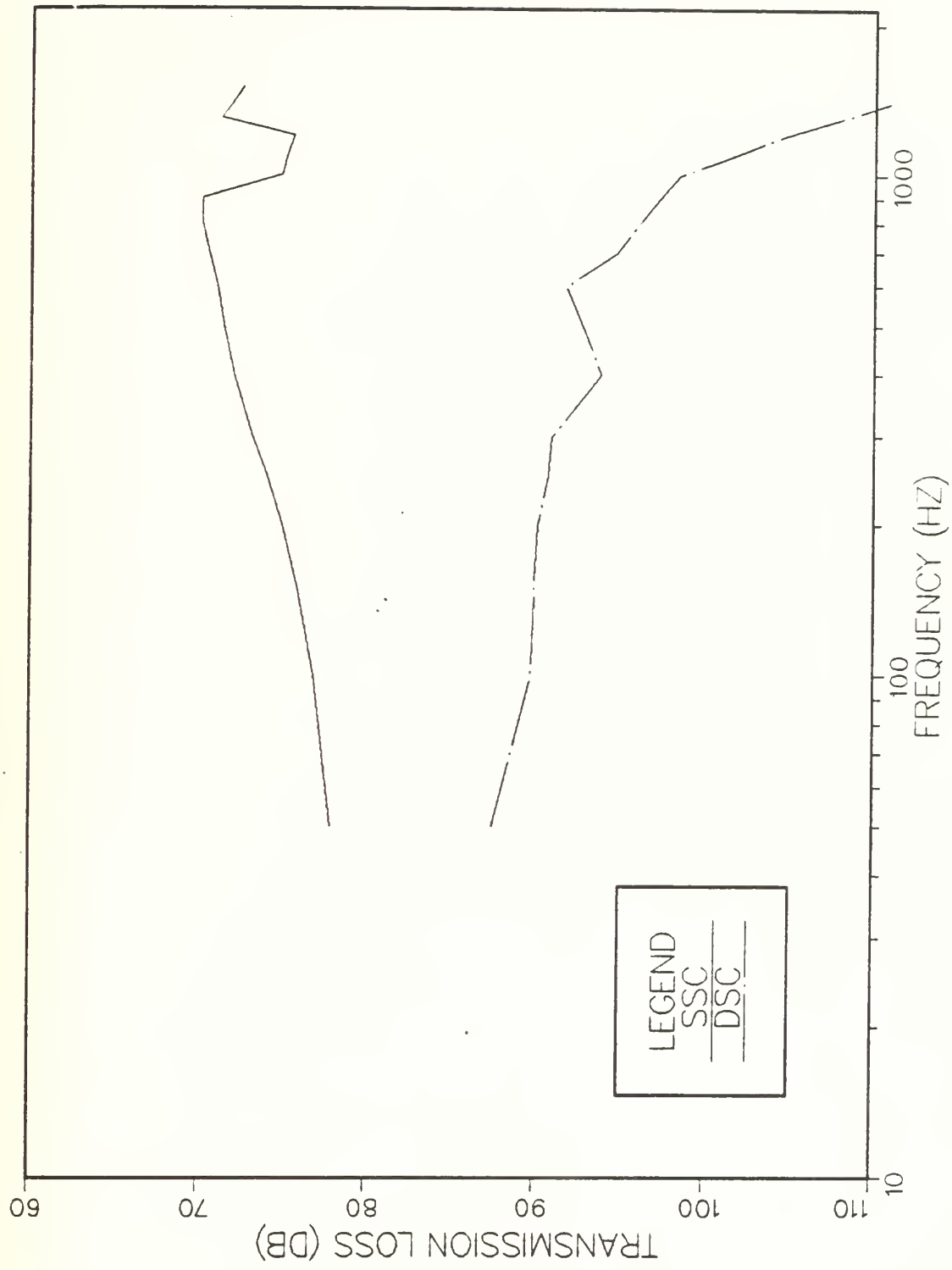

Figure 6.1 Transmission loss versus frequency, Dosso and Chapman (NPS FACT 9H model).

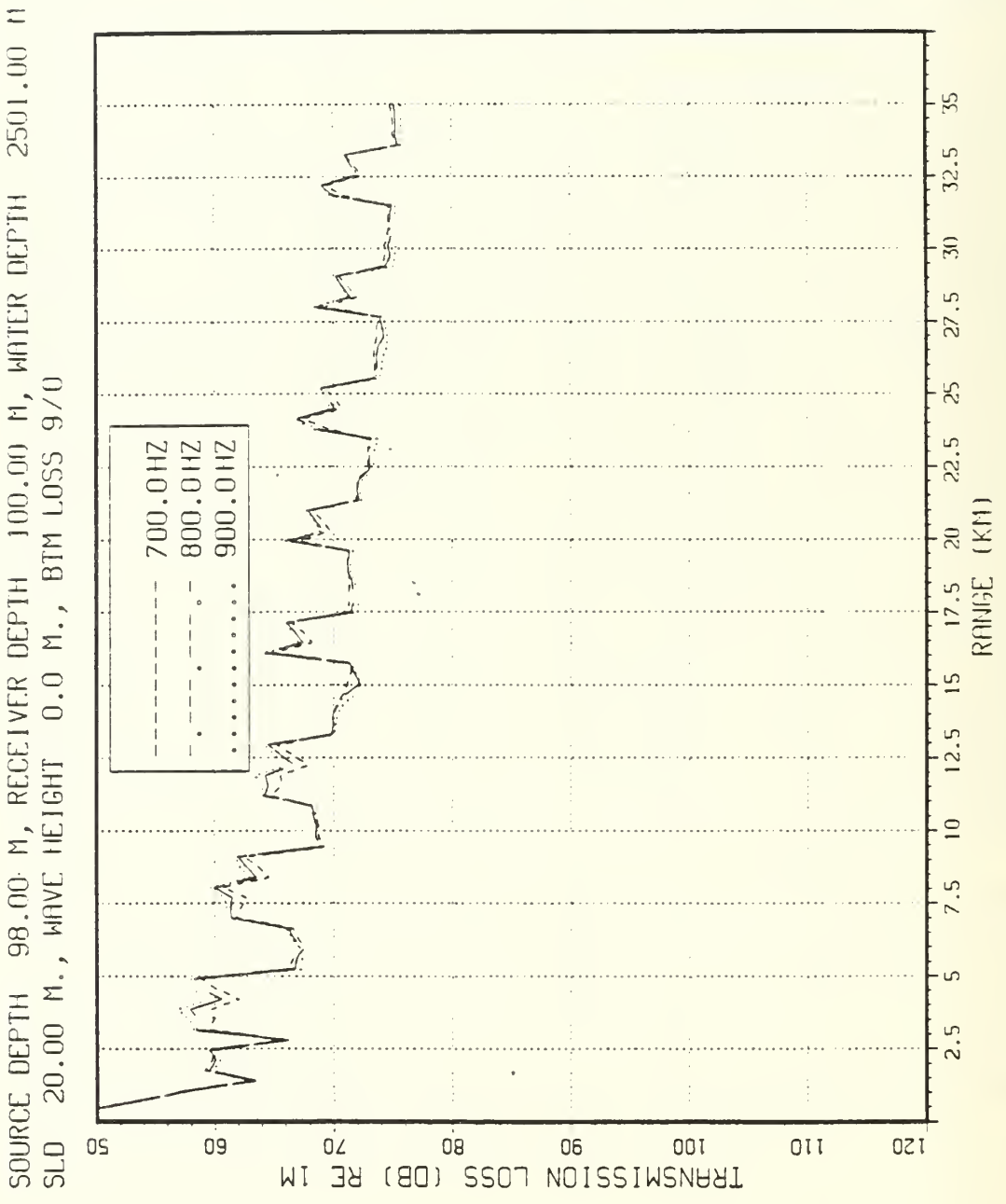

Figure 6.2 Transmission loss in the shallow sound channel, Dosso and Chapman (NPS FACT 9H model).

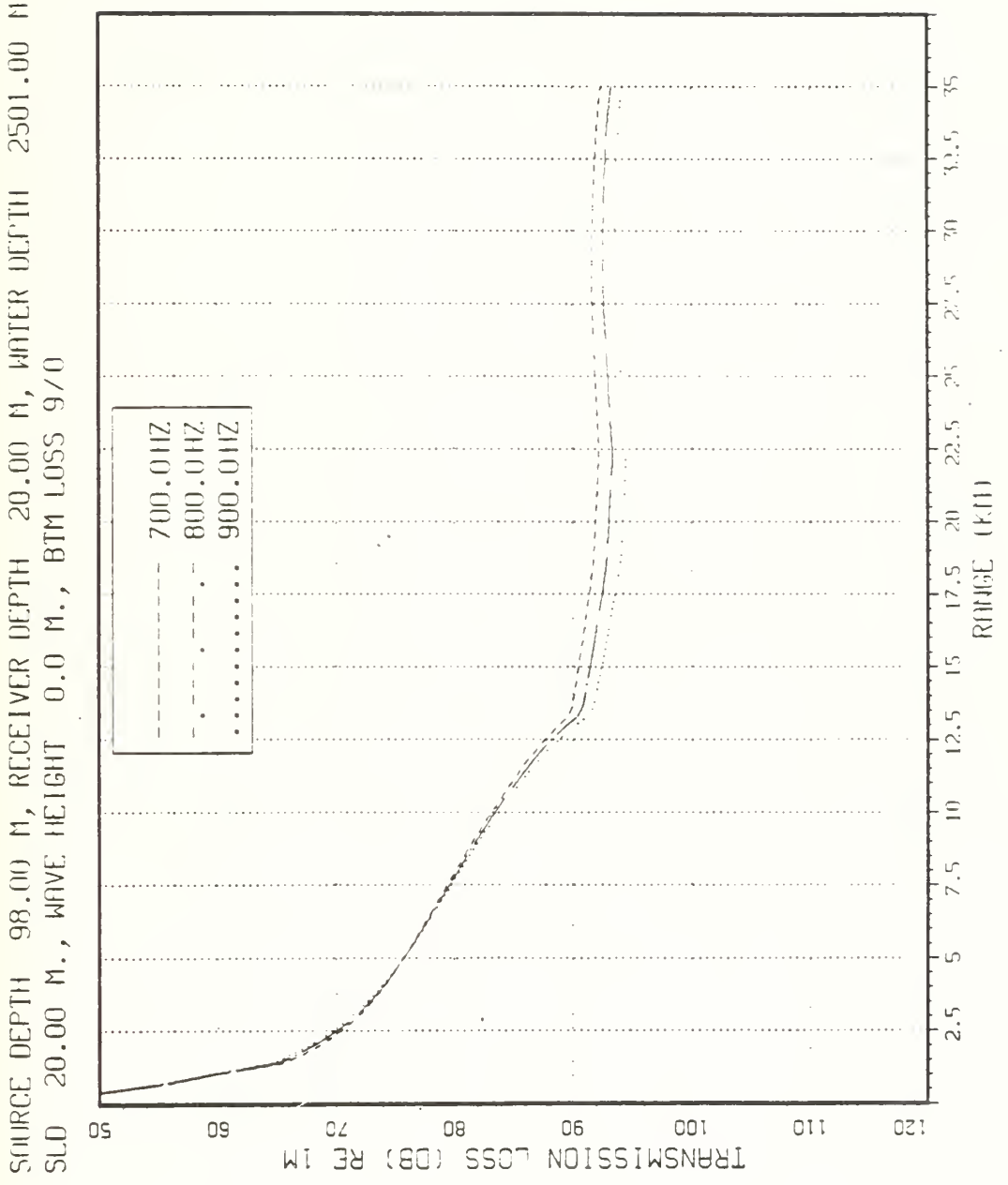

Figure 6.3 Transmission loss between SSC and DSC, Dosso and Chapman (NPS FACT 9H model).

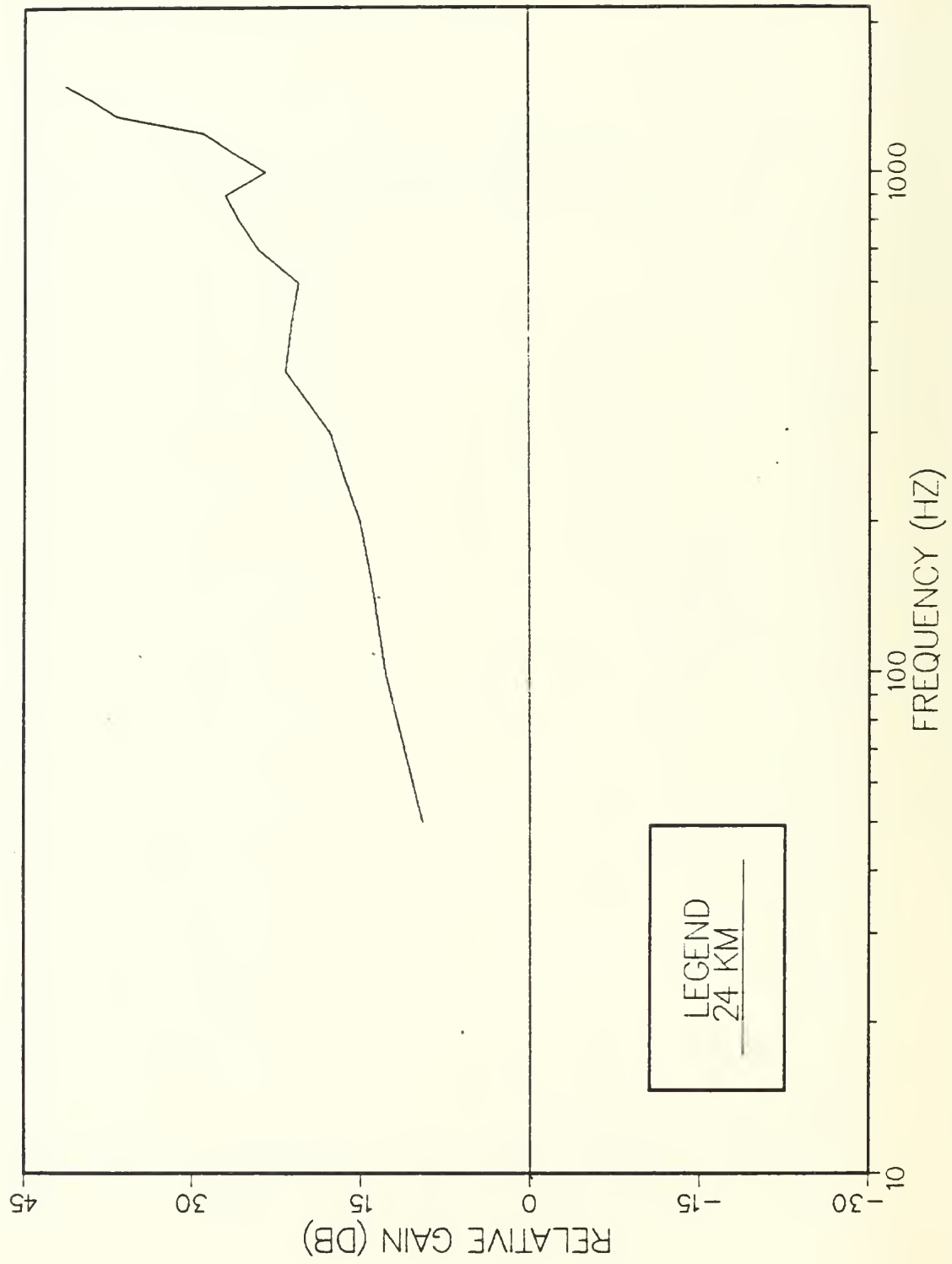

Figure 6.4 Relative gain, Dosso and Chapman (NPS FACT 9H model).

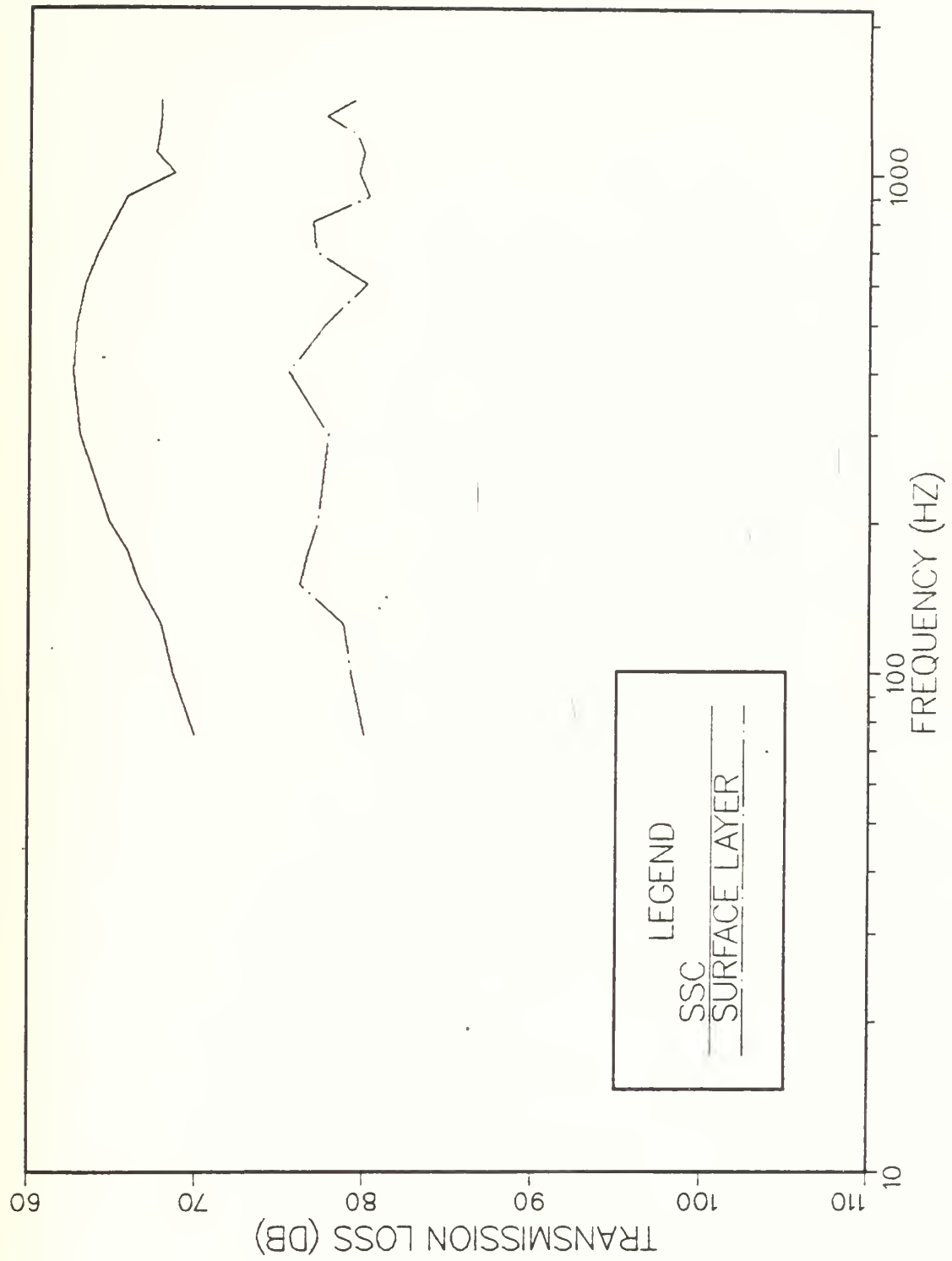

Figure 6.5 Transmission loss versus frequency, 28 June (NPS FACT 9H model).

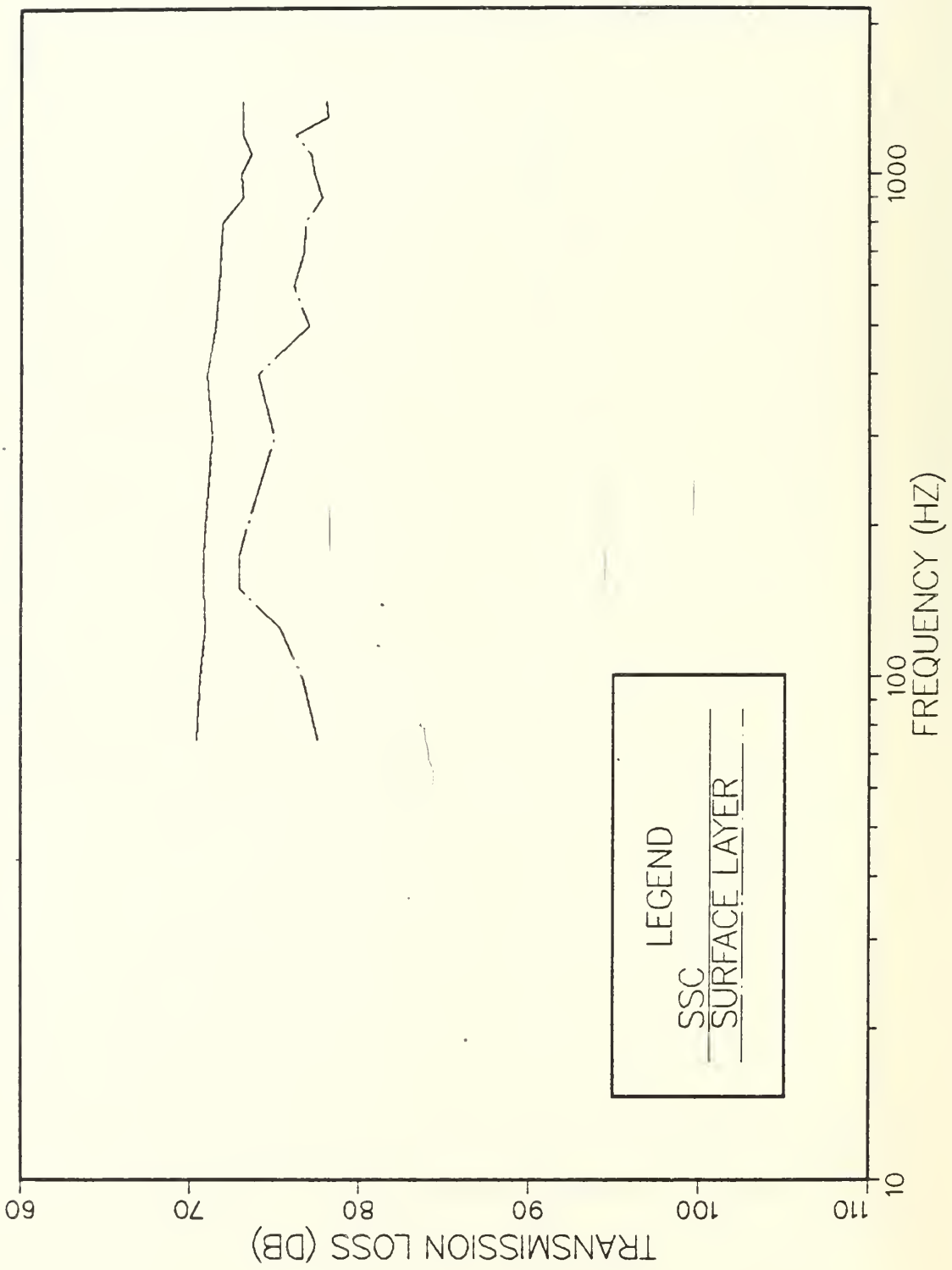

Figure 6.6 Transmission loss versus frequency, 10 June (NPS FACT 9H model).

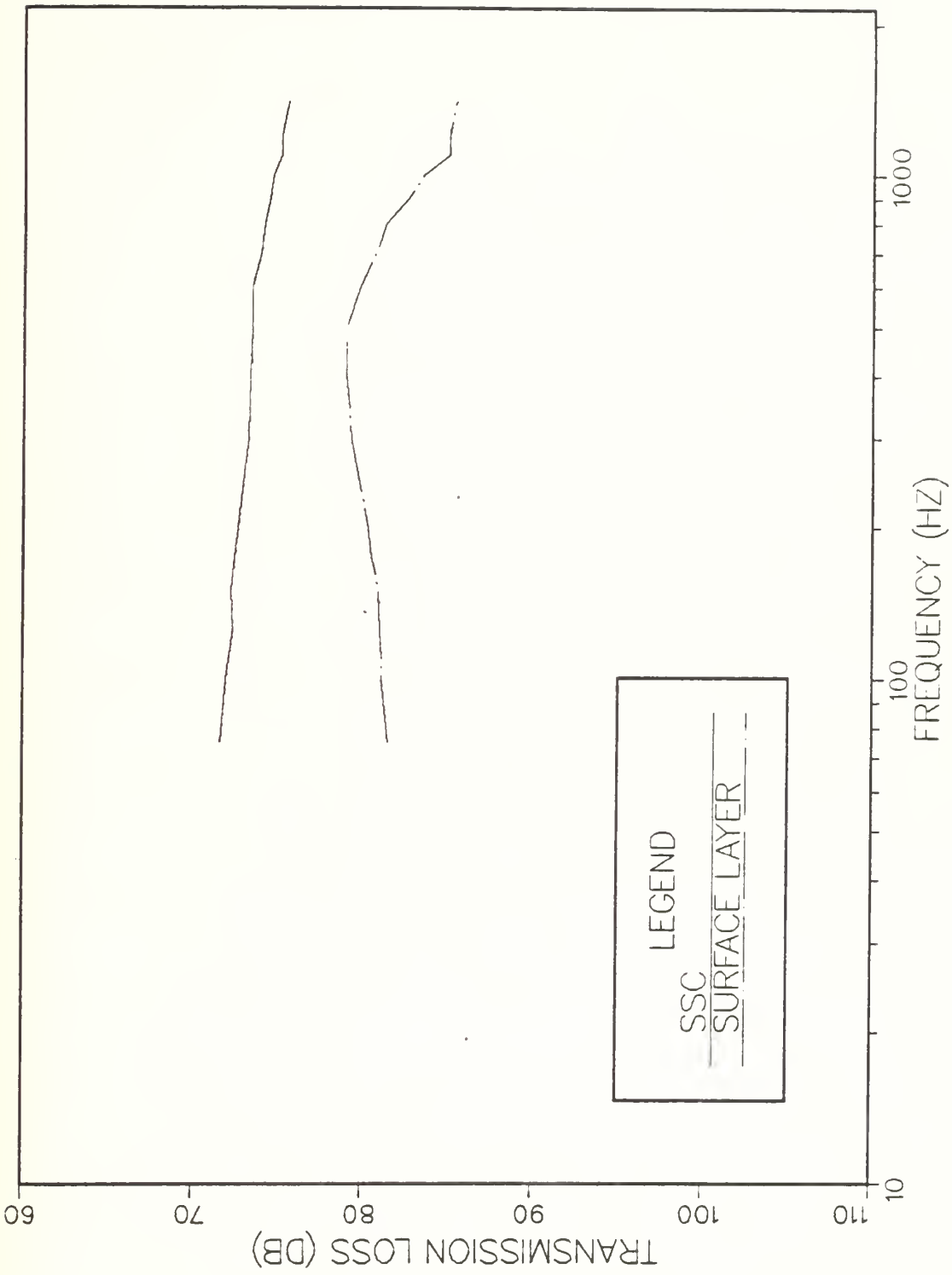

Figure 6.7 Transmission loss versus frequency, truncated profile (NPS FACT 9H model).

VII. CONCLUSIONS

A. RESULTS AND DISCUSSION

Two acoustic transmission loss models were examined to determine how well they predicted the optimum frequency for propagation of sound in shallow sound channels. The split-step Parabolic Equation (PE) model performed satisfactorily, while the Fast Asymptotic Coherent Transmission (FACT 9H) model was less satisfactory.

The PE model has two advantages: it allows for a range-dependent environment and it is a full-wave approximation for the wave equation. These two factors enable the PE model to deal with wave phenomena like diffraction and ducting with a degree of success. The PE model predicted optimum frequencies of 600-900 Hz for the shallow sound channels under study, consistent with the 800 Hz actually measured by Dosso and Chapman. The model seemed to produce better results when the sound velocity gradient between the overlying surface layer and the shallow sound channel was pronounced. The 28 June case, where the gradient was 0.1871/s, yielded 600-900 Hz for optimum frequency, but the 10 June case, where the gradient was only 0.0737/s, did not produce an optimum frequency. The 10 June prediction was improved somewhat by introducing a fully absorbing bottom at the lower boundary of the shallow sound channel.

The FACT 9H model has its advantages, too: it is efficient in terms of computational time and it has had significant operational use. As a ray theory model, it was not expected to handle situations involving surface ducts or shallow sound channels as successfully as the PE model, even with the semi-empirical surface duct module built into this

version of FACT. The Dosso and Chapman sound velocity profiles resulted in a surprisingly good prediction of 800-900 Hz, which agreed well with the experimental results. The 28 June case, however, predicted an optimum of about 400 Hz; and the 10 June case did not predict any reasonable optimum. Again the strength of the sound velocity gradient may explain these different results.

Of our two choices, the PE model, despite its long computation time, appears to be the better candidate for predicting optimum frequency of propagation in a shallow sound channel. The FACT model, despite its widespread use in the fleet, may not be a good predictor for optimum frequency. The predictions for both models seem to be better when there is a large sound velocity gradient between the surface layer and the axis of the shallow sound channel.

B. RECOMMENDATIONS AND AREAS FOR FURTHER STUDY

The fleet user presently has no easy access to a Parabolic Equation model to assess optimum frequencies for real-time environmental conditions. While this study predicts an optimum range of 600-900 Hz where both source and receiver are contained within 80 to 110 meter thick channels, it would be helpful to draw up a table for other source-receiver depth combinations and channels of varying thickness.

Several areas merit further investigation. First, this study uses a fully absorbing bottom throughout. This is unrealistic. It would be of interest to assess bottom losses more accurately and determine what difference, if any, this makes in the prediction of optimum frequency. Another area for investigation is the relative strength of shallow sound channels. A strong channel, where the sound velocity gradient between the bottom of the surface layer

and the axis of the shallow sound channel, appears to trap sound more strongly and may produce a clearer prediction of optimum frequency. It would be helpful to find out how much of a velocity gradient is required to produce an optimum frequency from each of the models, and whether the predicted optimum varies with the strength of the channel.

Finally, other acoustic transmission loss models are available. The implicit finite difference (IFD) PE model is advertised as being able to handle boundary conditions at the ocean bottom more successfully than the split-step PE model. The IFD model should be investigated. The most recent revision of the FACT model, version 10A, is nearly ready for implementation at the Naval Postgraduate School. Technical documents [Ref. 10] indicate that FACT 10A will, among other things, handle ducting situations and boundary conditions better than FACT 9H--this may affect performance for shallow sound channels. A third type of acoustic model is also available--the RAYMODE model. This model may produce better results than FACT when applied to surface ducts and sound channels. The RAYMODE model has recently been designated as the Navy's new standard acoustic propagation loss model, and its performance should be investigated for as wide a variety of environmental conditions as possible.

APPENDIX A

INPUT PARAMETERS FOR THE NPS PE AND FACT 9H MODELS

Table I describes the input options available to the user through the Naval Postgraduate School's split-step Parabolic Equation (PE) and Fast Asymptotic Coherent Transmission loss (FACT 9H) models. Tables II through VI are the sound velocity profiles used in this study.

TABLE I

Input Parameters for the NPS PE and FACT 9H Models

PARAMETERS	PE MODEL	FACT 9H
Input units	English or metric	English or metric
Source depths	One	One
Receiver depths	Maximum 20	One
Frequencies	One	Maximum 6
Maximum range	Unlimited	999 kilometers
Range step	Minimum .01 nm or selected by program	Selected by program
Number of SVPs	Maximum 50	One
Depth levels in SVPs	Maximum 50	Maximum 50
Bottom loss	1) Fully absorbing	1) Bottom type 0 (reflecting) to 9 (absorbing)
	2) User's loss vs grazing angle table	2) User's loss vs grazing angle table
	3) User's depth vs attenuation table	3) Internal loss vs grazing angle table
Variable bottom depth	Maximum 100 ranges/ depths	No
Correction for spherical earth	Available	Available
Correction for for volume attenuation	Available	Available
Vertical beam size of source	1-33 degrees	No
Special handling for surface duct	Not required	Yes
Wave height	No	Yes
Critical angle	Not required	1) Preset value 28.65 degrees
		2) User input

TABLE II

Dosso and Chapman's Sound Velocity Profile at 0 Kilometers

DEPTH(FT)	C(FT/S)	DEPTH(M)	C(M/S)
0.	4927.82	0.	1502.00
45.	4927.82	14.	1502.00
66.	4922.90	20.	1500.50
87.	4906.50	26.	1495.50
115.	4890.75	35.	1490.70
137.	4885.17	42.	1489.00
169.	4879.92	52.	1487.40
198.	4873.36	60.	1485.40
232.	4867.45	71.	1483.60
251.	4866.47	76.	1483.30
273.	4865.48	83.	1483.00
291.	4864.83	89.	1482.80
310.	4864.83	95.	1482.80
325.	4864.50	99.	1482.70
338.	4864.50	103.	1482.70
357.	4863.52	109.	1482.40
369.	4863.84	112.	1482.50
384.	4864.83	117.	1482.80
403.	4865.48	123.	1483.00
433.	4866.14	132.	1483.20
476.	4867.12	145.	1483.50
510.	4867.12	155.	1483.50
543.	4866.47	166.	1483.30
589.	4866.47	179.	1483.30
690.	4862.20	210.	1482.00
779.	4859.58	238.	1481.20
856.	4858.59	261.	1480.90
946.	4857.61	288.	1480.60
1026.	4854.66	313.	1479.70
1115.	4854.00	340.	1479.50
1312.	4849.41	400.	1478.10
1640.	4849.08	500.	1478.00
1969.	4849.73	600.	1478.20
2625.	4852.36	800.	1479.00
3281.	4856.62	1000.	1480.30
3937.	4860.89	1200.	1481.60
4921.	4870.08	1500.	1484.40
6562.	4891.07	2000.	1490.80
8202.	4916.01	2500.	1498.40

See Figure 3.1.

TABLE III

Dosso and Chapman's Sound Velocity Profile at 16 Kilometers

DEPTH(FT)	C(FT/S)	DEPTH(M)	C(M/S)
0.	4923.55	0.	1500.70
16.	4923.88	5.	1500.80
33.	4926.51	10.	1501.60
66.	4924.21	20.	1500.90
82.	4924.21	25.	1500.90
98.	4898.62	30.	1493.10
131.	4884.18	40.	1488.70
164.	4879.26	50.	1487.20
197.	4877.62	60.	1486.70
230.	4873.69	70.	1485.50
262.	4867.12	80.	1483.50
295.	4864.50	90.	1482.70
328.	4865.48	100.	1483.00
361.	4863.84	110.	1482.50
394.	4865.16	120.	1482.90
427.	4863.52	130.	1482.40
459.	4860.89	140.	1481.60
492.	4860.56	150.	1481.50
525.	4861.22	160.	1481.70
591.	4862.86	180.	1482.20
689.	4861.55	210.	1481.80
787.	4861.55	240.	1481.80
853.	4860.23	260.	1481.40
919.	4859.91	280.	1481.30
984.	4859.91	300.	1481.30
1050.	4858.59	320.	1480.90
1115.	4858.27	340.	1480.80
1148.	4857.61	350.	1480.60
1181.	4855.64	360.	1480.00
1214.	4853.67	370.	1479.40
1247.	4852.69	380.	1479.10
1280.	4850.72	390.	1478.50
1312.	4851.37	400.	1478.70
1345.	4850.39	410.	1478.40
1411.	4850.39	430.	1478.40
1444.	4849.73	440.	1478.20
1509.	4849.41	460.	1478.10
1640.	4850.39	500.	1478.40
1969.	4850.72	600.	1478.50
2625.	4852.69	800.	1479.10
3281.	4856.62	1000.	1480.30
3937.	4860.89	1200.	1481.60
4921.	4870.08	1500.	1484.40
6562.	4891.07	2000.	1490.80
8202.	4916.01	2500.	1498.40
9514.	4937.01	2900.	1504.80

See Figure 3.2.

TABLE IV

Dosso and Chapman's Sound Velocity Profile at 20 and 33 Kilometers

DEPTH(FT)	C(FT/S)	DEPTH(M)	C(M/S)
0.	4922.57	0.	1500.40
33.	4921.26	10.	1500.00
66.	4896.32	20.	1492.40
98.	4885.82	30.	1489.20
131.	4878.28	40.	1486.90
164.	4875.66	50.	1486.10
197.	4875.33	60.	1486.00
230.	4873.69	70.	1485.50
262.	4871.06	80.	1484.70
279.	4866.47	85.	1483.30
295.	4864.50	90.	1482.70
312.	4863.52	95.	1482.40
328.	4864.17	100.	1482.60
344.	4863.84	105.	1482.50
361.	4863.84	110.	1482.50
394.	4865.16	120.	1482.90
427.	4864.83	130.	1482.80
459.	4865.81	140.	1483.10
492.	4865.48	150.	1483.00
558.	4865.81	170.	1483.10
591.	4864.17	180.	1482.60
623.	4863.52	190.	1482.40
656.	4860.56	200.	1481.50
722.	4860.23	220.	1481.40
787.	4857.61	240.	1480.60
853.	4856.30	260.	1480.20
919.	4853.67	280.	1479.40
984.	4850.72	300.	1478.50
1083.	4849.73	330.	1478.20
1148.	4851.05	350.	1478.60
1312.	4848.75	400.	1477.90
1640.	4849.08	500.	1478.00
1969.	4849.41	600.	1478.10
2625.	4851.70	800.	1478.80
3281.	4855.97	1000.	1480.10
3937.	4860.89	1200.	1481.60
4921.	4870.08	1500.	1484.40
6562.	4891.07	2000.	1490.80
8202.	4916.01	2500.	1498.40
8858.	4927.82	2700.	1502.00

See Figure 3.3.

TABLE V

High-latitude Sound Velocity Profile for 10 June

DEPTH(FT)	C(FT/S)	DEPTH(M)	C(M/S)
0.	4796.59	0.	1462.00
131.	4796.59	40.	1462.00
164.	4780.18	50.	1457.00
328.	4780.18	100.	1457.00
443.	4773.62	135.	1455.00
492.	4798.23	150.	1462.50
820.	4842.52	250.	1476.00
1640.	4824.47	500.	1470.50
3281.	4847.11	1000.	1477.40
6562.	4890.42	2000.	1490.60
9843.	4943.57	3000.	1506.80
13123.	4999.34	4000.	1523.80

See Figure 5.1.

TABLE VI

High-latitude Sound Velocity Profile for 28 June

DEPTH(FT)	C(FT/S)	DEPTH(M)	C(M/S)
0.	4806.43	0.	1465.00
115.	4804.46	35.	1464.40
164.	4775.26	50.	1455.50
262.	4771.65	80.	1454.40
328.	4765.42	100.	1452.50
459.	4799.54	140.	1462.90
656.	4811.68	200.	1466.60
1640.	4827.43	500.	1471.40
3281.	4847.11	1000.	1477.40
6562.	4890.42	2000.	1490.60
9843.	4943.57	3000.	1506.80
13123.	4999.34	4000.	1523.80

See Figure 5.2.

LIST OF REFERENCES

1. Dunlap, C. R., "Shallow sound channels in ASW," ICAPS On Scene, Environmental Systems Division Newsletter, Naval Oceanographic Office, v. 4, no. 1, pp. 1-2, January 1982.

2. Dosso, S. E., and Chapman, N. R., "Acoustic propagation in a shallow sound channel in the Northeast Pacific Ocean," Journal of the Acoustical Society of America, v. 75, no. 2, pp. 413-418, February 1984.

3. Urick, Robert J., Principles of Underwater Sound, 3d edition, McGraw-Hill Book Company, 1983.

4. Kinsler, Lawrence E., Frey, Austin R., Coppens, Alan B., and Sanders, James W., Fundamentals of Acoustics, 3d edition, John Wiley & Sons, 1982.

5. Thorp, W. H., "Deep-ocean sound attenuation in the sub- and low kilocycle per-second region," Scientific and Engineering Studies, v. II, 1981: Attenuation of Low Frequency Sound in the Sea, Naval Underwater Systems Center, 1981.

6. Mellen, R. H., Simmons, V. P., and Browning, D. G., "Low-frequency sound absorption in sea water: A borate-complex relaxation," Scientific and Engineering Studies, v. II, 1981: Attenuation of Low Frequency Sound in the Sea, Naval Underwater Systems Center, 1981.

7. Naval Ocean Research and Development Activity Technical Note 12, The AESD Parabolic Equation Model, by H. K. Brock, January, 1978.

8. Chapman, N. R., private communication, 21 January 1985.

9. Acoustic Environmental Support Detachment, Maury Center Report 109, The FACT Model, by C. W. Spofford, November 1974.

10. Naval Ocean Research and Development Agency Report 70, Technical Evaluation of FACT 10A, by R. McGirr, D. White, and C. Bartberger, June 1984.

INITIAL DISTRIBUTION LIST

No.		Copies
1.	Defense Technical Information Center Cameron Station Alexandria, Virginia 22314	2
2.	Superintendent Attn: Library, Code 1424 Naval Postgraduate School Monterey, California 93943	2
3.	Superintendent Attn: Prof. C. R. Dunlap, Code 68Du Naval Postgraduate School Monterey, California 93943	8
4.	President Attn: Dr. S. W. Yoon, Physics Dept. Sung Kyun Kwan University Chunchun Dong Suwon, Kyeongki Do Republic of Korea	10
5.	Chief of Naval Operations Attn: LCDR W. L. Bradfield-Smith Naval Observatory 34th and Massachusetts ave.,N.W. Washington D.C. 20390	1
6.	Superintendent Attn: 61Sq Naval Postgraduate School Monterey,California 93943	1
7.	Superintendent Attn: 68Jg Naval Postgraduate School Monterey, California 93943	1
8.	Commander Space and Naval Warfare Systems Command Washington D.C. 20363-5100	1
9.	Commander Oceanographic System, Pacific Box 1390 Pearl Harbor, Hawaii 96860	1
10.	Commander Attn: Code 541 Naval Ocean Systems Center San Diego, California 92152	1
11.	Chief of Naval Operations Attn: OP951F Navy Department Washington D.C. 20350	1
12.	Commanding Officer Naval Ocean Research and Development Activity	3

NSTL
Bay St Louis, Mississippi 39522

13. Commanding Officer 1
Attn: Dr. William Jobst, Code 7300
Naval Oceanographic Office
NSTL
Bay St Louis, Mississippi 39522

14. Chief of Naval Research 1
Arlington, Va 22217

15. Director 1
Attn: Dr. Loyd Hampton
Applied Research Laboratories
The University of Texas at Austin
Austin, Texas 78713-8029

16. Director 1
Attn: Dr. Thomas A. Griffy
Applied Research Laboratories
The University of Texas at Austin
Austin, Texas 78713-8029

17. President 2
Attn: Library
Sung Kyun Kwan University
Chunchun Dong
Suwon, Kyeongki Do
Republic of Korea

18. President 1
Attn: Chairman, Physics Dept.
Sung Kyun Kwan University
Chunchun Dong
Suwon, Kyeongki Do
Republic of Korea

19. Director 1
Attn: Dr. Un Taek Son
Chinhae Research Laboratory
P.O.Box 18
Chinhae, Kyeong Nam
Republic of Korea

20. Director 1
Attn: Dr. Jungyul Na
Chinhae Research Laboratory
P.O.Box 18
Chinhae, Kyeong Nam
Republic of Korea

21. Commanding Officer 1
Attn: Dr. T. B. Gabrielson, Code 3031
Naval Air Development Center
Warminster, PA 18974

22. Superintendent 1
Attn: 61Cz
Naval Postgraduate School
Monterey, California 93943

23. Superintendent 1
Attn: 61Gx
Naval Postgraduate School
Monterey, California 93943

24. Superintendent 1
Attn: 61Sd

Naval Postgraduate School
Monterey, California 93943

25. Superintendent 1
Attn: 61W1
Naval Postgraduate School
Monterey, California 93943

26. Superintendent 1
Attn: 68Bf
Naval Postgraduate School
Monterey, California 93943

27. Superintendent 1
Attn: 012
Naval Postgraduate School
Monterey, California 93943